Development of highly porous polylactic acid-based monoliths containing sol-gel-derived 45S5 Bioglass®

Ehsan Rezabeigi

A Thesis

In the Department

of

Mechanical and Industrial Engineering

Presented in Partial Fulfillment of the Requirements

For the Degree of Doctor of Philosophy at

Concordia University

Montreal, Quebec, Canada

February 2015

CONCORDIA UNIVERSITY
SCHOOL OF GRADUATE STUDIES

This is to certify that the thesis prepared

By: **Ehsan Rezabeigi**

Entitled: **Development of highly porous polylactic acid-based monoliths containing sol-gel-derived 45S5 Bioglass®**

and submitted in partial fulfillment of the requirements for the degree of

Doctor of Philosophy (Mechanical Engineering)

Complies with the regulations of the University and meets the accepted standards with respect to originality and quality.

Signed by final examining committee

————————————————	Chair
Dr. Hashem Akbari	
————————————————	External Examiner
Dr. Tom Troczynski	
————————————————	External to Program
Dr. Michelle Nokken	
————————————————	Examiner
Dr. Suong V. Hoa	
————————————————	Examiner
Dr. Martin Pugh	
————————————————	Thesis Supervisor
Dr. Robin A.L. Drew	
————————————————	Thesis Supervisor
Dr. Paula M. Wood-Adams	

Approved by

————————————————————————————

Chair of Department or Graduate Program Director

————————— 2015   ————————————————

Dean of Faculty

ABSTRACT

Development of highly porous polylactic acid-based monoliths
containing sol-gel-derived 45S5 Bioglass®

Ehsan Rezabeigi, Ph.D.
Concordia University, 2015

It has been shown that highly porous composite scaffolds consisting of biodegradable polymeric matrices and well-dispersed bioactive glass nanoparticles have a great potential for creating the ideal scaffold for tissue engineering purposes. In spite of this, the scaffold with ideal morphology, degradation rate and mechanical properties has not yet been developed.

In the first stage of this study, the most bioactive glass composition, 45S5 Bioglass® (45% SiO_2, 24.5% CaO, 24.5% Na_2O and 6% P_2O_5 (wt.%)), was synthesized by a straightforward, nitrate-free sol-gel method. This route allowed for the production of a fully amorphous product with an appropriately high specific surface area (11.75 m^2/g), which is expected to have an excellent bioactivity for bone regeneration applications.

In the second stage, a fundamental study was performed on the PLA – dichloromethane (solvent) – hexane (nonsolvent) ternary system which was essential for the subsequent production of porous PLA monoliths from this system. The ternary phase diagram of this system was experimentally developed at room conditions in order to identify the liquid-liquid phase separated region. The phase separation kinetics were also studied using turbidity measurements, showing that a small increase in PLA content can significantly increase the phase separation rate of the system.

The third stage of this study involved the fabrication of PLA foams using a solvent-based foaming process: nonsolvent induced phase separation (NIPS), which is a template-free and a very versatile technique. For this purpose, systems from the liquid-liquid phase separated region were selected and allowed to phase separate at various

temperatures and then gel. Shrinkage of the gels during drying was monitored in order to identify compositions with minimum shrinkage and highest porosity. This method was able to produce semi-crystalline PLA foams with high specific surface area (up to 54.14 m^2/g), high porosity (up to 90.8%) and compressive modulus ranging from 1.8 to 57 MPa. Crystallization during phase separation and the phase separation mechanisms were explained and discussed for various compositions and conditions. Depending on the ternary composition and the phase separation standing temperature, mesoporous and combined meso/macroporous morphologies were produced. The latter morphology is very promising for bone scaffold applications since the macropores are vital for vascularization and bone ingrowth whereas the mesopores are expected to enhance cell attachment onto the structure.

In the last stage of this study, the sol-gel-derived 45S5 Bioglass[®] was surface modified with a silane coupling agent (methacryloxypropyltriethoxysilane) in order to improve its interfacial compatibility with PLA. This process effectively increased the stability of the glass particles in PLA solutions. It also diminished the agglomeration of glass particles. Surface modified glass particles (2 wt.%) were subsequently incorporated into the NIPS foaming process to produce composite foams. It was shown that the particle incorporation route (via solvent or nonsolvent) had the greatest impact on morphology, porosity and crystallinity of the resulting foams. An incorporation of 2 wt.% of particles via nonsolvent significantly decreased the porosity and crystallinity of the PLA matrix. The incorporation of particles via solvent increased the average size of the macropores and made them more homogeneous in terms of size. It also slightly increased the porosity of the foams whereas no impact on the crystallinity of their PLA matrices was observed. SEM examination revealed that the surface modified particles were incorporated within the open mesoporous structure of the foams where they can simultaneously be in contact with the physiological fluids.

Dedicated to

My Mom Mehrangiz and My Dad Aliashraf

Acknowledgement

First and foremost, I would like to express my deepest appreciation to my supervisors, Dr. Robin Drew and Dr. Paula Wood-Adams for their guidance, advice and support during my research. They always encouraged me to learn more and think better.

I would like to thank all of the administrative staff of Mechanical and Industrial Engineering, especially Leslie Hosein, Maureen Thuringer and Arlene Zimmerman. I would also like to thank Heng Wang, Ahmad Omar Mostafa and Mazen Samara for their technical assistance.

My special thanks to my lovely, amazing family and all of my friends especially, Ali Alem, Sina Chaeichian and Alireza Zandi Karimi who always supported and encouraged me.

Contributions of Authors

1. Ehsan Rezabeigi, Paula M. Wood-Adams and Robin A.L. Drew, "Synthesis of 45S5 Bioglass$^{®}$ via a straightforward organic, nitrate-free sol-gel process", Materials Science and Engineering: C, vol. 40, pp. 248 – 252, 2014.
   [**Chapter 3 of this thesis**]

   ➢ The experimental work of this article was performed by the author Ehsan Rezabeigi as a part of this PhD dissertation. The particles size analysis and BET were performed by Monique Riendeau - McGill University. The original ideal for working on bioactive glasses was proposed by Robin Drew. Rolf Schmidt kindly helped by giving suggestions for the stabilization of the gel. The first draft of the article was written by Ehsan Rezabeigi which was revised and modified by the other authors before submission. Robin Drew and Paula Wood-Adams supervised this work during the entire research.

2. Ehsan Rezabeigi, Paula M. Wood-Adams, Robin A.L. Drew, "Isothermal ternary phase diagram of the polylactic acid-dichloromethane-hexane system", Polymer, vol. 55, pp. 3100 – 3106, 2014.
   [**Chapter 4 of this thesis**]

   ➢ The experimental work of this article was performed by the author Ehsan Rezabeigi as a part of this PhD dissertation. The ideal of developing the ternary phase diagram was originally proposed by Paula Wood-Adams. The first draft of the article was written by Ehsan Rezabeigi which was revised and modified by the other authors before submission. Robin Drew and Paula Wood-Adams supervised this work during the entire research.

3. Ehsan Rezabeigi, Paula M. Wood-Adams, Robin A.L. Drew, "Production of porous polylactic acid monoliths via nonsolvent induced phase separation", Polymer, vol. 55, pp. 6743 – 6753, 2014.
   [**Chapter 5 of this thesis**]

   ➢ The experimental work of this article was performed by the author Ehsan Rezabeigi as a part of this PhD dissertation. Micro-CT analysis was kindly performed by Saadallah Bouhanik at Sainte Justine Hospital - Research Center. The BET analysis was performed by Monique Riendeau - McGill University. The first draft of the article was written by Ehsan Rezabeigi which was revised and modified by the other authors. Robin Drew and Paula Wood-Adams supervised this work during the entire research.

4. Ehsan Rezabeigi, Paula M. Wood-Adams and Robin A.L. Drew, "The incorporation of surface modified sol-gel-derived 45S5 Bioglass$^{®}$ in highly porous polylactic acid monoliths", *will be published shortly*.
   [**Chapter 6 of this thesis**]

   ➢ The experimental work of this article was performed by the author Ehsan Rezabeigi as a part of this PhD dissertation. The particles size analysis was performed by Monique Riendeau - McGill University. The first draft of the article was written by Ehsan Rezabeigi which was revised and modified by the other authors before submission. Robin Drew and Paula Wood-Adams supervised this work during the entire research.

Two conference papers have also been published based on this work, which are not presented in this thesis as chapters, but mentioned in Appendix C.

TABLE OF CONTENTS

List of Figures

List of Tables

Abbreviations

(A/W) glass-ceramic	Apatite-wollastonite glass-ceramic
APTS	3-aminopropyltriethoxysilane
BET	Brunauer, Emmett and Teller (N2 adsorption–desorption)
DMF	Dimethylformamide
DI water	Deionized water
DCM	Dichloromethane
DSC	Differential scanning calorimetry
EDS	Energy-dispersive X-ray spectroscopy
FSP	Flame Spray Pyrolysis
FDA	Food and Drug Administration
FTIR	Fourier transform infrared spectroscopy
GRAS	Generally Recognized as Safe
HCA	Hydroxycarbonate apatite
HA	Hydroxyapatite
MPTES	3-methacryloxypropyltriethoxysilane
NIPS	Nonsolvent induced phase separation
NTU	Nephelometric turbidity units
PLA	Polylactic acid
PE	Poly(ethylene)
PET	Poly(ethylene terephthalate)
PHA	Polyhydroxyalkanoates
P(3HB) or PHB	Poly-3-hydroxybutyrate
PHBV	3-hydroxyvalerate
P4HB	Poly-4-hydroxybutyrate
PBSu	Poly(1,4-butylene succinate)
(PUR)s	Poly(urethane)s
PPF	Poly(propylene fumarate)
PVA	Poly(vinyl alcohol)

PVDF	Poly(vinylidene fluoride)
PSA	Particle size distribution analysis
SBF	Simulated body fluid
SEM	Scanning electron microscope
SD	Standard deviation
TCP	Tricalcium phosphate
T_g	Glass transition temperature
T_m	Melting temperature
TEOS	Tetraethylorthosilicate
TIPS	Thermally-induced phase separation
TEP	Triethyl phosphate
USP	Ultrasonic Spray Pyrolysis
VIPS	Vapor-induced-phase-separation
XRD	X-ray diffractometry analysis
YSZ	Yttria-stabilized zirconia

Chapter 1

Introduction

1.1. Overview

Since earliest times, bone is one of the tissues with the most need for repair. This is due to the important role of the skeleton in locomotion, support and protection of the vital organs [1, 2]. Bone can heal itself if the defect is small; but in the case of a large defect or diseased bone, the bone needs a supportive structure to regenerate. Using natural bone grafts (allo- or autografts) is not always an ideal alternative because they may cause problems such as pathogen transfer and/or rejection by the body [2, 3].

Ever since 1950, various types of biomaterials have been developed and used as bone implants including metals and alloys, glasses, ceramics and polymers [1-7]. The discovery of the first bioactive material, 45S5 Bioglass®, by Larry Hench in late 1969 [5], revolutionized biomaterials. This composition is able to bond to both hard and soft tissues *in vivo* and it can encourage bone cells to differentiate and proliferate. To date, 45S5 Bioglass® is still the most bioactive and promising composition for bone regeneration having Class A bioactivity. In 1991, it was shown that many bioactive glass compositions can be produced via sol-gel processing [5, 8]. Sol-gel-derived bioactive glasses usually have higher bioactivity due to higher specific surface area and a typical surface covered with hydroxyl groups [2, 3, 5-7]. Production of the 45S5 composition via sol-gel methods is challenging and the product may in fact be too bioactive to be useful for bone regeneration applications [9-12].

In spite of high bioactivity, bone scaffolds[1] made of bioactive glasses do not always exhibit the desirable mechanical properties and degradation rates. As an alternative, composite scaffolds consisting of a biocompatible, bioresorbable, polymeric matrix such as polylactic acid (PLA) and well-dispersed bioactive particles have been

---

1. Bone scaffold is a highly porous 3D structure which supports the defective bone to regenerate. The characteristics of an ideal scaffold for bone regeneration are explained in section 2.4.

developed. An ideal composite scaffold must be highly porous (up to 95%) with both meso- and macropores in order to promote the attachment of bone cells and vascularization, respectively[1] [1-7]. The production method of scaffolds determines their porosity and pore morphology. Solution phase separation methods including thermally-induced or nonsolvent induced phase separation, have great potential to fabricate highly porous scaffolds with interesting morphologies via template-free, versatile routes [7, 13, 14].

The problems associated with the current scaffolds such as insufficient mechanical properties and undesirable degradation behavior can be partly overcome by improving the interfacial compatibility between their organic and inorganic phases. Surface modification of bioactive particles with silane coupling agents diminishes their agglomeration and improves their dispersibility in the polymeric matrix. Furthermore, this promotes bioactivity and good mechanical properties of the final composite scaffold [7, 15, 16].

1.2. Objectives

The main objectives of each step of this study are now presented according to the sequence of chapters in this thesis.

- ➢ To develop a sol-gel process for synthesis of a fully amorphous 45S5 bioglass with an appropriate specific surface area. For this purpose, a combination of appropriate precursors and testing conditions (e.g., pH) must be selected, which result in a gel with a stabilization temperature below its crystallization temperature (*1st stage of this study presented in Chapter 3*).
- ➢ To produce knowledge of phase equilibria behavior and phase separation kinetics of the PLA – dichloromethane – hexane system, which is essential for the design of solution phase separation-based techniques for the production of porous PLA

---

1. Tissue engineered nanocomposite scaffolds which are designed to be biomimetic are the advanced generation of bone scaffolds [1, 3, 7]. Tissue engineering is defined as "application of scientific principles to the design, construction, modification, growth and maintenance of living tissues" [4].

structures. For this purpose, the ternary phase diagram of this system must be developed at room temperature (*2nd stage of this study presented in Chapter 4*).

➢ To develop a template-free foaming process for PLA that allows for the production of foams with predetermined characteristics such as high porosity and morphologies including both mesopores and macropores. For this purpose we will use nonsolvent induced liquid-liquid phase separation in PLA – dichloromethane – hexane system. Also, to describe the dependency of foam characteristics including porosity, crystallinity and morphology on their initial composition and phase separation temperature. The final goal here is to select the compositions and conditions leading to highly porous PLA foams with desirable morphologies and mechanical properties for scaffold applications (*3rd stage of this study presented in Chapter 5*).

➢ To improve the dispersibility of the sol-gel-derived 45S5 bioactive glass in PLA, and investigate their incorporation for the production of highly porous composite monoliths. Also, to describe the effect of incorporation of the surface modified glass particles on PLA foams and evaluate the characteristics of the final PLA/bioglass scaffolds (*4th stage of this study presented in Chapter 6*).

1.3. Thesis organization

This thesis has seven chapters which are briefly described here. The first chapter provides a brief introduction to bone healing and bone substitutes including polymer-based composite scaffolds. The objectives of the thesis are also presented in this chapter.

Chapter 2 includes a comprehensive literature review on bioactive materials including bioactive glasses; in particular 45S5 Bioglass®. The sol-gel technique method for synthesizing bioactive glasses is also reviewed. Biocompatible and bioresorbable polymers used in bone regeneration are discussed with a focus on PLA. The organic/inorganic interfaces and methods for improving them are discussed. The last section of Chapter 2 describes the characteristics of an ideal bone scaffold. Polymer foaming techniques, especially solution phase separation methods including TIPS and NIPS, which are used for scaffold production, are also reviewed.

Chapter 3[1] starts with a brief to 45S5 Bioglass® and then focuses on synthesizing this glass composition via an organic, nitrate-free sol-gel route. Chapter 4[2] includes a fundamental study of the PLA-DCM-hexane system in order to develop its ternary phase diagram at room temperature. The phase separation kinetics are also studied. The theory of phase separation in such ternary systems is explained based on the Flory-Huggins equations.

The production of PLA foams via NIPS is discussed in Chapter 5[3]. The effects of composition and the phase separation standing temperature on the characteristics of the final foams are explored and highly porous systems with desirable morphologies for scaffold production are selected. Phase separation mechanisms such as nucleation and growth and spinodal decomposition are also elaborated for various compositions of this system.

In Chapter 6[4], the sol-gel-derived 45S5 Bioglass® is coated with a silane coupling agent under basic conditions. The incorporation of the surface modified particles into PLA via NIPS in order to produce composite scaffolds is also investigated. The effects of this incorporation on the properties of the PLA foams are examined.

Chapter 7 summarizes the conclusions and contributions of this study and presents a list of recommendations for future work.

---

1. Chapter 3 is published as: Ehsan Rezabeigi, Paula M. Wood-Adams and Robin A.L. Drew, "Synthesis of 45S5 Bioglass® via a straightforward organic, nitrate-free sol-gel process", Materials Science and Engineering: C, vol. 40, pp. 248 – 252, 2014.

2. Chapter 4 is published as: Ehsan Rezabeigi, Paula M. Wood-Adams, Robin A.L. Drew, "Isothermal ternary phase diagram of the polylactic acid-dichloromethane-hexane system", Polymer, vol. 55, pp. 3100 – 3106, 2014.

3. Chapter 5 is published as: Ehsan Rezabeigi, Paula M. Wood-Adams, Robin A.L. Drew, "Production of porous polylactic acid monoliths via nonsolvent induced phase separation", Polymer, vol. 55, pp. 6743 – 6753, 2014.

4. This Chapter *will be published shortly*: Ehsan Rezabeigi, Paula M. Wood-Adams and Robin A.L. Drew, "The incorporation of surface modified sol-gel-derived 45S5 Bioglass® in highly porous polylactic acid monoliths".

Chapter 2

Literature review

2.1. Bioactive materials

The first requirement for a biomaterial is biocompatibility which is defined as "the ability of a material to perform with an appropriate host response in a specific application" [4]. Any type of foreign material implanted into the body causes some response from the body, although in the case of biomaterials it is expected to be minimum [1]. A biocompatible material should not cause any "unresolved inflammatory response, demonstrate immunogenicity or cytotoxicity" [7]. Some metals, ceramic and glass compositions as well as polymers are classified as biocompatible materials used for tissue engineering [7].

A bioactive material is not only biocompatible but can also induce a certain interfacial biological response *in vivo*[1], which may result in bonding with the tissue. Bioactive materials are able to produce hydroxyapatite (HA; $Ca_{10}(PO_4)_6(OH)_2$) upon placing *in vitro*[2] or *in vivo* via which they can bond to the defective bone. That is due to the fact that this hydroxyapatite is chemically and structurally similar to the mineral of the bone (carbonated hydroxyapatite) [1-7]. HA crystals form bonds to the layers of collagen fibrils produced by osteoblasts at the interface [5]. The rate of HA formation on the bioactive material indicates its bioactivity level. The HA formation rate and its thickness as well as the strength and stability of the bond formed between the biomaterial and the tissue depend on the composition, microstructure and surface texture of the bioactive material [1, 8, 17]. For example, the shear strength of the bond between 45S5 Bioglass® and the cortical bone of rats and monkeys is the same or more than that of the host bone [5].

---

1. "Pertaining to a biological process occurring within the living organism or cell" [4].

2. "Pertaining to a situation which involves the experimental reproduction of biological processes in the more easily defined environment such as a culture vessel" [4].

Hench classified bioactive materials into Class A and Class B based on the rate of bone regeneration induced by the material. Class A bioactivity includes those compositions which are able to bond with both soft and hard tissues. These materials are osteoconductive and osteoproductive resulting in a high rate of hydroxyapatite formation and fast bone bonding [1, 18-21]. Class B bioactive materials only exhibit osteoconductivity and they normally cannot provide a fully suitable environment to stimulate the few osteoprogenitor cells to mitosis [5, 22]. Class A bioactivity is explained further in section 2.1.1.

Bioactivity has been reported for various types of materials which can be classified in three main groups [1-7]: 1) *calcium phosphates*, 2) *bioactive glasses and glass-ceramics* and 3) *other bioactive materials*. These three groups of material are briefly reviewed in the following.

The most common bioactive calcium phosphates are synthetic HA and tricalcium phosphate (TCP; $Ca_3(PO_4)_2$). TCP has four polymorphs among which α and β are the most commonly used forms [2]. The Ca/P molar ratio in the composition of a calcium phosphate determines the type of the material (Table 2.1) [1].

Table 2. 1. Various types of calcium phosphates based on their Ca/P molar ratio [1]

Ca/P molar ratio	Calcium phosphates type
< 1.67	α or β-TCP
>1.67	CaO+HA phase
= 1.667 (= 2.151 in weight ratio)	HA

Although synthetic HA has been extensively studied due to its similarity to the mineral of the bone as well as its thermal and chemical stability in the body, its Class B bioactivity, relatively poor mechanical properties (especially toughness) and slow degradation rate *in vivo* have limited its applications. The HA resorption rate can be increased to some extent by creating silicon or carbonate substituted apatites. The β-TCP shows relatively higher mechanical properties and dissolution rate compared to those of HA [1-3]. The dissolution rates of these calcium phosphates are as follows [7]: Amorphous HA > α-TCP > β-TCP > Crystalline HA. It has been shown that, the

incorporation of β-TCP and HA creates a new material known as biphasic calcium phosphate with improved dissolution and mechanical properties [2, 3].

After the advent of 45S5 Bioglass®, new bioactive glass and glass-ceramic compositions have been developed and studied over the past four decades [2, 5]. They are the only materials which can bond with both soft and hard tissues *in vivo* (Class A bioactivity) [5, 22-24]. Bioactive glasses can be synthesized in various compositions and forms (powders, fibers, bulks and porous monoliths), resulting in wide range of properties suitable for various applications [1, 7, 25]. Bioactive glasses are reviewed further in section 2.1.1.

Apatite-wollastonite (A/W) glass-ceramic which was created in Japan (1982) [1] is one of the most important modifications of bioactive glasses. This material comprises 34 wt.% of oxyfluorapatite ($Ca_{10}(PO_4)_6(O,F)_2$) crystals (50–100 nm) and 28 wt.% wollastonite (CaO•SiO$_2$), in a glassy matrix (17 MgO, 24 CaO, 59 SiO$_2$ in wt.%) [1, 5]. According to Table 2.2, the mechanical properties of the A/W glass-ceramic are much higher than those of 45S5 Bioglass® and calcium phosphates as well as other bioactive glasses and glass-ceramics [1, 5, 26]. This material can be used as bone replacement in load-bearing parts of the skeleton since it has good bioactivity and mechanical properties [1].

Table 2. 2. Mechanical properties of HA, 45S5 Bioglass® and (A/W) glass-ceramic [7].

Materials (Dense)	Compressive strength (MPa)	Tensile strength (MPa)	Young's modulus (GPa)	Fracture toughness (MPa m$^{1/2}$)
HA	>400	~40	~100	~1.0
45S5 Bioglass	~500	42	35	0.5-1
(A/W) glass-ceramic	1080	215	118	2.0

Although calcium phosphates and bioactive glasses are the most well-known bioactive materials, bioactivity is not limited only to them. It has been reported that some bioinert metals and ceramics can also achieve some level of bioactivity after "a simple chemical heat treatment" [7]. For example, after a chemical treatment by NaOH combined with heat treatments on titanium and its biocompatible alloys, HA has been formed on their surface *in vitro* [7].

2.1.1. Bioactive glasses and glass-ceramics

Bioactive glasses have shown more advantages for tissue repairing purposes among all of the bioactive materials. These surface-reactive materials are biocompatible, bioresorbable and bioactive [1-5]. Their biocompatibility is due to the fact that their dissolution by-products include elements such as Si, Ca and Na which are naturally found in the body [27]. Rejection of a material by forming scar tissues generally occurs because those tissues do not contain the components of the material and its by-products [5].

Bioactive glasses comprise elements which are glass formers (network formers) or glass modifiers (network modifiers). Glass formers (e.g., Si and P) develop the glass structure via covalent bonding and glass modifiers (e.g., Ca and Na) bond ionically to this structure. Higher glass former content in a glass composition makes it more chemically stable meaning the glass is less soluble and bioactive. Although most of the bioactive glasses are silica-based, some phosphorus-based bioactive glasses have been also studied. Note that the introduction of multi-valent cations, such as Al^{3+} and Ti^{4+} into the glass composition diminishes the bioactivity and reduces bone bonding [5, 19].

All melt-derived silica-based glass compositions in the system of SiO_2–Na_2O–CaO with 6 wt.% P_2O_5 are illustrated in Fig. 2.1. No glass can be formed in the silica-poor region of the diagram (region D) due to the lack of glass former content. On the contrary, for the silica-rich region of the diagram (> 60 wt.%; region B), the composition is not reactive and soluble enough to be considered bioactive (bio-inert) [1, 8]. Bone bonding only occurs within the compositional region of A in which glasses with high silica contents (52 – 60 wt.%) [5] can bond to the hard tissues within 2 – 4 weeks. The compositions in region S (SiO_2 = 42 – 52 wt.%) are able to rapidly bond to both hard and soft tissues (Class A bioactivity). The glass compositions such as 45S5 which are located in the small region of E have the highest bioactivity index [1, 5].

The dissolution of Class A bioactive glasses (region S) starts rapidly upon placing *in vitro* or *in vivo* resulting in HA formation and releasing critical concentrations of soluble ions, for example 15 – 30 ppm Si and 60 – 90 ppm Ca in the case of 45S5 Bioglass[®] [22]. It provides an environment which simulates the bone cells to differentiate and proliferate (osteogenic properties) [19, 22] via the activation of seven groups of

genes in osteoprogenitor cells resulting in a fast bone formation [1, 22]. The genetic aspect of this phenomenon is not completely understood [6, 22, 28]. These ions also promote blood vessel formation which is a vital stage for bone regeneration (angiogenesis properties) [3, 22].

Region	Description
A	Bone bonding
B	Too low reactivity (non-bonding)
C	Too high reactivity (non-bonding)
D	No glass formation
S	Soft and hard (bone) tissue bonding
E	Bioactive glasses with the highest level of bioactivity (rapidly bond to bone)
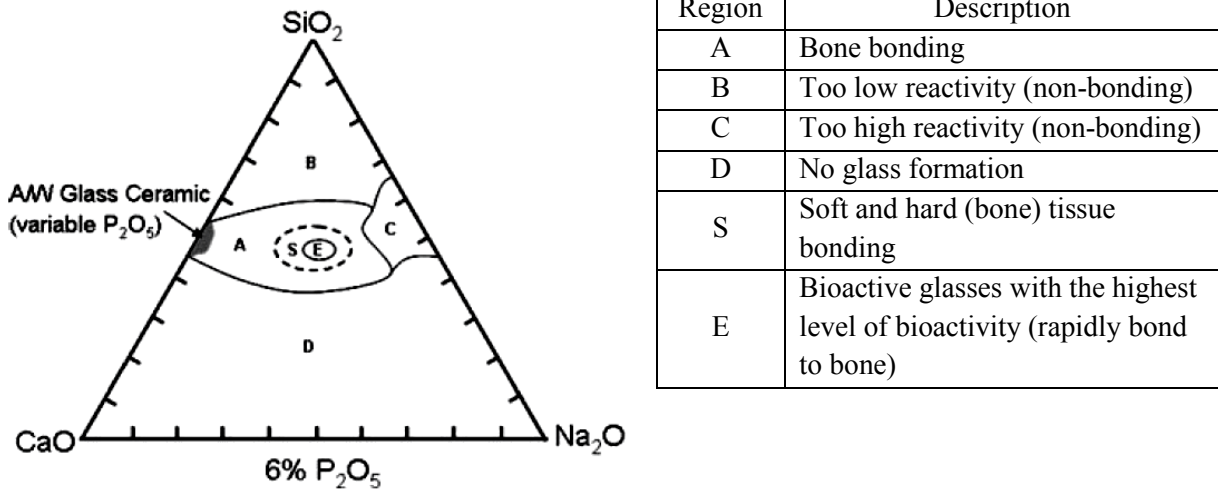
Fig. 2. 1. Compositional diagram of melt-derived glasses in $SiO_2 - CaO - Na_2O$ system with 6% P_2O_5 (wt.%). The boundaries in this diagram are kinetic boundaries [5].

The bioactivity, physical and mechanical properties of a bioactive glass depend on not only its composition but also its crystallinity, microstructure and surface chemistry which are affected by the production method of the glass (section 2.1.2) [3, 5, 8, 17, 29-33]. Low crystallinity and high specific surface area result in higher bioactivity due to lower chemical stability and larger surface to react with the physiological fluids, respectively. For example, melt-derived silica-rich glass compositions which are not bioactive (Fig 2.1) show a high level of bioactivity if produced by sol-gel methods. Chen et al. [29], studied the HA formation on 3 bioactive glasses with different compositions and characteristics (Fig. 2.2). Although the glass former contents of 58S and 77S are very high (67 wt.% and 86 wt.%, respectively), HA has formed on their surface after 4 days of immersion in simulated body fluid (SBF). This is due to their high specific surface area since they have been produced via the sol-gel process. Note that according to Fig. 2.1, the melt-derived composition of 77S is expected to exhibit a very low level of bioactivity. The sol-gel technique is discussed further in section 2.1.2.5. The type of hydroxyapatite

9

formed on each bioactive glass in Fig. 2.2 depends on their composition and other characteristics such as specific surface area and surface chemistry.

Bioactive glass	Composition (wt.%)				Method of production	Specific surface area (m^2/g)
	SiO_2	CaO	Na_2O	P_2O_5		
45S5	45	24.5	24.5	6	Conventional melting-quenching	3.22±0.14
58S	58	33	-	9	Sol-gel	115.89±0.74
77S	77	14	-	9	Sol-gel	369.19±1.45
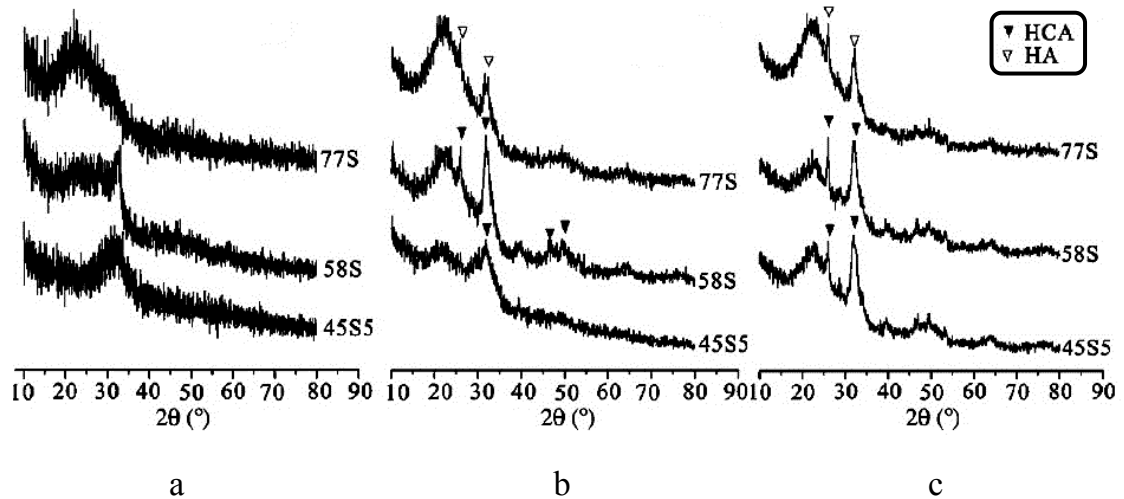
Fig. 2. 2. XRD patterns of the bioactive glasses presented in the table: before (a) and after 4 h (b) and 96 h (c) immersion in SBF [29].

The *in vitro* HA formation on a silica-based bioactive glass involves 5 major steps which are briefly presented in Fig 2.3. For a Class A bioactive glass, it takes only minutes after exposure to SBF to reach step 3 of this process [34]. For example, the hydroxyapatite crystals nucleate on the surface of melt-derived 45S5 Bioglass® within 2 – 6 hours *in vitro* (step 5). This timeframe can be as long as 2 – 30 days for a melt-derived glass with Class B bioactivity [24].

Step 1 — Rapid exchange of modifier cations such as Na^+ and/or Ca^{+2} with H^+

Step 2 — Formation of SiOH and release of $Si(OH)_4$

Step 3 — Polycondensation of Si-OH + Si-OH to form Si-O-Si

Step 4 — Diffusion of Ca^{2+} and PO_4^{3-} through the surface SiO_2 layer and form a CaO-P_2O_5–rich film (*Incorporation of soluble Ca and P cations from the solution helps the amorphous layer to grow*)

Step 5 — Crystallization of HA layer on the surface of the bioactive glass

Fig. 2. 3. The HA formation steps on silica-based bioactive glasses in vitro [35-39].

2.1.1.1. 45S5 Bioglass®

As mentioned in the introduction, the first bioactive material which was able to bond to living tissues was discovered by Hench [5] in 1969 as a result of tremendous demand for bone repair during the Vietnam War. This glass was named 45S5 based on its composition: 45S represents 45 wt.% SiO_2 which is the main glass former in this composition and 5 is the key molar ratio of Ca/P [1].

There is an eutectic close to the 45S5 composition in the equilibrium phase diagram of SiO_2-CaO-Na_2O making this composition melt at a relatively low temperature so that it can be produced via the conventional melting and quenching method [1, 5]. 45S5 Bioglass® has the highest bioactivity index (I_B= 12.5)[1] among the compositions of region E of the diagram shown in Fig. 2.1 making it the most bioactive composition [5, 40, 41]. In addition to high bioactivity, osteogenic and angiogenesis properties, antibacterial properties has been reported for high specific surface area 45S5 Bioglass® powder due to its high dissolution rate resulting in rapid increase in pH of the surrounding medium which is not tolerable for microbiota. This characteristic can be very

---

1. Hench proposed this *in vivo* bioactivity index (I_B) in order to evaluate and compare the bioactivity of the materials. This index is defined as a 100 divided by t_{50bb} which is the time required for more than 50% of the materials surface bonds to the surrounding tissue(s) [1, 5].

important in tissue repairing, especially in dentistry involving infected root canals [35, 42, 43].

In the network structure of 45S5 Bioglass[®] (Fig. 2.4), Si and P are the network formers which covalently bond together via oxygen atoms and the network modifiers, Na and Ca, are ionically bonded to the structure via broken oxygen bonds. These modifiers bond to the non-bridging oxygen atoms in order to maintain the system electroneutrality [21, 27, 38]. Network modifiers can diminish the physical, chemical and mechanical stability of the glass. They can accelerate the HA formation *in vitro* according to Fig. 2.3 (first step). The high bioactivity of 45S5 Bioglass[®] is attributed to the high content of network modifier in its composition (49 wt.%) making the dissolution process faster due to the easier network break down [23, 24, 35-38, 44]. Some level of bioactivity has been reported for crystalline 45S5 [36, 45] showing the high bioactivity of this composition, although crystallization of bioactive glasses generally diminishes or even neutralizes their bioactivity [46, 47]. Chen et al. [9], reported that after a 14 day *in vitro* test a layer of amorphous HA is formed on the fully crystalline sol-gel-derived 45S5 composition ($Na_2CaSi_2O_6$).

Silicon atoms, which are bonded covalently to the oxygen atoms

Oxygen atoms bonding the network formers together

Phosphorous atoms, which are bonded covalently to the oxygen atoms

Sodium and calcium atoms attaching to the network via ionic bonds
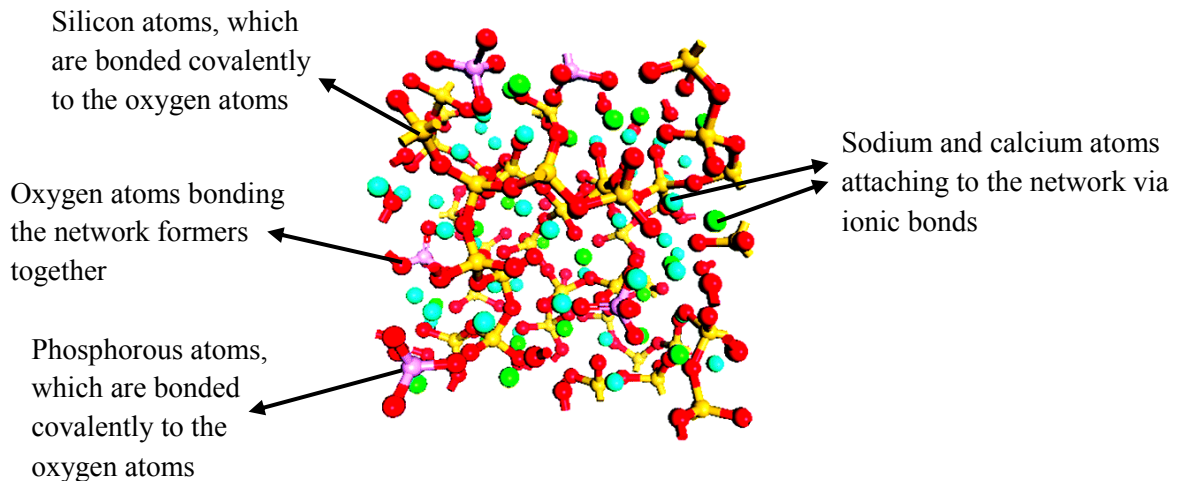
Fig. 2. 4. Network structure of 45S5 Bioglass[®] [21, 48].

There are several studies focusing on the thermal behavior of 45S5 Bioglass[®] in order to determine its phase transformation pattern and critical temperatures: glass

transition temperature (T_g), crystallization temperature (T_p) and melting temperature (T_m). The crystallization temperature of this glass varies with the heating rate as shown in Fig. 2.5. It reaches full crystallinity before its sintering temperature which is at 1000-1100 °C [49-51]. In some cases where mechanical properties play a key role, fully or partially crystalline 45S5 glass-ceramic ($Na_2CaSi_2O_6$ or $Na_2Ca_2Si_3O_9$) is used [36, 45].

These characteristics combined with more than 25 years of successful clinical applications, make this material one of the most useful bioactive compositions to date [1-7]. The future biomaterials are expected to be designed to prevent or delay tissue loss and the presence of 45S5 Bioglass® in the preliminary studies of this field shows its great potential in tissue engineering [52]. The properties, advantages, challenges and potential of 45S5 Bioglass® are explained and discussed further in Chapter 3.

Rate (°C/min)	T_g (°C)	T_p (°C)	T_m (°C)
5	505	650	1174
10	536	664	1172
15	544	674	1168
20	549	676	1165
25	553	686	1160
30	551	690	1155

550°C	Glass transition 1
580°C	Glass-in-glass phase separation
610°C	$Na_2CaSi_2O_6$ Crystallisation
800°C	$Na_2Ca_4(PO4)_2SiO_4$ Crystallisation
850°C	Glass transition 2
1200°C	Melting
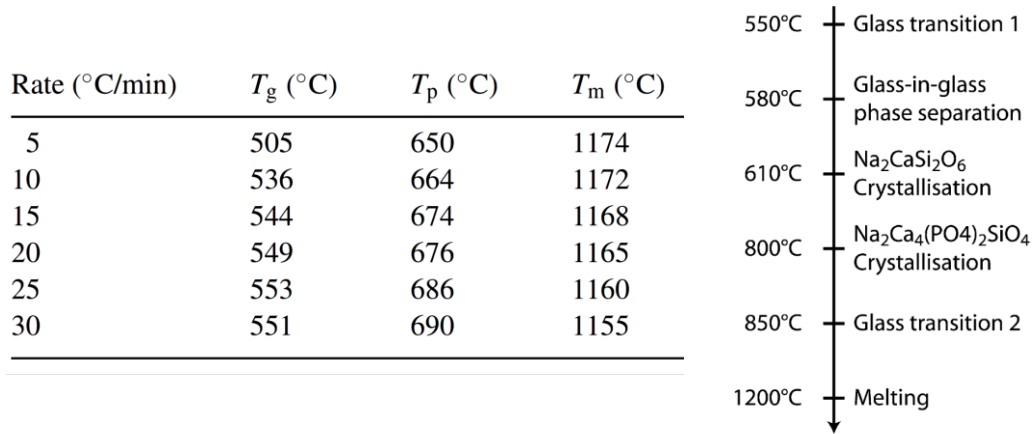
Fig. 2. 5. The critical temperatures and structural transformation of 45S5 Bioglass® in different studies. Left: Ref. [50] and right: Ref. [49] (heating rate of 5°C/min).

2.1.2. Production methods of bioactive glasses

As discussed in the introduction, composite scaffolds containing bioactive nanoparticles are among the most promising bone substitutes. The advantages of submicron bioactive glass particles as the second phase in composite scaffolds are discussed in section 2.4. The techniques for production of submicron bioactive glass particles and fibers with various compositions and properties are explained in this section. The advantages and disadvantages of each method are also briefly discussed.

2.1.2.1. Conventional melting and quenching

The first bioactive glass compositions were produced via melting and quenching since this is the oldest and most well-documented technique for the production of any type of glass. No chemical, which may be potentially hazardous to the living tissues, is involved in this process. Briefly, the glass precursors are weighed and appropriate amounts are mixed together normally by a simple roller mill. Subsequently, the mixture is melted at high temperatures until homogeneity in the molten material is achieved. This is followed by quenching the melt into water and rinsing the product. Melt-derived glasses are normally in the form of a bulk or large dense particles with angular shapes resulting in a low specific surface area and bioactivity [36]. Alternatively, wet mechanical grinding (ball milling) as an additional step is used to obtain finer glass particles. This involves several hours of ball milling (preferably planetary ball milling) in the presence of ethanol, followed by freeze drying and sieving. Freeze drying prevents particle agglomeration to some extent, since there is no liquid phase involved in the drying process [33].

The number of bioactive glass compositions which can be produced by this technique is limited due to very high melting temperatures and/or the absence of bioactivity in the final glass. At high temperatures some of the precursors such as the phosphorous may partially evaporate making it more difficult to obtain the equilibrium composition of the glass. Also, this process can be costly since it requires a high temperature furnace and expensive platinum crucibles. Furthermore, ball milling may introduce contamination to the glass. To avoid this problem yttria-stabilized zirconia (YSZ) balls and containers are used which are also very expensive. Freeze drying and sieving can be also time consuming and expensive [21, 36, 46].

2.1.2.2. Flame Spray Pyrolysis (FSP)

Mixed metal oxide powders (1 – 200 nm) can be synthesized by FSP using inexpensive precursors with a production rate as high as 250 g/h [53]. In this method, precursors which are carried by an appropriate fuel such as iso-octane, are transferred into a flame, melted and then droplets are rapidly cooled down forming the nanoparticles. A filter is placed on top of the flame to gather the nanoparticles. The FSP-derived products are fully amorphous since the droplets are rapidly quenched. One of the advantages of these nanoparticles is their low tendency to agglomerate due to few surface hydroxyl groups [53, 54].

Brunner et al. [54], have successfully synthesized FSP-derived nanoparticles with various compositions from SiO_2-CaO-Na_2O-P_2O_5-B_2O_5 systems including 45S5 Bioglass®. Although FSP uses inexpensive starting materials, its dependency on the specific flame and filtering equipment increase the overall cost and complexity of the technique.

2.1.2.3. Ultrasonic Spray Pyrolysis (USP)

USP is a novel method for producing submicron spherical particles of bioactive glass and glass-ceramics (Fig. 2.6). This method involves spraying an aqueous solution of proper precursors (e.g., salts), into a chamber where the solution is subjected to ultrasonic generators and atomized. The atomized particles are dried, decomposed and melted in a "hot reaction column" which is followed by a rapid cooling [55].

The flow rate of air as the carrier gas, the processing temperature and cooling rate determine the crystalline status of the final product [55]. USP-derived particles also exhibit a low degree of agglomeration (Fig. 2.6) for the same reason as FSP-derived particles. This production method has not been commonly used since it requires specialized equipment making the process costly and complex. Furthermore, USP has a relatively low production rate (on the order of 5 g/h) resulting in a low efficiency especially for industrial scale production.
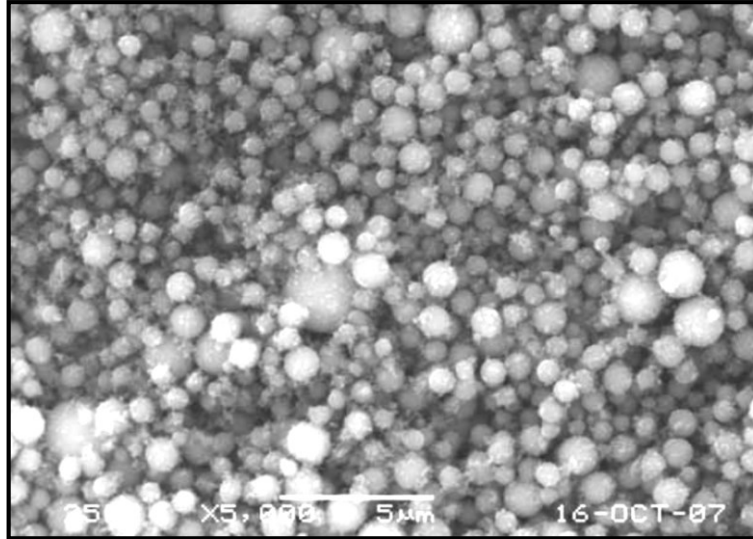
Fig. 2. 6. SEM image of a typical bioactive glass particles produced by USP (at processing temperature of 1400°C) [55].

2.1.2.4. Production of glass nanofibers

Most of the methods designed for producing (bioactive) glass fibers such as gel spinning [56] and melt-extraction technique [57] result in production of fibers with several microns in diameter. Quintero et al. [58], introduced laser spinning which is a novel technique for producing glass nanofibers (average of ~ 200 - 300 nm in diameter). In this method, a ceramic plate (precursor) with suitable composition is locally melted by means of a high power laser beam (Fig. 2.7a). The molten material is simultaneously stretched and cooled down using a high velocity gas jet. The final product is an amorphous bundle of long, thin glass fibers (Fig. 2.7c).

16
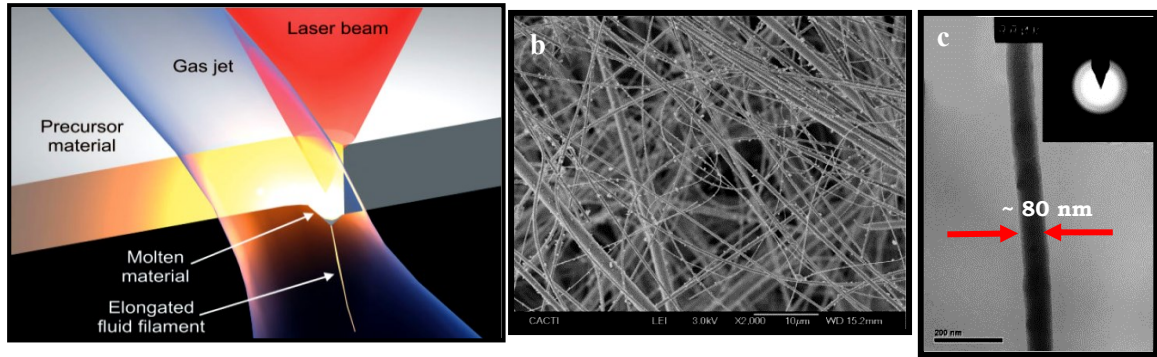
Fig. 2. 7. a) Schematic illustration of the laser spinning processing; b) SEM image of 45S5 Bioglass® fibers produced by laser spinning and c) TEM image of an individual fiber [58].

No chemical and post treatment are involved in laser spinning which are important advantages especially for producing biomaterials. However, the need for specialized equipment (laser and gas jet) and the use of high temperature for melting the precursor which may result in heterogeneity in the final composition, limit the application of laser spinning [58]. Deliormanli [59] has recently synthesized 45S5 glass-ceramic nanofibers (average diameter = 377 ± 81 nm) via a combination of sol-gel and electrospinning. The fibers are semicrystalline after the final calcination (heat treatment).

2.1.2.5. Sol-gel and sol-gel-derived bioactive glasses

Sol-gel is an inexpensive, straightforward method which has been commonly used for producing a wide range of materials including bioactive glasses. Highly pure and homogeneous glasses in various forms of particles, fibers and foams with enhanced bioactivity can be produced at room temperature via sol-gel [17, 21, 60].

In 1991, Li, Clark and Hench [8] discovered that bioactive glasses can also be produced via sol-gel extending the compositional range of bioactive glasses (Fig. 2.8). Although, melt-derived bioactive glasses containing more than 60 wt.% SiO_2 are not bioactive (Fig. 2.1) [38], silica-based sol-gel-derived glasses with SiO_2 content up to 100% have exhibited bioactivity [1, 8, 61]. The rate of hydroxyapatite formation for the sol-gel-derived glasses is much faster compared to those of the melt-derived bioactive

glasses almost regardless of the composition [62-64]. This is due to the fact that bioactivity is dependent not only on composition, but also on the glass surface chemistry and microstructure which depend on their production technique [24]. Sol-gel-derived glasses inherently have high specific area and high concentration of surface OH groups which result in high bioactivity [21, 40]. The former increases the glass dissolution rate due to higher reacting surface and the latter induces the HA formation onto the glass surface via accelerating the first two steps of HA formation *in vitro* (Fig. 2.3). The formation of HA as a function of SiO_2 content in sol-gel-derived glasses of SiO_2–CaO–P_2O_5 system has been reviewed in Ref. [8].
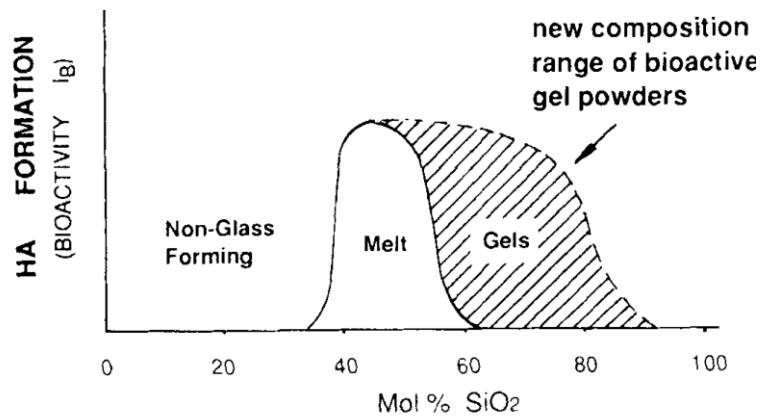
Fig. 2. 8. A comparison between the melt-derived and sol-gel-derived silica-based bioactive glasses in terms of SiO_2 mol% [8]. Note that, it has been shown that sol-gel is able to extend the compositional range of bioactivity up to 100% SiO_2 [1].

The sol-gel process involves the hydrolysis of appropriate precursors (e.g., alkoxides) to form a sol which subsequently converts into a gel as a result of condensation reactions. Finally, the aged gel is dried and stabilized in order to obtain the final glass or glass-ceramic product [3]. Alkoxides are the most common sol-gel precursors. A metal alkoxide is generally presented as $M(OR)_x$ where M represents a metal of valency x and R is an alkyl or aryl group [65]. The hydrolysis and condensation reactions for tetraethylorthosilicate (TEOS; $SiC_8H_{20}O_4$), one of the most common silicon alkoxides, are shown in Eqs. 2.1 to 2.3. The structure of the silica-based glass forms via the condensation reactions (Eqs. 2.2 and 2.3). Eqs. 2.4 and 2.5 show how the glass

modifiers (Na^+ and Ca^{2+}) ionically bond to the structure via broken oxygen bonds as discussed in section 2.1.1.1 [60, 66, 67].

$$Si\,(OC_2H_5)_4 + nH_2O \iff Si\,(OC_2H_5)_{4-n}(OH)_n + nC_2H_5OH \qquad \textit{Hydrolysis} \qquad \text{Eq. 2.1}$$

$$\equiv SiOH + OC_2H_5 - Si \equiv \iff \equiv Si - O - Si \equiv + C_2H_5OH \qquad \textit{Dealcoholation} \qquad \text{Eq. 2.2}$$

$$\equiv SiOH + \equiv SiOH \iff \equiv Si - O - Si \equiv + H_2O \qquad \textit{Dehydration} \qquad \text{Eq. 2.3}$$

$$Na(C_3H_5O_3) + \equiv Si - OH \iff \equiv Si - O^- Na^+ + C_3H_6O_3 \qquad \text{Eq. 2.4}$$

$$Ca(C_3H_5O_3)_2 + 2(\equiv Si - OH) \iff \equiv Si - O^-Ca^{2+}O^- - Si \equiv + 2C_3H_6O_3 \qquad \text{Eq. 2.5}$$

The gelation of a system may take a few minutes up to several days depending on its composition. In some cases a hydrolysis accelerator such as nitric acid and a gelation catalyst such as ammonium hydroxide are added to the system in order to adjust the pH and control the hydrolysis and gelation rates [32, 33, 66]. Under acidic conditions, hydrolysis starts by rapid formation of a protonated oxygen-alkyl group since the concentration of H^+ is high in the solution. This makes the silicon more electrophilic and more prone to be attacked by H_2O (Eq. 2.6). Thus, the hydrolysis reaction (Eq. 2.1) under acidic condition is accelerated as shown in Eq. 2.6 [60].

$$\equiv Si - O - C_2H_5 + H_2O \iff \equiv Si \cdots \overset{\overset{\textstyle H^{\delta+}}{\vdots}}{\underset{\underset{\textstyle H}{OH^{\delta+}}}{O}} - C_2H_5 \iff \equiv Si - O - H + C_2H_5OH \qquad \text{Eq. 2.6}$$

H^+ (Released from the acid)

H^+

Fast hydrolysis under acidic conditions results in higher concentration of SiOH (if n = 4 in Eq. 2.1) monomers in the sol. Polymerization of these monomers gradually occurs via the "cluster-cluster growth" mechanism. The polymer chains are tangled and cross-linked developing a three-dimensional structure known as a polymeric gel. If a base

is used as the hydrolysis catalyst (Eq. 2.7), the polymerization mechanism is mainly "monomer-cluster growth" leading to a colloidal gel [60, 68].

$$\equiv Si-O-C_2H_5 \Leftrightarrow \equiv Si\cdots\overset{\delta-}{O}-C_2H_5 \Leftrightarrow \equiv Si-O-H + C_2H_5O^- \qquad \text{Eq. 2.7}$$

$$\underset{OH^-}{\overset{\nearrow}{\vert}} \qquad \underset{OH^{\delta-}}{\vdots}$$

OH^-
(Released from the base)
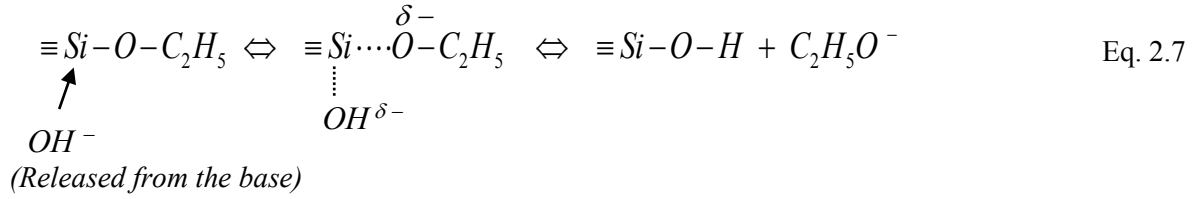
Sol-gel is a very sensitive method and the composition of the precursors, type and concentration of the hydrolysis catalyst (the pH of the system), and the test conditions such as temperature and atmosphere significantly affect the characteristics of the final product [10, 32, 43, 69-72]. Controlling the sol-gel process becomes more difficult, as the number of precursors with different rates of reactivity increases, or inclusions such as Na_2O whose precursors have high rates of hydrolysis, are introduced to the system [36, 73]. This combined with the fact that highly bioactive systems without Na_2O can be easily synthesized by sol-gel, has limited the number of studies on sol-gel-derived 45S5 Bioglass® [9-12]. Furthermore, producing highly bioactive compositions such as 45S5 via sol-gel may significantly increase the bioactivity of the glass, making it too soluble to be useful for tissue repairing. All the challenges and studies on the synthesis of 45S5 bioactive glass and glass-ceramic via sol-gel conducted as a part of this research are discussed in Chapter 3.

To date, the clinical use and the commercial production of 45S5 Bioglass® are mainly limited to the conventional melt-derived type [21] which is normally in the form of dense micron-sized particles. Considering the advantages of sol-gel, more studies are necessary to produce sol-gel-derived 45S5 Bioglass® with desirable properties. This thesis aims to provide some much needed understanding in this regard.

2.2. Biocompatible polymers

Biocompatible polymers have been widely used in medical applications because of their light weight, desirable mechanical properties, and formability. The biocompatible polymers which are used in the bone healing field can be categorized into two major

groups: biodegradable and nonbiodegradable. The nonbiodegradable polymers such as poly(ethylene) (PE) and poly(ethylene terephthalate) (PET) cannot be used for the fabrication of bone scaffolds since these scaffolds are designed to be bioresorbable [2, 7, 74].

Biodegradable polymers are also an excellent alternative for unrecyclable plastics which are extensively used (up to 140 million tons every year), resulting in significant environmental pollution [75]. Biodegradable polymers are currently being used in a wide range of applications from biomedical to packaging industries [75-77]. The degradation of these polymers generally occurs via scission of their main or side chains through thermal, chemical (e.g., hydrolysis and oxidation) or biological routes [75]. The biodegradable, bioresorbable polymers are either synthetic or with natural origins[1] which are both briefly reviewed in this section. A classification of biodegradable polymers which have been studied/used for the bone and/or cartilage healing purposes, is presented in Fig. 2.9 [7, 74].

It has been shown that natural polymers normally exhibit very low toxicity and can improve cell adhesion *in vivo*. Polysaccharides (Fig. 2.9) such as chitosan are the most used natural polymers for biomedical applications [74]. Natural polymers are especially good candidates for the fabrication of hybrid composite scaffolds in which the polymer and the inorganic nanoparticles are strongly (covalently) bonded at the molecular level [3]. Collagen is a particularly good candidate for this purpose. About 20 wt.% of natural bone is comprised of collagen fibrils resulting in a good compatibility between the defective bone and the scaffold [3, 78]. It also has relatively good mechanical properties (tensile strength and toughness) comparable to those of the bone [3]. Hybrid composite scaffolds are reviewed further in section 2.4.

Polyhydroxyalkanoates (PHA) such as Poly-3-hydroxybutyrate (P(3HB) or PHB [5, 27]), copolymers of 3-hydroxybutyrate and 3-hydroxyvalerate (PHBV) and Poly-4-hydroxybutyrate (P4HB) are also classified as natural polymers (Fig. 2.9). They are microbial aliphatic polyester which are degraded via hydrolysis [7, 74]. It has been reported that PHB has piezoelectric properties which may stimulate the defective bone

---

1. In Williams's dictionary [4], biopolymers are defined as: "naturally occurring long-chain molecules e.g. polysaccharides, proteins, DNA" [4].

improving the healing process [79] without inflammatory response over a long *in vivo* period of up to a year [7]. The application of PHA polymers is limited due to the lack of availability since they are produced by microorganisms and the extraction process from bacterial cultures, especially at the industrial scale, can be expensive [7, 74].

Despite all the advantages of natural biodegradable polymers, their application is generally limited because of relatively fast degradation, low mechanical strength and chemical stability, risk of rejection by body and the possibility of disease transmission [7, 74, 79]. The rapid degradation of natural polymers such as collagen can potentially lead to a drop in mechanical properties of the scaffold structure, increasing the likelihood of premature collapse *in vivo*. Modification of some of these polymers in order to improve their characteristics is being investigated [74].

Synthetic bioresorbable polymers (Fig. 2.9) have been of more interest for the fabrication of bone scaffolds due to their controllable and reproducible characteristics. The synthesis process provides the possibility of designing and producing suitable polymers for a certain application. The impurities in the final polymer can be also controlled during the production process. Furthermore, the risk of toxicity, rejection by the immune system and causing infection is normally lower for the highly pure synthetic polymers compared to that of natural polymers [2, 7, 74]. Note that, natural polymers such as PHAs and PURs are still being studied and examined for clinical applications whereas; synthetic biocompatible polymers such as PLA, PLGA and PLC have already been successfully used in many clinical products [74].

Saturated aliphatic polyesters are the most commonly used synthetic polymers for bone regeneration purposes: PLA, PGA and their copolymer PLGA[1] as well as PCL [7, 74]. The hydrolysis of these polymers starts upon exposure to the aqueous environment in the body where the cellular and/or enzymatic pathways promote degradation [78]. These polyesters are degraded via water absorption followed by hydrolysis of the ester bond [7]. Thus, the degradation behavior of these polymers depends on their wettability by water. In general, degradation behavior of these polymers also depends on their composition, chemical structure, molecular weight distribution, degree of crystallinity, the temperature and pH of the medium, the presence of any enzyme or bacteria, type and amount of

---

1. PLA, PGA and their copolymers are classified as poly(α-hydroxyacids) (Fig. 2.9) [7, 74].

second phase (e.g., a bioactive glass particle), specific surface area, porosity and pore morphology [75, 76, 80-86]. Mechanical properties and degradation time of some of these polyesters are presented in Table 2.3 and compared with mechanical properties of the human bone.

Any parameter that increases the hydrophilicity of the polymer results in a higher degradation rate. For example, the incorporation of bioactive glass particles, which are known to be highly hydrophilic, into the polymer increases the overall hydrophilicity causing the polymer to degrade more rapidly. Boccaccini et al. [87], showed that the addition of small amounts (up to 5 wt.%) of melt-derived 45S5 Bioglass® to PDLLA/TiO$_2$ scaffold can significantly increase the *in vitro* degradation rate due to a higher water absorption. Misra et al [79] showed that using bioglass nanoparticles have a more significant impact on the overall degradation rate of the scaffold compared to that of the large micron-sized particles. They showed that the water contact angle on the pure P(3HB) is 87±9°; whereas, this value decreases to 71.8±0.3° and 62±2° as 30 wt.% micron-sized and nano-sized 45S5 Bioglass® particles are respectively added to the polymer [79]. Similar observations are also reported for other scaffold systems such as PLGA/tricalcium phosphate nanoparticles [2] and PLLA/HA nanoparticles [2, 3].

Table 2. 3. Biodegradation time and mechanical properties of some common polyesters [7, 78] . The mechanical properties of the human bone are also presented as Ref. [78].

Polymer [a]	PDLLA	PLLA	PGA	PLGA	PCL	Human bone	
						Cortical	Cancellous
Biodegradation period (months)	12-16	>24	6-12	1-12	>24	-	-
Young's modulus (GPa) [b]	1.9	2.7	7-14 [c]	1.4-2.8	0.4	12-20	0.05-0.5
Tensile strength (MPa) [b]	29	50	340-920 [c]	41.4-55.2	16	50-151	10-20

(a) Note that the mechanical properties and degradation rate of polymers depend on not only their composition, but also molecular weight, crystallinity, and thermal history [78, 80-84].

(b) The Young's modulus and tensile strength of typical biocompatible polymers (resorbable and nonresorbable) are in the range of 0.4 – 2.8 GPa and 16 – 61 MPa, respectively [2].

(c) These values are reported for PGA fibers [7].
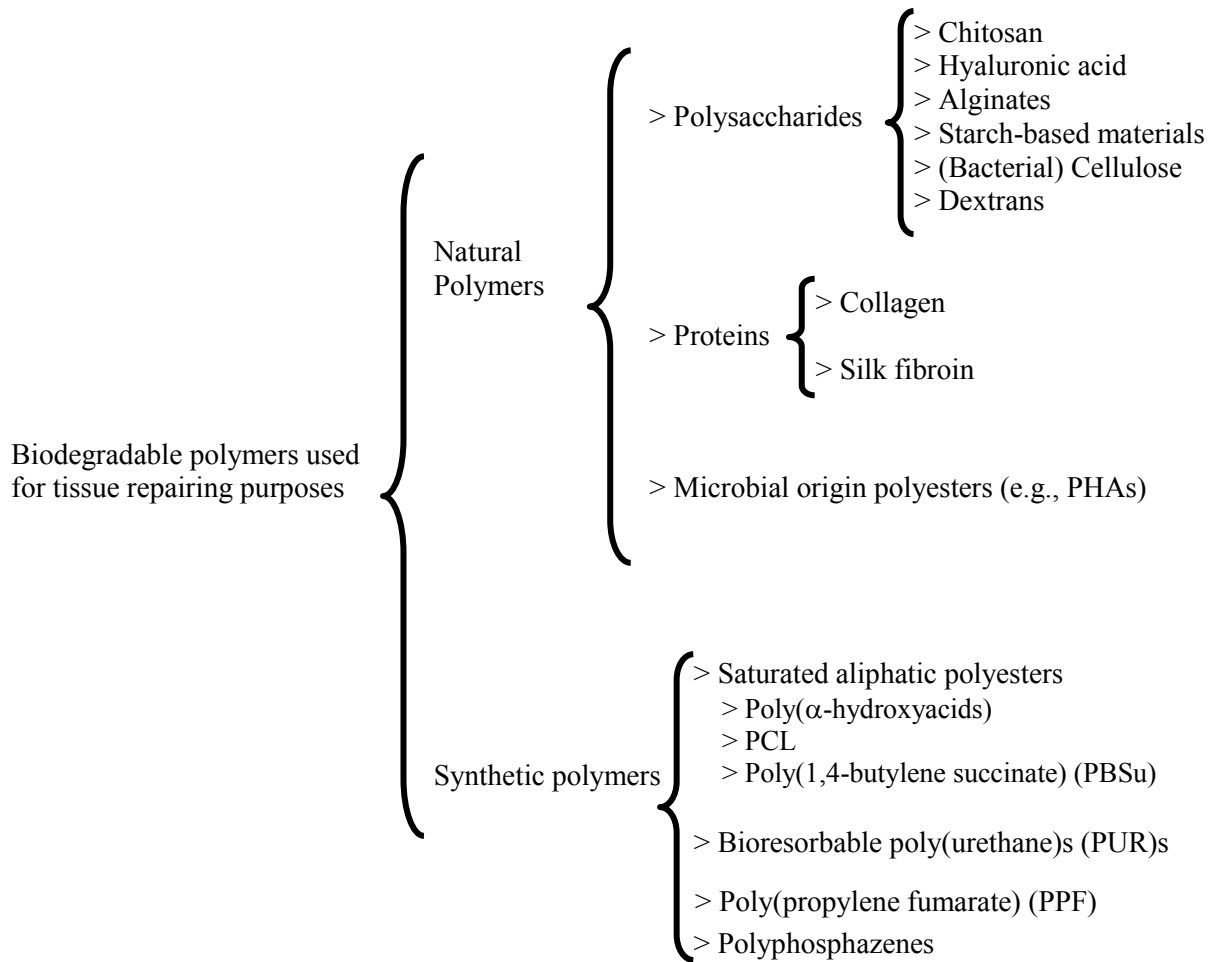
Fig. 2. 9. A typical classification of biodegradable polymers used for bone and cartilage repairing [7, 74].

Degradation rate is inversely correlated to the degree of crystallinity of the polymers [7, 74]. PCL with a high molecular weight may take several years for complete degradation *in vivo* [7]. However, in the natural environment, PCL has shown a more rapid degradation due to more variety of microorganisms which are involved in its degradation process [75, 76]. On the contrary, PGA degrades fast at a rate which is generally higher than that of the PLA family due to the more acidic degradation by-products (mainly glycolide acid), accelerating the degradation process[1]. Furthermore, PGA which has a

---

1. Note that the acidity (pKa) of glycolide acid and lactic acid which are the main degradation by-products of PGA and PLA are 3.83 and 3.86 respectively [175].

more hydrophilic nature results in more water uptake facilitating the hydrolysis. The hydrophobic behavior of PLA is because of its nonpolar methyl groups (Fig. 2.10 and 2.11). PLA has been studied the most among the saturated aliphatic polyesters for the biomedical applications, in particular as the matrix of bone scaffolds. PLA is reviewed further in the next section.

2.2.1. PLA

PLA is a biodegradable, bioresorbable synthetic polymer which is one of the most promising thermoplastics for a wide range of applications. After a high molecular weight PLA was patented by DuPont in 1954, this polymer attracted the attention of researchers [75]. This polymer was initially used only for biomedical applications, but it is also being used for consumer products, thanks to new production techniques making PLA with various molecular weights more available and less expensive [88]. The ease of production makes PLA relatively inexpensive [76], although its price is still high as compared to petroleum-based polymers [75].

PLA has a relatively high melting point (~ 170 °C [76]), high transparency, excellent biocompatibility, good mechanical properties and diverse degradation rates (Table 2.3) which mainly depend on the stereochemistry, polymerization degree, copolymerization and the presence of any additives [75, 81]. PLA can be synthesized via polymerization of lactic acid monomers or ring opening polymerization of lactides (a dimer of lactic acid [89]) [75, 89]. The monomer lactic acid (Fig. 2.10 a and b) are polymerized via polycondensation reactions to create polylactic acid since the hydroxyl and carboxyl groups coexist in the monomers. In this case, the conventional polymerization process can be very long and normally results in PLA with low molecular weights. The second synthesis method, ring opening polymerization of lactide (Fig. 2.10 c, d and e), is more common for producing high molecular weight polylactide[1] [75, 76, 89]. The monomer lactic acid can be produced from the glucose of renewable resources

---

1. Although both terms of **polylactic acid** and **polylactide** represent PLA, they are used typically when PLA is a product of lactic acid polymerization or ring opening polymerization of lactide, respectively [89]. In this thesis, **PLA** and **polylactic acid** have been mostly used.

such as cane sugar and corn via a fermentation process [76, 81, 88]. Note that most of the bacteria involved in this process, produce only the L- form of lactic acid [89].
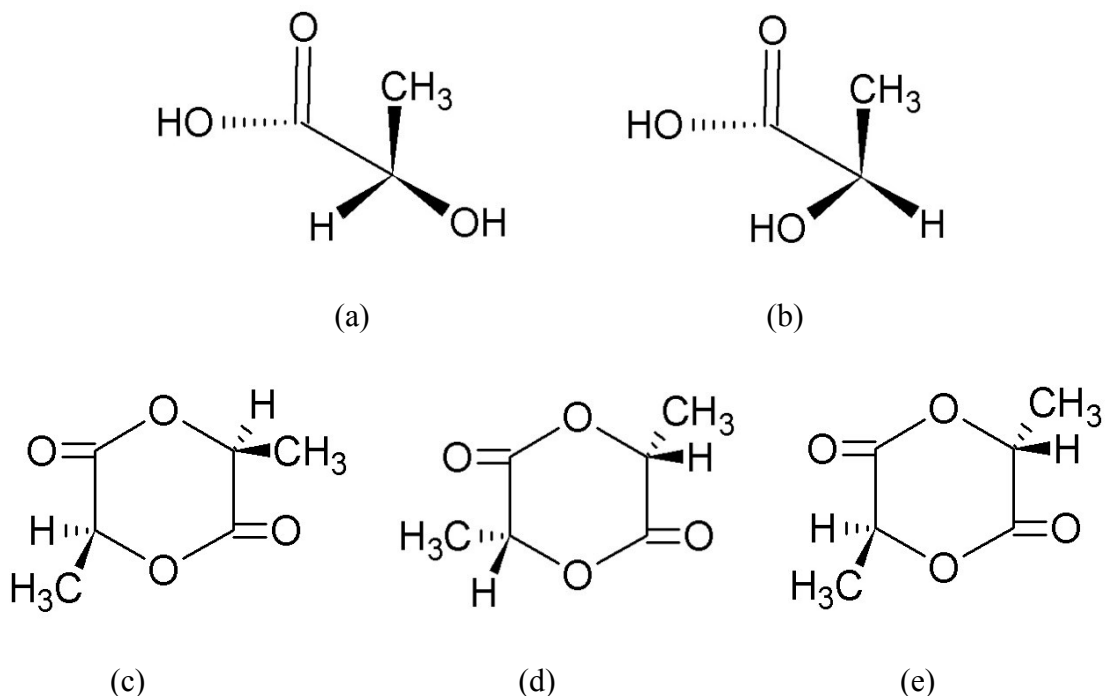
Fig. 2. 10. Stereochemistry of PLA monomers a) L-lactic acid, b) D-lactic acid, c) LL-lactide, d) DD-lactide and e) LD-lactide [89].

Since lactic acid has an asymmetric molecular structure (Fig. 2.10 a and b), PLA exists in three forms: L-PLA (PLLA), D-PLA (PDLA), and D,L-PLA (PDLLA) [74, 76, 80-82]. The D and L isomeric content generally determines whether the polymer is semi-crystalline or amorphous [78]. PLLA and PDLA are semi-crystalline[1] and PDLLA is mainly amorphous, if the D-content is more than 5%, due to the randomly distributed L and D isomeric content. As a result, PLLA generally exhibits better mechanical properties and slower degradation rates compared to those of PDLLA (Table 2.3) [7, 74, 83]. Note that, degree of crystallinity particularly affects the elastic modulus of a polymer [83]. The density of PLA also depends on its crystallinity. For example, the density of a

---

1. For example PLLA has a crystallinity of ~ 37% [75].

crystalline PLLA is ~1.290 g/cm^3 which is higher than that of the amorphous PLLA (1.248 g/cm^3) due to the more packed, ordered chain arrangement [75]. PLA can crystallize into different crystal structures (e.g., α, β and γ) depending on the conditions under which crystallization occurs. The most common and stable crystal structure of PLA is α which forms via crystallization from melt and solutions [88, 89]. Crystallization of PLA and the characteristics of its crystal structures are comprehensively reviewed in Ref. [88]. Crystallization of PLA as the result of phase separation phenomenon in a ternary system of PLA-solvent-nonsolvent is studied in Chapter 5.

(a)

(b)   (c)

Fig. 2. 11. Molecular structure of a) PLA in general, b) PLLA and c) PDLA [74].

PLA is biocompatible since lactic acid, its main hydrolytic degradation by-product, is naturally found in the body as a product of muscle contraction [27, 82]. PLLA is considered to be the more biocompatible stereochemistry of PLA since L-lactic acid is the naturally occurring form of this monomer [75]. PLA has been approved by the U.S. Food and Drug Administration (FDA) for clinical applications. For example, bioresorbable PLA sutures which were initially proposed in 1960 [82] are commonly used. Many studies have also focused on the potential of this polymer in orthopedics [82], drug delivery and tissue engineering [75]. Although PLA is biocompatible, in some cases

sudden release of its acidic degradation by-products results in a local drop in pH which may cause minor adverse biological responses [7, 74]. Poly (lactic-glycolic acid)[1] is the most well-known copolymer of PLA and PGA in the field of tissue engineering and is also approved by FDA and is used in clinical applications [75, 86].

As discussed in section 2.2, the degradation kinetics of PLA depend on its ability to absorb water. PLA is commonly blended with starch to improve its biodegradation although diminishing the mechanical properties especially its toughness [75]. Fukushima et al. [81], showed that the addition of clay to PLA also increases the degradation rate since the clay is hydrophilic, thus enhancing water uptake. They found that the presence of clay also influences microbial degradation of PLA in a composter [81]. Ozkoc et al. [83], found that incorporation of 3% clay nanoparticles into PLA increases the elastic modulus on the order of 33%. Obtaining a PLA with high strength and stiffness as well as an enhanced toughness is a big challenge for industry [75]. Another challenge is the glass transition temperature of PLA (Tg; ~ 60 – 65 °C) which is not high enough to meet the required criteria of some of its potential consumer applications [89]. However, the Tg is not an issue for medical applications since the application temperature, the body temperature, is well below of 65 °C. The glass transition and melting temperature of PLA is compared with some other thermoplastics in Fig. 2.12. Note that the Tg of PLLA increases with increasing molecular weight until it reaches a plateau for molecular weights of ~ 20 – 40 kg/mol [89].

---

1. Lactic acid / glycolic acid = 2/23 [75]. This ratio can vary to control the degradation rate and mechanical properties of the final copolymer.
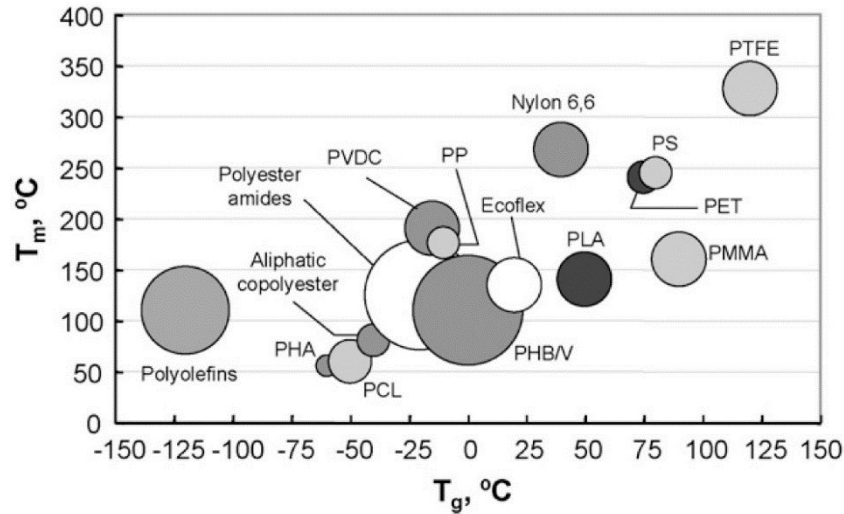
Fig. 2. 12. Glass transition and melting temperature of some thermoplastics, including PLA [88].

PLA has been successful in replacing nonbiodegradable polymers in some applications such as packing materials and tableware [75, 77, 88]. In general, chemical and/or biological (i.e., enzymatic and/or microbial) mechanisms are involved in the degradation process of PLA. Enzymes produced by cells may act as a hydrolysis catalyst via absorption onto the surface of the polymer and aiding the de-esterification process. The degradation of PLA *in vivo* starts with hydrolysis, producing soluble oligomers which are subsequently metabolized by cells [76]. During degradation, lactic acid enters the tricarboxylic acid cycle whereby it is excreted easily by the body in the forms of H_2O and CO_2 [82].

PLA is also degraded under controlled composting conditions[1] which favor a microbial population [75, 76]. It has been shown that this process can take from a few weeks to 3 months depending on the environment where the degradation is occurring. In such environment, PLA beaks down to low molecular weight chains via hydrolysis in which pH, temperature, moisture and the role of microorganisms are important. The microorganisms eventually convert the low molecular weight oligomers to mainly CO_2 and H_2O as well as humus. Low molecular weight PLA with and low crystallinity is more

1. Commercial compost with various compositions can be purchased from some suppliers such as Societa` Metropolitana Acque Torino (SMAT). The degradation test on the samples in such environment is usually performed under humidity [81].

easily degraded in such conditions by microorganisms such as the *Bacillus licheniformis*[1] and *Pseudonocardiaceae* family [75, 76, 81]. Furthermore, crystalline segments diminish the water permeability of the polymer, resulting in a slower degradation for crystalline PLA compared to that of amorphous PLA [76, 80, 83, 84].

Thermo-mechanical history and molecular weight have an impact on the crystallinity of PLA and subsequently its degradation behavior. The tendency of PLA to crystallize is inversely related to its molecular weight such that almost regardless of the cooling rate from the melt state, PLA with very high molecular weight undergoes little or no crystallization (from melt). However, during annealing after quenching, the crystallinity increases for all molecular weights with the higher the molecular weight the lower the crystallinity [74, 80].

PLA can be also decomposed to lactic acid by heating; in a humid environment. It also undergoes pyrolysis by heating in the range of 180 °C – 350 °C over 30 minutes [75, 88]. A pre-drying step (~ 40 – 100 °C)[2] is important to control thermal degradation of PLA during the fabrication process. Several techniques such as "stretch blow molding" and "casting and extrusion" which are commonly used for producing PLA products such as bottles and sheets, are reviewed in Ref. [88]. The common foaming methods for the fabrication of highly porous PLA-based scaffolds normally do not involve such high temperatures (section 2.4.1 and Chapters 5 and 6) [7, 88].

Thick/large three-dimensional PLA pieces may undergo heterogeneous degradation behavior: initially the degradation is faster on the surface due to higher water content and then, over the time, it becomes faster inside the sample due to the autocatalysis. Autocatalysis is a result of higher concentration of acidic by-products of PLA degradation inside of the material acting as hydrolysis catalysts. Once chain scission begins, the molecular weight and the pH of the surrounding medium drop, which subsequently accelerates the degradation process. Note that on the surface of the monolith, the carboxylic end groups may be neutralized more rapidly by the surrounding fluid resulting in a slower degradation on the surface of the monolith at this point [7, 74,

---

1. Fukushima et al. [81], claimed that among the bacterium which are mostly present in commercial composts, *Bacillus licheniformis* plays a key role for the PLA degradation.

2. The drying time changes with the drying temperature and crystallinity of the PLA [88].

82, 90]. Although highly porous and fully interconnected scaffolds are partially able to allow for the dilution of the acidic degradation by-products, autocatalysis can still lead to premature collapse and failure of such scaffolds. The incorporation of bioactive glasses with alkali dissolution by-products can lower the effect of autocatalysis [7].

The PLA family offers a wide range of properties for scaffold applications based on their range of crystallinity, mechanical properties and degradation rates. Thus, one can select a suitable PLA with appropriate characteristics for specific applications. In this regard, the foaming process for and characteristics and applications of PLA are reviewed and discussed further in Chapters 4, 5 and 6.

2.3. Organic-inorganic interface

One of the applications for the incorporation of an inorganic phase (e.g., a bioactive glass) into a polymeric matrix is to fabricate a composite bone scaffold. The common biocompatible, bioresorbable polymers are not bioactive, and their mechanical properties are not normally sufficient for supporting the defective bone [7, 13]. Furthermore, high concentration acidic degradation by-products of these polymers (e.g., PLA), may cause some adverse biological responses *in vivo* [2, 74]. The addition of bioactive glasses to the polymeric scaffolds not only induces bioactivity to the structure but also partly buffers the acidic by-products due to the release of alkali ions. Also, such a nanocomposite scaffold can more closely mimic the natural bone, since the bone itself is a nanocomposite comprising a polymeric matrix (mostly collagen) and nano-sized HA crystals [3, 78]. The incorporation of bioactive phases with better compressive strength and Young's modulus compared to those of the common biodegradable polymers, may reinforce the structure and increase the overall mechanical properties. However, in some cases this incorporation has worsened the mechanical properties of the final scaffold. This is often due to the incompatibility between the glass and polymer phases since they are hydrophilic and hydrophobic, respectively [3, 7]. Surface OH groups make the glass particles hydrophilic whereas, the nonpolar species in polymers such as methyl groups in PLA (section 2.3), are responsible for their hydrophobic nature. Rezwan et al. [7], claim that the "the lack of interfacial bonding strength" due to this incompatibility is the main

reason for the overall poor mechanical properties of composite scaffolds which are far worse than those of the pure polymeric scaffolds (Fig. 2.13) [7]. This incompatibility makes it impossible to properly disperse inorganic particles throughout the polymeric matrix. Agglomeration of inorganic particles in organic solutions can also diminish the mechanical properties of the composite scaffold. In particular, in the case of a highly porous scaffold where the skeleton is very thin, large micron-sized agglomerates may act as stress concentrators increasing the likelihood of the entire structure collapsing [16, 91]. It has been also reported that, decreasing the particle size of the second phase, increases the modulus of the composite [16, 79]. Agglomeration can also lower the overall bioactivity of the scaffold due to the inhomogeneous distribution of bioactive particles throughout the matrix [3, 16, 91].
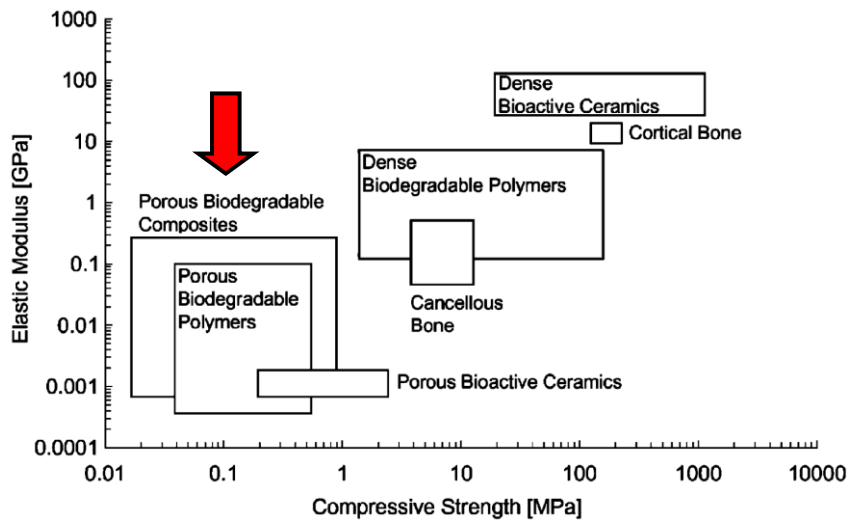
Fig. 2. 13. The elastic modulus and compressive strength of the materials used for bone regeneration purposes. The incorporation of inorganic phases (glasses or ceramics) with polymers to develop "porous biodegradable composites" results in a very small increase in their mechanical properties [7].

Surface modification of the inorganic phase can help to create a better composite scaffold in which the two phases form a compatible interface and the inorganic particles are well-dispersed throughout the polymeric matrix. In this manner, good mechanical properties and bioactivity are also ensured [3].

The methods proposed for surface modification of bioactive phases (mostly bioactive glasses) can be classified into physical, chemical and biological routes with their own advantages, disadvantages and applications [15, 92-96]. For example, surface treatments involving acids (e.g., HCl and HF) or bases (e.g., NH4OH) [93, 94] attacking the surface of a glass, can change the surface texture and morphology of the particles, and consequently change their interaction with the physiological fluids and cells [94]. Li et al. [94], claimed that the surface roughness as a result of such chemical treatment at different pHs can enhance cell adhesion and interfacial bonding. Among all surface modification methods, the chemical approach including surface deposition of a silane coupling agent is the most effective. There is another similar method, in which the grafted molecules on the surface of the glass particles form in situ via polymerization of monomers [15, 97]. In the next section, the most common surface modification approach for silica-based glasses via deposition of silane coupling agents is reviewed.

2.3.1. Surface modification using silane coupling agents

The molecular structure of silane coupling agents enables them to form covalent bonds to both glasses and polymers acting as cross-linkers. The molecular structure of a typical silane (Fig. 2.14) consists of a polar end compatible with the glass (typically hydrolysable groups) and a nonpolar end compatible with polymers which includes organofunctional groups. These two ends are normally connected by alkyl groups (Fig. 2.14). The length of this alkyl bridge (n) affects the reactivity and physical properties of the silane [15, 33, 91]. Table 2.4 summarizes some silane agents which are commonly used for coupling polymers and glasses. Silane coupling agents with a methacryl organofunctional group such as 3-methacryloxypropyltriethoxysilane (MPTES) are known to be highly reactive with unsaturated polyesters such as PPF (Fig. 2.9) [92].

$$R-(CH_2)_n-Si-X_3$$

	X	e.g., acyloxy, alkoxy, amine or halogen
	R	e.g., amino, methacryl or glycidoxy
	n	0, 1, 2 …

Linker

Hydrolysable group

Organofunctional group
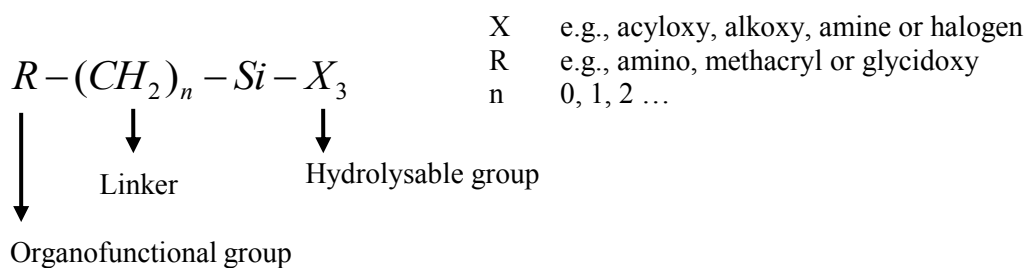
Fig. 2. 14. The general chemical formula of a silane coupling agent [98].

Table 2. 4. Some silane coupling agents commonly used for the surface modification of glasses [15, 91, 98]

Chemical name	Chemical formula according to Fig. 2.14		
	R	n	X
methacryloxymethyltriethoxysilane	$CH_2=C(CH_3)COO$	1	OC_2H_5
3-methacryloxypropyltrimethoxysilane	$CH_2=C(CH_3)COO$	3	OCH_3
3-methacryloxypropyltriethoxysilane (MPTES)	$CH_2=C(CH_3)COO$	3	OC_2H_5
vinyltrimethoxysilane	$CH_2=CH$	0	OCH_3
3-aminopropyltriethoxysilane (APTS)	H_2N	3	OC_2H_5
3-glycidoxypropyltrimethoxysilane	$CH_2(O)CHCH_2O$	3	OCH_3
methyltriethoxysilane	CH_3	0	OC_2H_5
(3-acryloxypropyl)trimethoxysilane	$CH_2=CHCOO$	3	OCH_3
dimethyldichlorosilane	$(CH_3)_2$	0	Cl

The silane molecules bond to the surface of the inorganic material via their surface OH groups which are very reactive sites. This reaction can occur via an anhydrous or a hydrolytic route. In anhydrous deposition (Fig. 2.15), the silane molecule directly bonds to hydroxyl groups on the glass surface in the absence of water and catalyst. This procedure is time consuming and needs high temperatures. Of the alkoxysilanes, only methoxysilanes can be deposited without catalysis via this anhydrous route [92, 98].
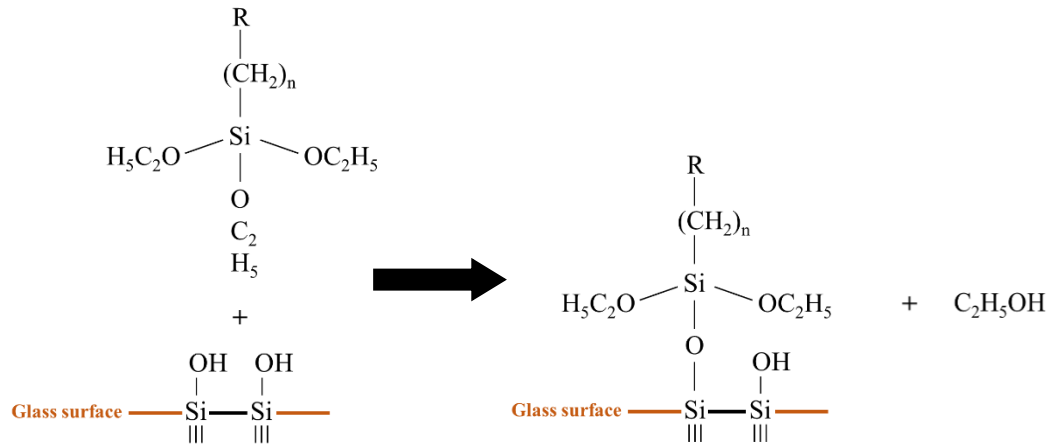
Fig. 2. 15. Anhydrous depositions of a triethoxysilane onto the surface of a silica-based glass [98]. Note that the hydrolytic deposition is schematically presented in Chapter 6 (Fig. 6.1).

In hydrolytic deposition the silane molecules undergo hydrolysis, attach to the surface hydroxyl groups via secondary bonds and then the covalent bonds form during subsequent refluxing at ~70 – 100 °C and/or drying[1] [92, 98]. The hydrolytic route normally includes a catalyst (an acid or a base) to control the rates of hydrolysis and condensation reactions. This matter is discussed in the next section.

2.3.1.1. Parameters affecting the surface modification process

The water content, amount of added silane and the pH as well as the nature, morphology, specific surface area and surface chemistry of the glass [16], are the most important parameters affecting a surface modification process [15, 16, 91-93, 97-100].

The water content in a surface modification process has a significant impact on the hydrolysis and self-polymerization rate of the silane molecules [98]. Silane molecules easily hydrolyze; and in many cases, water molecules in the atmosphere or minor a water content in the starting material(s) are enough to initiate the hydrolysis reaction. Excess

---

1. The hydrolytic deposition route is explained further in Chapter 6.

water in the system can result in undesirable self-polymerization[1] and/or multi-layer deposition of the silane onto the surface of the glass as a result of rapid hydrolysis [33, 98, 101, 102]. To minimize self-polymerization and multi-layer deposition, the amount of water in the system must be carefully controlled.

The theoretical quantity of a silane coupling agent (W in μg) required to yield a surface coverage density of ρ (μmol/m^2) on silica-based glass particles (w_g in grams) with a specific surface area of S_g (m^2/g) is given by Eq. 2.8.

$$W = w_g S_g M_w \rho$$

Eq. 2.8

where M_w is the molecular weight of the silane (g/mol). The surface coverage density is also presented often as molecules/nm^2 which is equal to 0.6ρ. This equation is valid if we assume that the entire surface of the glass particles is covered by hydroxyl groups which are all accessible to the silane molecules. Also, all the silane molecules must only react with these hydroxyl groups (i.e., no unreacted silane[2] or self-polymerization). However, in practice, much more silane (~ 10 – 100 times) than this calculated value is required to obtain the desirable surface coverage since these assumptions are not met in reality [15, 16, 91-93, 97-100].

It has been shown that adding more silane to a surface modification process increases the density of the surface coverage, until it reaches a plateau as the surface is completely saturated. At this stage, adding more silane does not increase the coverage density and they mostly self-polymerized [97, 99]. Pryce et al. [99], investigated the final amount of modifier grafted onto the surface of a bioactive glass as a function of initial concentration of the modifier added to the process (Fig. 2.16).

---

1. The silane molecules can be self-condensed into three different forms (dimer, linear siloxane and three-dimensional polysiloxane) as presented and explained in reference [92].

2. Unreacted silane also includes those molecules which are weakly attached to the surface of the glass particles via physisorption. A throughout rinsing step is required at the end of the surface modification process to remove the physisorbed molecules [98]. This issue is explained further in Chapter 6.
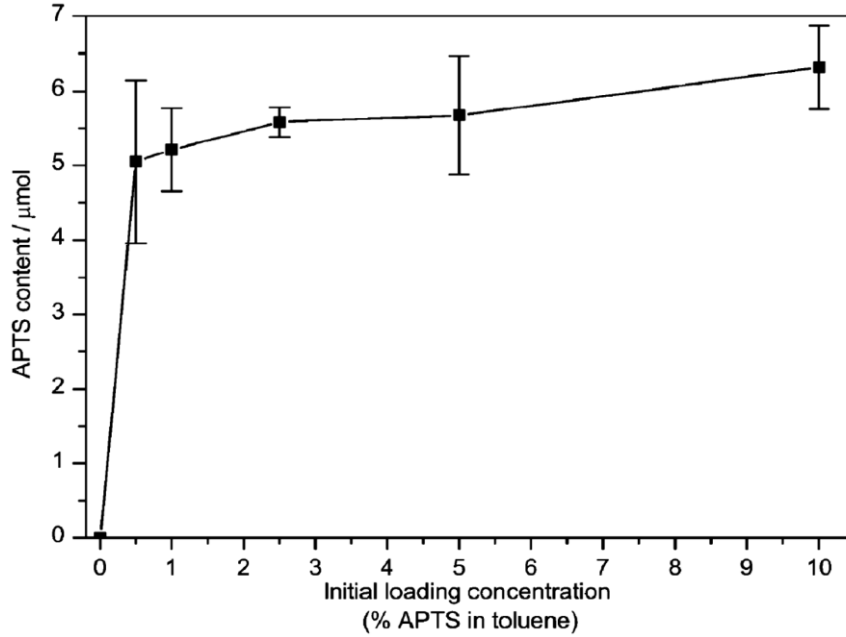
Fig. 2. 16. Modifier content grafted onto the surface of sol-gel-derived 58S[1] glass particles versus the amount of modifier added initially to the reaction mixture [99]. According to Table 2.4, APTS stands for 3-aminopropyltriethoxysilane.

The presence of an acid or a base controls the rates of the hydrolysis and condensation reactions (Eqs. 2.6 and 2.7). In a report prepared by Gelest[2] [98], using acetic acid as the catalyst to maintain the pH in the range of 4.5 to 5.5 is recommended. They indicate that this pH range catalyzes both hydrolysis and condensation reactions. However, employing a base such as ammonium hydroxide (NH_4OH) to adjust the pH (8-10), is also common [15, 16, 97]. In addition to catalyzing the hydrolysis reaction (Eq. 2.7), basic conditions also allow for effective catalyzation of the condensation reaction resulting in an efficient deposition.

The surface chemistry of a glass is affected by its production method (section 2.1.2). For example, the high concentration of OH groups on the surface of sol-gel-derived glasses are attributed to the nature of sol-gel which involves hydrolysis and condensation reactions through which hydroxyl groups are massively formed (Eqs. 2.1 –

1. Composition of 58S bioactive glass (mol%): 60% SiO_2, 36mol% CaO and 4 mol% P_2O_5 [99].

2. Gelest, Inc. is one of the largest suppliers of silane coupling agents.

2.3). The concentration of these surface hydroxyl groups decreases by increasing the stabilization temperature of the sol-gel process (Fig. 2.17) [3, 16].
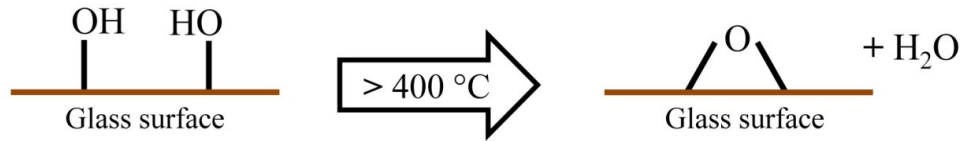
Fig. 2. 17. The effect of temperature on the concentration of surface hydroxyl groups [100].

The high density of surface hydroxyl groups combined with the high specific surface area makes sol-gel-derived bioactive glasses potentially more susceptible to surface modification with coupling agents since there are more active hydroxyl sites on their surface [3]. Gao et al. [16], showed experimentally that mesoporous sol-gel-derived 58S bioactive glass is surface modified more efficiently compared to melt-derived 45S5 Bioglass[®]. They showed that PDLLA films containing surface modified sol-gel-derived glass particles exhibit higher tensile strength compared to that of not only pure PDLLA film (~ 60% higher) but also the PDLLA film containing the same glass particles but unmodified (~ 80% higher) (Fig. 2.18). In the case of melt-derived 45S5 Bioglass[®], the improvement in tensile strength of the PDLLA film with surface modified particles is negligible and still lower than that of the pure PDLLA film [16].
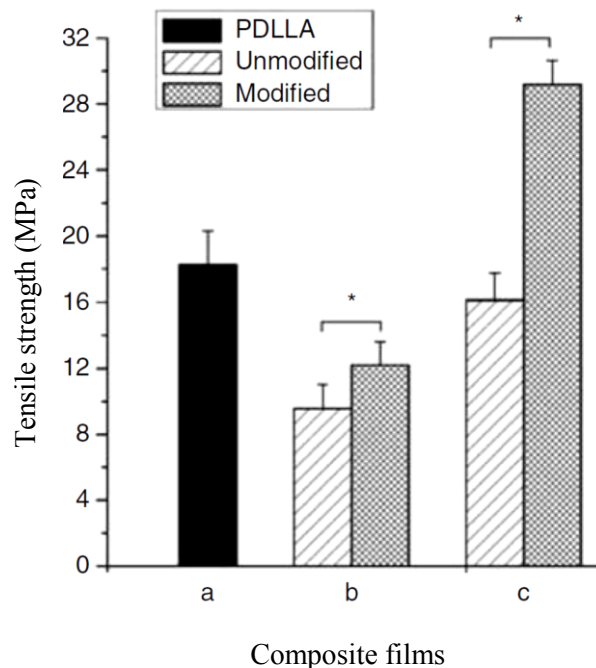
Fig. 2. 18. Tensile strength of PDLLA-based films: a) pure polymer, b) containing 15 wt.% melt-derived 45S5 Bioglass® c) containing 15 wt.% sol-gel-derived 58S bioactive glass [16]. Note that the mean particle size of the as-received melt-derived and sol-gel-derived glasses (before surface modification) is reported 20 μm and 1 μm) [16].

2.3.1.2. Advantages of surface modification

After successful surface modification, the glass particles are expected to be more hydrophobic resulting in a more stable suspension in a polymer solution with less agglomeration (Fig. 2.19b) [15, 16, 91]. According to colloid stability theory, inorganic particles are prone to agglomerate, especially in organic solutions [16]. Glass particles hydrogen bond to each other via their surface hydroxyl groups forming the agglomerates (Fig. 2.19a) [91]. Mechanical stirring and ultrasonication have only short-term effects on breaking the agglomerates; whereas, surface modification of particles provides a much longer-term effect (Fig. 2.19b) [15, 16].

A stable suspension of well-dispersed surface modified glass particles in the polymer solution provides for a composite scaffold with well-dispersed particles and a strong interfacial bond. As mentioned before, this can ensure good mechanical properties

and bioactivity of the final scaffold. It has also been shown that well-dispersed bioactive particles lead to the formation of a homogeneous distribution of hydroxyapatite in vitro [15, 16, 79, 97]. Misra et al. [79], showed that the exposure of bioactive nanoparticles on the surface of the scaffold is considerably higher than that of larger micron-sized particles. This leads to many advantages since the bioactive phase is not completely embedded in the polymer matrix and is directly in contact with the physiological fluid and cells (higher overall bioactivity).

The surface modification process for a sol-gel-derived 45S5 Bioglass® using MPTES is presented and discussed in Chapter 6. The effect of this modification process on the agglomeration of particles and the incorporation of surface modified particles in PLA to develop porous composite monoliths, are also investigated in that chapter.

(a)

(b)
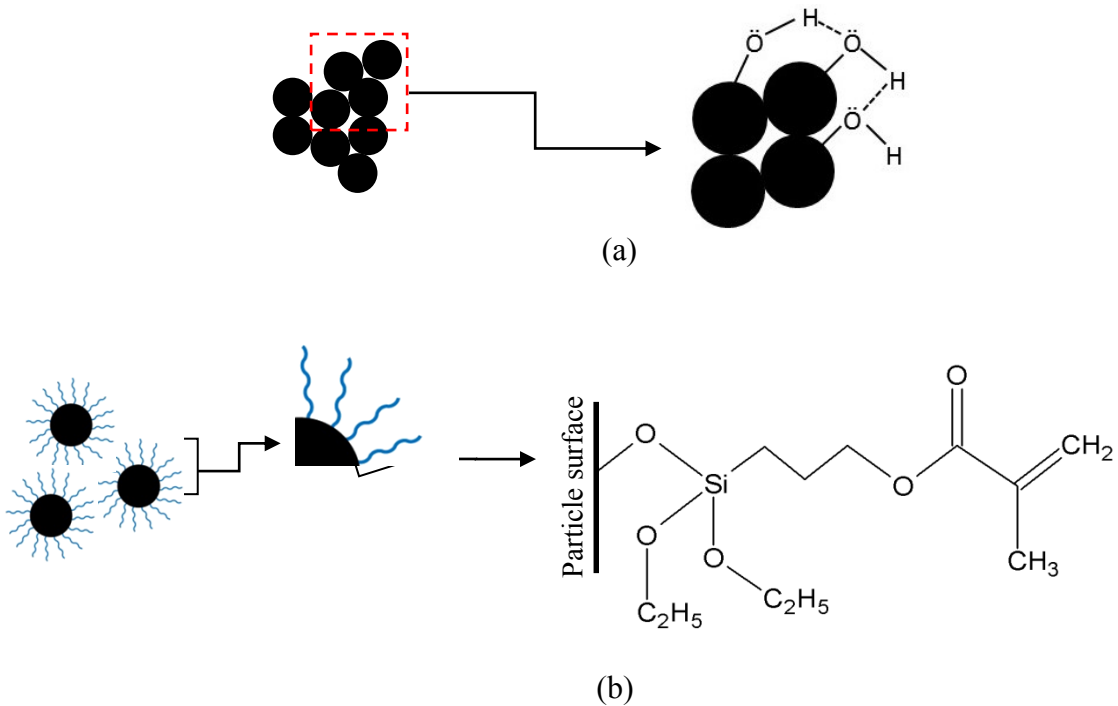
Fig. 2. 19. a) Schematic of hydrogen bonding between glass particles resulting in agglomeration; adapted from Ref. [15]; b) Schematic of grafted silane molecules preventing agglomeration. The silane presented in this figure is grafted MPTES. This figure is reproduced in Chapter 6 (Fig. 6.4).

2.4. The ideal scaffold and remaining challenges

Although scaffolds made of bioactive glasses have high levels of bioactivity and relatively good compressive strength [7]; they cannot be used in load-bearing sites of the skeleton, because of poor tensile strength and toughness. On the other hand, biodegradable polymers are not bioactive and their acidic degradation by-products may be inflammatory [2, 3]. **Biodegradable polymer/bioactive glass** composites have the potential to overcome these problems: an ideal bone scaffold is a highly porous monolith containing a bioresorbable polymeric matrix and well-dispersed bioactive glass nanoparticles[1].

Characteristics of a scaffold including materials type, mechanical properties and morphology depend on its application [87]. The important characteristics of an ideal scaffold for bone regeneration purposes are briefly explained in the following (a – e):

a) It must be biocompatible, bioresorbable and bioactive (Class A) so that it improves bone ingrowth [3]. The scaffold must bond to the defective bone without forming scar tissue [2]. MG-63 cells are a typical cell culture used for studying the biocompatibility and scaffold behavior *in vitro* [79]. The bioactivity level of a scaffold depends on the characteristics, compositions and weight ratio of its constituents and their interaction as well as the porous morphology of the framework [5].

b) It must act as a 3D, interconnected, highly porous (80-90%) framework which includes both mesopores and macropores (> 100 μm) [3, 74]. The high porosity of the structure provides enough space for new tissue to penetrate and the degradation by-products to disperse [74, 87]. The mesopores promote cell adhesion onto the scaffold and the macropores allow cellular ingrowth and vascularisation. It is believed that mesopores significantly affect cell responses (particularly osteoblasts) and the degradation rate of the scaffold [1, 2, 3, 7]. However, the characteristics of an ideal morphology for bone scaffolds are not yet fully understood [3]. Pore size, morphology and interconnectivity strongly depend on the fabrication process of the scaffold (section 2.4.1) [7].

---

1. All the advantages of using submicron (preferably nanosized < 100 nm) bioactive particles in a polymer-based scaffold are explained in section 2.3.

c) It must exhibit mechanical properties comparable to those of the defective bone (Table 2.3 and section 2.3). The scaffold should not collapse during handling, surgical operation and ordinary body activities when it has been implanted. The mechanical support of the scaffold must be maintained during the entire healing process [3, 7, 74, 78].

d) It must exhibit a relatively linear degradation rate[1] similar to the rate of defective bone ingrowth. The rate of bone regeneration itself depends on sex, age, and the location of defective bone in the skeleton. Thus, there is not just one desirable degradation rate for scaffolds [3]. Composite scaffolds are ideally designed to degrade as one material, without any mismatch between the degradation of the components. This can be achieved by developing a hybrid nanocomposite scaffold wherein the nanoscale interactions between both organic and inorganic phases make them come into contact simultaneously with the cells and physiological fluids [1, 3, 7]. In hybrid scaffolds the organic and inorganic phases are covalently bonded at molecular scales and the inorganic phase is normally formed in situ via sol-gel[2] [3, 15]. In order to incorporate the polymer into the sol-gel process, the polymer must be soluble in aqueous media; for example natural polymers (section 2.2). Some hybrid nanocomposite scaffolds consisting of bioactive glass particles and poly(vinyl alcohol)(PVA) or collagen matrix have been developed; but no desirable covalent bond is seen between the phases in those systems [3]. Hybrid nanocomposite scaffolds are still under investigation [3, 15, 21, 103].

e) The fabrication method of the scaffold must be flexible in terms of the shape of the final product in order to match the geometry of the defective bone [3].

The ideal polymer-based scaffold has not been yet developed; mainly due to insufficient mechanical properties, undesirable degradation behavior and morphology [1, 2, 3, 7]. The complexity of the hierarchical structure of bone makes the creation of a

---

1. Degradation rate can be defined as the rate of hydrolysis, dissolution and weight loss (%) of the polymeric matrix, bioactive second phase and the composite scaffold, respectively [3, 7, 37].

2. Composite scaffolds in which the organic and inorganic phases are bonded weakly via secondary bonds are considered as class 1 hybrid composites [15]. Class 2 hybrid composites are explained in this section and are usually referred to as hybrid composites.

similar structure very difficult. Furthermore, a better understanding of the biological systems and their interaction with biomaterials is still needed to design an ideal scaffold for bone healing [1-7, 17].

2.4.1. Scaffold production methods

Scaffold fabrication methods are basically polymer foaming techniques which result in highly porous monoliths with the characteristics mentioned in the previous section. In general, polymeric foams can be produced from thermoplastics or thermosets; however, thermosets are not normally used for scaffold production since they are not biodegradable and biocompatible[1] [104]. Scaffold fabrication methods include conventional techniques such as solvent casting and particle leaching [7], template [103, 105] and gas [105, 106] based techniques, and more advanced methods such as "supercritical CO_2 assisted" [107] processing and 3D printing [105, 108]. The sol-gel process is one of the most promising methods which is able to produce not only bioactive glass scaffolds but also hybrid composite scaffolds as explained in the previous section [3, 21]. A review of scaffold fabrication methods is presented by Dhandayuthapani et al. [14] and their common applications in tissue engineering. The advantages and disadvantages of these methods are also summarized in Ref. [7], [109] and [14].

Solution phase separation methods are template-free techniques used for fabrication of porous structures such as scaffolds. These techniques are reviewed further in the following sections since one such method is used in this work (Chapters 4, 5 and 6) is classified in this group.

2.4.1.1. Solution phase separation methods

Solution phase separation techniques have been studied for more than 50 years for the production of porous polymer structures [110]. The theory behind these phase inversion techniques are explained in Chapter 4 using Flory-Huggins equations. The addition of a nonsolvent to or changing the temperature of a polymer solution changes the

---

1. Most cross-linkers commonly used for curing thermosets are toxic to living cells [104].

Gibbs free energy of the system making it unstable, and resulting in a phase separation (solid-liquid or liquid-liquid) [111]. Phase separation occurs if the two-phase system including polymer-rich and polymer-lean, has a lower free energy than that of the initial system. The polymer-rich phase generally forms a 3D structure and the polymer-lean phase flows through it. After drying, the phase separated system is transformed into a foam in which the polymer-rich and polymer-lean phases have formed the skeleton and the pores, respectively. The methods in which the phase separation is induced by changing the temperature or adding a nonsolvent are known as thermally-induced phase separation (TIPS) and nonsolvent induced phase separation (NIPS), respectively [7, 109]. There are two main nonsolvent-based methods used for producing porous polymer structures: immersion precipitation and NIPS which are normally used to fabricate polymer membranes and foams, respectively.

Polymer-solvent-nonsolvent ternary phase diagrams (Fig. 2.20) are used in order to depict the phase separation phenomena and mechanisms at equilibrium for systems with various compositions. These phase diagrams can be developed experimentally (explained in Chapter 4) or theoretically using the Flory–Huggins approach [112-116]. The binodal curve separates the single phase and two-phase regions and the spinodal curve represents the systems in which any compositional fluctuation leads to instability and phase separation via spinodal decomposition. The compositions which lie in the area between the binodal and spinodal curves exhibit metastability and their phase separation is mainly driven by nucleation and growth. The spinodal curve separates the metastable and unstable regions [108,113]. The porous structures produced via spinodal decomposition are known to have interconnected, fine pores (~1 − 10 μm in diameter) [117]. In general, depending on the system and conditions, (liquid-liquid or solid-liquid) phase separation, crystallization or vitrification may occur. For example **gelation** in high polymer concentration systems is normally induced by **crystallization** during **phase separation** [111, 118].
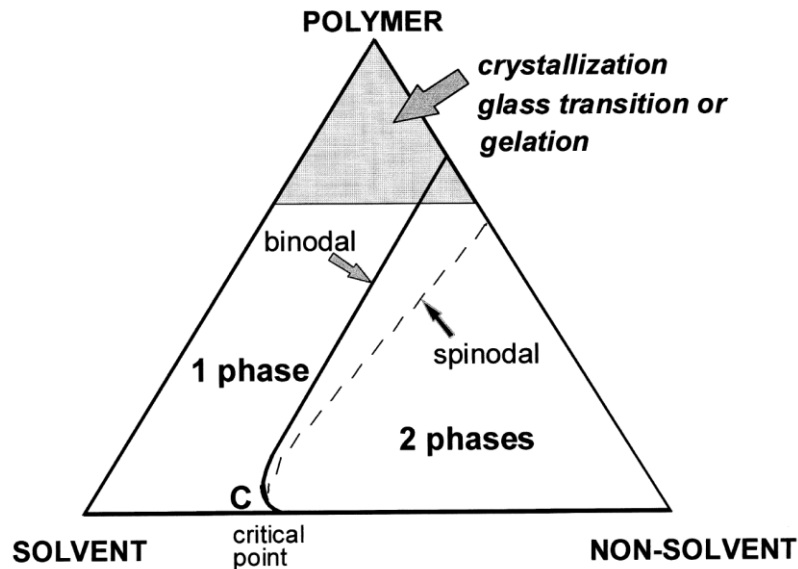
Fig. 2. 20. A typical polymer-solvent-nonsolvent phase diagram [111]. Point C, where the binodal and spinodal intersect, is known as the critical point [119].

2.4.1.1.1. TIPS

TIPS is able to produce highly porous (up to ~ 97% [7]) scaffolds with anisotropic, well-interconnected morphologies (Fig. 2.21a) comprising macropores and micropores [7, 87, 105]. In this technique, a homogeneous polymer solution is quenched inducing phase separation (liquid-liquid or solid-liquid [13, 120]) to occur. The phase separated system is then freeze dried to minimize shrinkage and a porous structure is obtained [7, 13, 87, 120]. Bioactive particles can be also added to the polymer solution prior to the quenching to produce bioactive composite scaffolds (Fig. 2.21b). The quenching temperature, characteristics of the starting materials (polymer and solvent) and the initial concentration of the solution are the most important parameters affecting the final properties of the TIPS-derived scaffolds [7, 13]. Higher polymer concentrations combined with lower quenching temperatures encourage solid-liquid phase separation in which the system is transformed into a concentrated polymer solution and frozen. In the case of liquid-liquid phase separation, polymer-rich and polymer-lean phases are formed [120]. TIPS-derived scaffolds typically have good mechanical properties [105].
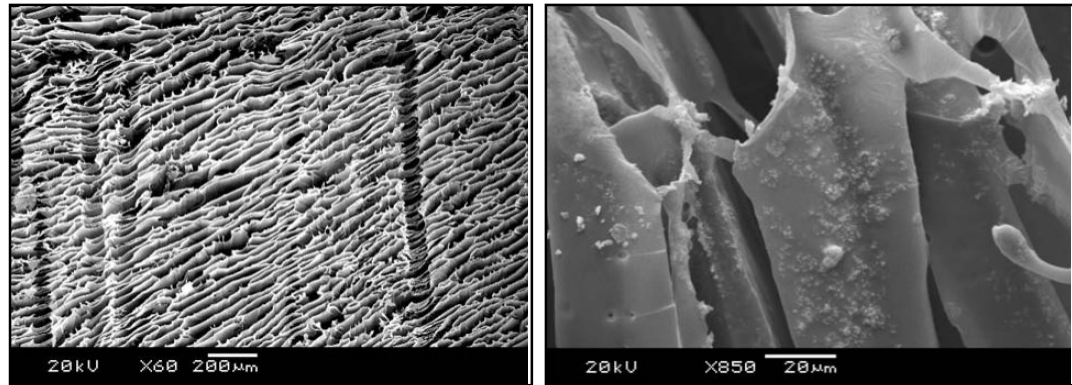
<div style="text-align:center">(a)   (b)</div>

Fig. 2. 21. a) The typical anisotropic, tubular morphology of a TIPS-derived PDLLA scaffold; b) The second phase particles can be seen on the scaffold [87].

Composite scaffolds containing bioactive particles have been also produced via TIPS. Hong et al. [121], fabricated TIPS-derived PLLA scaffolds containing bioactive glass-ceramic nanoparticles (SiO_2:CaO:P_2O_5 = 55:40:5 in mol%). They showed that incorporation of up to 20 wt.% glass-ceramic does not significantly change the porosity (91 – 92%) and morphology of the scaffolds. The porosity drops to ~ 88% for a scaffold with 30 wt.% glass-ceramic content. Also, the compressive modulus and compressive strength of the scaffolds increased from 5.5 to 8 MPa and 0.28 to 0.35 MPa, respectively, as the glass content increased from zero to 30 wt.% [121].

There are several studies on production of porous monoliths via a modified TIPS process with the incorporation of a small amount of nonsolvent to promote phase separation [122-126]. In modified TIPS, the nonsolvent/solvent ratio is an important parameter affecting the phase separation behavior of the system. It has been shown that the nonsolvent content has the greatest impact on the cloud-point temperature of the ternary systems [123, 124]. Chen et al. [122], showed that by incorporation of a nonsolvent into a TIPS process the tubular anisotropic morphology is changed to an isotropic structure consisting of macropores (Fig. 2.22) with slightly higher porosity. This is due to different phase separation mechanism for these systems which is solid-liquid phase separation induced by crystallization of the solvent (Fig, 2.22a) and liquid-liquid phase separation (Fig. 2.22 b and c) [122].

<div style="text-align:center">46</div>

<div align="center">(a)   (b)   (c)</div>
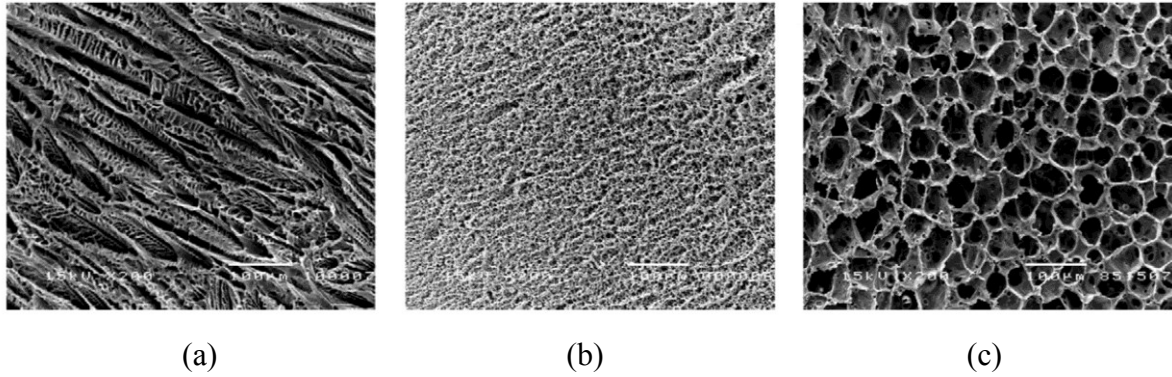
Fig. 2. 22. The morphology of PDLLA scaffolds from anisotropic TIPS-derived (a) to isotropic after the addition of a nonsolvent to the TIPS process (modified TIPS): nonsolvent/solvent = 10/90 (b) and 15/85 (c) [122].

Hua et al. [123, 124] produced scaffolds with interconnected macroporous (50 – 150 μm) via liquid-liquid phase separation with the PLLA–dioxane–water [123] and PLGA–dioxane–water [124] systems. They show that by increasing the aging time at various quenching temperatures and polymer concentrations, the pore morphology becomes coarser [123, 124].

It has been shown that the incorporation of surface active substances (e.g., surfactants) to the modified TIPS process can decrease the interfacial energy between the polymer-rich and polymer-lean phases and stabilize the morphology [122, 124, 126].

2.4.1.1.2. Immersion precipitation

There are several methods for fabrication of polymeric membranes from polymer-solvent-nonsolvent systems; for example, casting the ternary mixture on a substrate and allowing evaporation of the solvent to increase the nonsolvent/solvent ratio leading to phase separation in the system. In vapor-induced-phase-separation (VIPS), the cast polymer solution is exposed to the nonsolvent vapor; e.g., water vapor [110]. Immersion precipitation is the most promising and well-known type of phase inversion used to produce polymer membranes with a range of morphologies and properties [111, 119, 127, 128]. These membranes are normally used for microfiltration purposes; e.g., PLLA

membranes for removing "cell and cell debris" [129] Immersion precipitation normally involves a nonsolvent bath[1] in which a polymer solution which is cast on a substrate (support) is directly immersed. Solvent exchange gradually occurs via diffusion of solvent and nonsolvent (Fig. 2.23); without mechanical stirring. After formation of the membrane skin, it is assumed that the overall polymer concentration is constant, the solvent content is decreasing and the nonsolvent content is increasing [130]. The mass transfer continues via diffusion until viscous effects stop the process [111]. The dry/wet method is a similar technique in which the polymer solution is partly dried in air prior to immersion in the coagulation bath [110]. This results in different morphology and properties for the final membrane compared to those membranes produced by immersion precipitation.
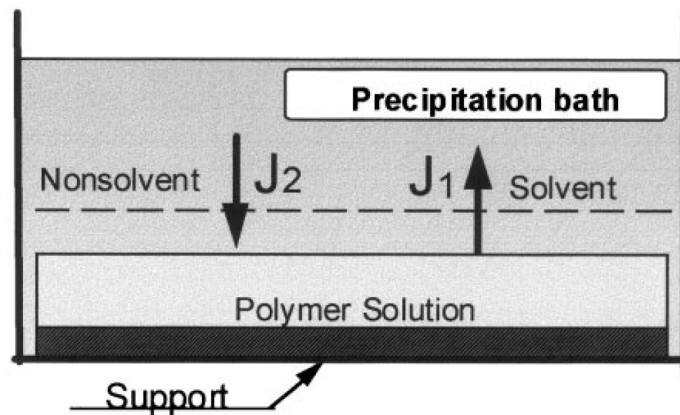
Fig. 2. 23. Schematic of immersion precipitation technique [111]. The support is normally a glass substrate on which the polymer solution is cast [128].

The type of solvent and nonsolvent, composition of the coagulation bath and the initial concentration of the polymer solution affect the phase separation mechanism. Zoppi et al. [127] produced PLLA membranes via immersion precipitation of the PLLA-chloroform-ethanol system. They explain that if a low concentration polymer solution is placed in a coagulation bath, the solvent exchange occurs rapidly and the system quickly passes the metastable region and enters the unstable area where spinodal decomposition

---

1. Also referred to as coagulation or precipitation bath [119, 127, 128].

is the predominant phase separation mechanism. In the case of a high concentration polymer solution, since the diffusion of the solvent and nonsolvent is slower, the system mainly stays in the metastable region during phase separation which is most likely driven by nucleation and growth [127]. Note that in general the energy barrier for phase separation by nucleation and growth is much higher than that of the spinodal decomposition where the energy barrier is negligible [131].

Young et al. [113], produced poly(vinylidene fluoride) (PVDF) membranes via immersion precipitation using the solvent dimethylformamide (DMF) and two nonsolvents: 1-octanol and water which are soft and harsh nonsolvents for PVDF respectively[1]. As shown in Fig. 2.24, using different nonsolvents significantly affects not only the ternary phase diagram but also the morphology of the membrane. The harsh nonsolvent (water) promotes phase separation, makes the single phase smaller and expands the unstable region compared to that of the soft nonsolvent.

Xing et al. [128], investigated the effect of using a coagulation bath consisting of two nonsolvents (ethanol and water) in various ratios on the properties of PLLA membranes. They showed that increasing the water content (harsh nonsolvent) in the coagulation bath decreases the porosity of the membranes and diminishes the uniformity of the pores. The same observations have been reported in other studies [113, 127].

The incorporation of the solvent in the coagulation bath has been also studied in order to control the diffusion rate (i.e., phase separation rate). It has been shown that increasing the solvent content in the coagulation bath, increases the pore size of the membranes due to the slower phase separation in the metastable region providing the pores with more time to grow. The membranes are crystalline due to this slow solvent exchange process providing the polymer chains with more time to crystallize [113, 125, 127, 128]. Crystallization during phase separation is discussed and assessed experimentally for PLLA−DCM−hexane system in Chapters 5 and 6.

Although the effect of polymer molecular weight is generally less significant than that of the other parameters mentioned above [122, 125, 124]; at low Mn, the effects of molecular weight and its distribution are more noticeable on the phase separation

---

1. The meaning of soft and harsh nonsolvent for a polymer can be explained by their *interaction parameter* which is explained in Chapter 4.

behavior [115, 122]. Polymers with high molecular weights exhibit a critical point closer to the solvent and nonsolvent axis of their phase diagram. This can be seen in the phase diagram of PLLA (300,000 g/mol)-chloroform–ethanol system developed by Zoppi et al. [127] as well as the experimentally developed phase diagram of PLLA (180,000 g/mol)-DCM-hexane presented in Chapter 4.

(a)   (b)
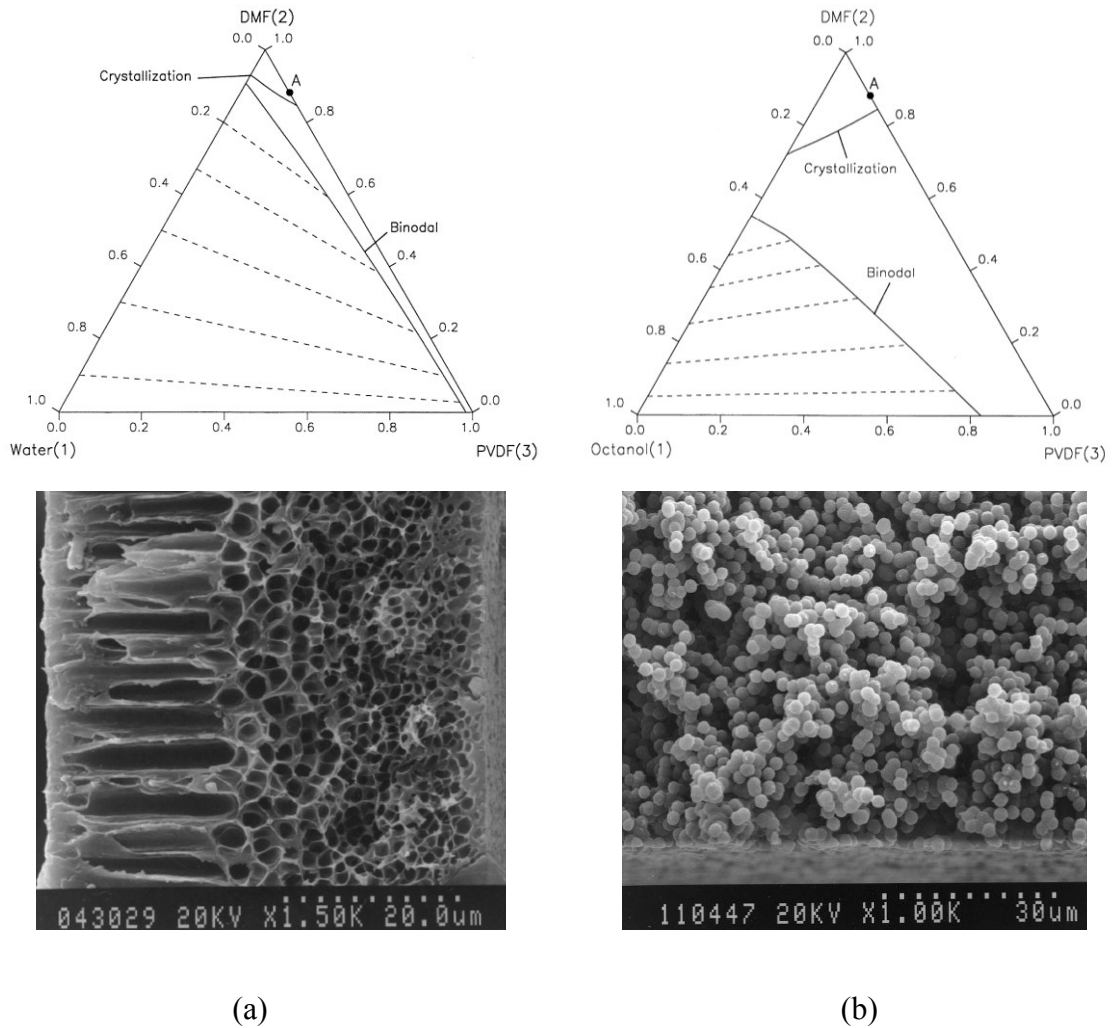
Fig. 2. 24. The phase diagram and morphology of the membranes produced via immersion
precipitation of systems: a) PVDF-DMF-water and b) PVDF-DMF-1-octanol [113].

Various types of inorganic particles such as TiO_2 [132] and ZnO [133] are incorporated into polymeric membranes in order to increase hydrophilicity and/or mechanical properties, reduce membrane foulding or improving their performance (e.g.,

50

gas separation) according to their application. The particles are normally dispersed in the polymer solution before casting and then the homogeneous cast layer is immersed in the coagulation bath [110, 132, 133]. Razmjou et al. [132] showed that incorporation of surface modified TiO_2 into the membranes makes the microvoids larger.

2.4.1.1.3. NIPS for the production of porous monoliths

Although most of the nonsolvent induced phase separation studies have been focused on the production of polymer membranes, porous monoliths can be also produced via NIPS using polymer-solvent-nonsolvent systems. The theory of phase separation for membrane production via immersion precipitation and foam production via NIPS are the same. However, the phase separation mechanism in these processes is different due to a key difference in their productions steps: immersion precipitation method involves a coagulation bath and no stirring, and the solvent exchange gradually occurs via diffusion; but in the NIPS process, normally the nonsolvent is mechanically mixed with the polymer solution. Due to the difference in material transport mechanism (diffusion vs mixing) the time that it takes for a system with high polymer concentration to enter the unstable region is much longer in immersion precipitation compared to a similar NIPS system [109, 122-125, 127]. This matter is discussed further in Chapter 5.

Xin et al. [125], produced porous polycarbonate monoliths via NIPS and showed that the pore and skeleton size of the foams decrease with increasing polymer concentration, nonsolvent/solvent ratio or molecular weight. The pore and skeleton size increase with increasing the phase separation standing temperature [125]. However, fabrication of scaffolds with desirable morphology and characteristics via NIPS is challenging [109].

In order to control the morphology of the final foam, phase separation standing temperature may be adjusted or sacrificial phases may be incorporated. The production of polymer scaffolds from phase separated polymer-solvent-nonsolvent systems via modified TIPS at various phase separation standing temperatures is explained previously in section 2.4.1.1.1. Reverchon et al. [134], produced PLA scaffolds from PLA-dioxane-ethanol system with a macroporous morphology due to addition of fructose particles (250

– 500 μm) as porogen to the gels. They also produced composite scaffolds by introducing hydroxyapatite nanoparticles (up to 50 wt.%) into the foams. They reported that the porosity decreases and compressive modulus increases (up to 123 kPa) by increasing the hydroxyapatite content. They also showed that due to the interesting fibrous nanostructure combined with macropores, the human mesenchymal stem cells can efficiently differentiate onto the scaffold [107].

Unlike TIPS and modified TIPS, the fabrication of porous monoliths via NIPS at various phase separation standing temperatures does not require quenching in liquid nitrogen or freeze drying. The nonsolvent content is normally enough for inducing phase separation throughout the system. PLA foams with different morphologies which are successfully produced from PLA-DCM-hexane systems via NIPS at various phase separation standing temperatures, are studied in Chapters 5 and 6. In Chapter 6, the effect of incorporation of glass particles on morphology of PLA foams are discussed. This template-free, versatile method has shown a great potential as a foaming technique which can be also used for producing scaffolds used in tissue engineering.

Chapter 3

Synthesis of 45S5 Bioglass® via a straightforward organic, nitrate-free sol-gel process[1]

Ehsan Rezabeigi, Paula M. Wood-Adams and Robin A.L. Drew

Department of Mechanical and Industrial Engineering, Concordia University
Montreal, QC H3G 1M8, Canada

Abstract

More than four decades after the discovery of 45S5 Bioglass® as the first bioactive material, this composition is still one of the most promising materials in the tissue engineering field. Sol-gel-derived bioactive glasses generally possess improved properties over other bioactive glasses, because of their highly porous microstructure and unique surface chemistry which accelerate hydroxyapatite formation. In the current study, a new combination of precursors with lactic acid as the hydrolysis catalyst have been employed to design an organic, nitrate-free sol-gel procedure for synthesizing of 45S5 Bioglass®. This straightforward route is able to produce fully amorphous submicron particles of this glass with an appropriately high specific surface area on the order of ten times higher than that of the melt-derived glasses. These characteristics are expected to lead to rapid hydroxyapatite formation and consequently more efficient bone bonding.

Keywords: Sol-gel; 45S5 Bioglass®; Organic; Nitrate-free; Lactic acid

3.1. Introduction

Bone repair has been an important issue since early times [3, 5]. After the first generation of biomaterials (metals and alloys) were applied to bone healing, the first

---

bioactive material, 45S5 Bioglass® (45% SiO_2, 24.5% CaO, 24.5% Na_2O and 6% P_2O_5 (wt.%)), developed by Hench et al. [5] in 1969, began a new era in this field. This glass has been the parent composition for many bioactive glasses. According to the ternary phase diagram of the Na_2O–CaO–SiO_2 system with 6 wt.% P_2O_5, few compositions exhibit Class A bioactivity, amongst which 45S5 Bioglass® has the highest bioactivity index making it the most bioactive composition [5, 38]. This glass is not only capable of in-situ hydroxyapatite formation [3, 5, 7, 20-22, 38], but also releases certain concentrations of soluble Si and Ca cations as it dissolves in physiological fluids, which consequently upregulate seven groups of genes providing osteogenic properties [3, 5, 7, 22]. The released ions can also promote vascularization which is vital for the bone healing process [3]. Additionally, 45S5 Bioglass® with high specific surface area has antimicrobial properties which can play an important role especially in dental applications involving infected root canals [42]. These characteristics along with an ability to chemically bond with both hard and soft tissues without scaring or inflammation, can most efficiently accelerate the healing process [135]. The next generation of biomaterials is being designed for the purpose of tissues loss prevention and the presence of 45S5 Bioglass® among the primarily investigations demonstrates the importance of this material in this field [52].

Bioactivity is not only dependent on composition, but also on glass microstructure and surface chemistry which are governed by the processing route [24]. The sol-gel technique provides a flexible, low-temperature method for developing a wide range of bioactive glass compositions with enhanced chemical homogeneity and purity [3, 10, 36, 136]. Silica-based sol-gel-derived glasses inherently have high specific surface area and high concentration of surface silanol groups, giving rise to higher bioactivity [3, 21]. This high specific surface area is due to their "interconnected nanoporous structure" [3] as a result of the condensation architecture of tetrahedral SiO_4 units [21]. These structural and chemical characteristics distinguish sol-gel-derived bioactive glasses from melt-derived and lead to faster hydrolysis and increased bioactivity. Based on these characteristics, even some glass compositions which were previously classified as low-level bioactive or non-bioactive materials could be rendered highly bioactive. Comparisons of the properties of melt-derived 45S5 Bioglass® with sol-gel-derived bioactive glasses mostly

in the SiO_2-CaO-P_2O_5 system such as 58S and 77S, demonstrated that, regardless of the composition, the rate of hydroxyapatite formation is faster for sol-gel-derived glasses [3, 10, 17, 21, 24, 36, 136]. The sol-gel technique is very sensitive to process conditions such as pH, type and ratios of reactants, temperature, and atmospheric conditions. These factors govern the characteristics of the final product [10, 69, 137]. Also, controlling the process becomes very difficult, as the number of precursors and/or their reactivity rates increase, especially in the case of the sodium precursors [9, 36, 60]. The presence of inclusions such as Na_2O in the glass network generally accelerates the first step of hydroxyapatite formation [24, 36, 38]. Substitution of Na_2O by other oxides such as K_2O_5 [138] and ZnO [139] have been investigated for some specific applications. However, 45S5 Bioglass® with a 25 year history of clinical applications [5, 21] in different fields such as orthopedics and dentistry [42, 49, 140] is still the most promising bioactive composition.

Sodium and calcium nitrates and nitric acid have been traditionally used in most bioactive glass sol-gel processes due to their high solubility, specificity, low cost, and ease of thermal decomposition. Heat treatments above 600 °C are required to remove the nitrate byproducts that are hazardous to living cells [3, 141]. Such heat treatment conditions are above the crystallization temperature (610-800 °C) of 45S5 Bioglass®, resulting in the formation of a crystalline phase (most likely either $Na_2CaSi_2O_6$ or $Na_2Ca_2Si_3O_9$) [49, 50]. Even though it has been reported that $Na_2Ca_2Si_3O_9$ has some level of bioactivity [9], crystallization of these glasses generally diminishes their bioactivity [7, 49]. Furthermore, high temperature heat treatments can lower the concentration of hydroxyl groups on the glass surface [3, 21].

Chen et al. [31] showed that lactic acid catalyzed hydrolysis produces nanoparticles with rough surface morphologies for the 60 mol% SiO_2, 36 mol% CaO, 4 mol% P_2O_5 system. Lactic acid and lactate are to a certain extent biocompatible. This organic acid is classified as "GRAS (Generally Recognized as Safe) for use as a food additive" by the US Food and Drug Administration (FDA) [142]. In this study, we will show that lactic acid is compatible with our new organic sol-gel system, leading to a stable, homogeneous and transparent sol. On the contrary with the other commonly used acids such as HCl and HNO_3, in this case there is no concern about miniscule amounts of

acid or its byproducts potentially being incorporated in the final bioactive glass. Furthermore, the complete conversion of precursors to the final oxides may occur at lower stabilization temperatures than those of the inorganic sol-gel routes [137, 143].

In spite of the superior properties of 45S5 Bioglass[®] as well as the advantages of the sol-gel technique, there have been few studies on sol-gel-derived 45S5 Bioglass[®] and most either involved nitrate-containing materials, or the synthesis of a glass-ceramic or ceramic [9-12]. Lucas-Girot et al. [137] were able to synthesize an amorphous bioactive glass (52S4) of the same four-component system as 45S5, via a nitrate-free sol-gel process using inorganic sodium and calcium precursors ($CaCO_3$ and Na_2CO_3) and acetic acid. Although, no in vitro test was reported, a very high dissolution rate is expected based on the glass composition combined with its high specific surface area (80.1 m^2/g). Specific surface area, which increases bioactivity, is a critical characteristic especially for Na_2O-containing sol-gel-derived bioactive glasses; because the final product is likely to possess super-high dissolution rates in vitro, resulting in overly high bioactivity to be used efficiently for bone regeneration purposes [21, 24, 38].

To the authors' knowledge, this is the first time, a fully amorphous, submicron 45S5 Bioglass[®] powder with appropriately high specific surface area has been synthesized via a straightforward, organic, nitrate-free sol-gel process using lactic acid as the hydrolysis catalyst. All precursors are stable under normal room conditions and are soluble in water and/or ethanol, making the sol preparation process very simple without the need for a glove box, freeze-drying, or refluxing.

3.2. Materials and methods

3.2.1. Materials

All materials were obtained commercially and used without further purification. Precursors include tetraethylorthosilicate (TEOS; Aldrich, ≥99.0%), triethyl phosphate (TEP; Aldrich, ≥99.8%), calcium L-lactate pentahydrate (Fisher; >98.0%) and sodium DL-lactate aqueous solution (Sigma-Aldrich; syrup, 60 % (w/w)). Absolute ethanol (Fisher, >95.5%) and DL-lactic acid (Fulka, ~90%) were used as solvent and hydrolysis

catalyst, respectively. Deionized water (DI water; Fisher, Deionized Ultra Filtered Water) was also used.

3.2.2. Sol-gel process

To produce 1g of the glass, TEOS (1.67 ml) is dissolved in absolute ethanol (2.62 ml), and then added to the dilute lactic acid (0.55 ml + 0.55 ml DI water), and stirred for 1 h until the solution becomes clear (Sol.1). Next, Sol.1 is added to [TEP (0.14 ml) + lactic acid (8 ml)] in order to prepare Sol. 2. After 45 min of stirring, Sol. 2 is added to the solution of calcium lactate pentahydrate [(1.35 g) + DI water (12.50 ml) + lactic acid (20 ml)] and subsequently stirred for 3 h (Sol. 3). Sol. 3 is added to the solution of commercial sodium lactate syrup (1.47 g) and 16 ml of lactic acid (Sol.4) and then stirred for 24 h. The final colorless, transparent sol (pH≈1.7) is sealed and put aside at room temperature for 45 days, during which gelation occurs and a few days are allowed for aging. The system is stirred briefly up to three times over the period of day 20 to day 40.

During the procedure, each new material is added dropwise to the next sol/solution, and the sequence, in which the precursors are added, is critical. Since atmospheric humidity can alter the water balance in the sol, the container should be sealed during stirring and storage. The water content of the starting materials must also be considered in determining the amount of DI water to add. The amounts of lactic acid added at each step were designed such that the pH was maintained between 1 and 2 during the sol preparation process, avoiding gelation and controlling the rates of hydrolysis and condensation [60, 69]. It is convenient to adjust the pH of each sol/solution before it is incorporated in the next step. In this manner, there is no need to continuously measure and adjust the pH of the sol.

The resultant gel is transferred to a wide quartz crucible and dried under high humidity at 170 °C for 4 days. TG (TA Instruments, TGA Q50)/DSC (Setaram, Setsys 12) analyses were performed on the dried gel in order to capture the thermal behavior of the material and to design an efficient heat treatment for the subsequent stabilization. The analyses were performed under nitrogen atmosphere with a heating rate of 5 °C/min using aluminum and alumina crucibles, respectively. Since the gel was previously

subjected to the drying step, the weight loss below 170 °C (Fig. 3.1) is mostly related to humidity absorption from the air. Most of the residual organic materials and water are eliminated from the gel below 550 °C (~ 57% out of 62% total weight loss). This temperature is below the crystallization temperature, which is 614 °C according to the DSC results. 45S5 Bioglass® crystallization temperatures of 610 °C [49] and 650-690 °C [50] for the heating rates of 5 °C/min and 5-30 °C/min, have been reported in the literature. Based on our results, 550 °C is selected for the stabilization procedure.
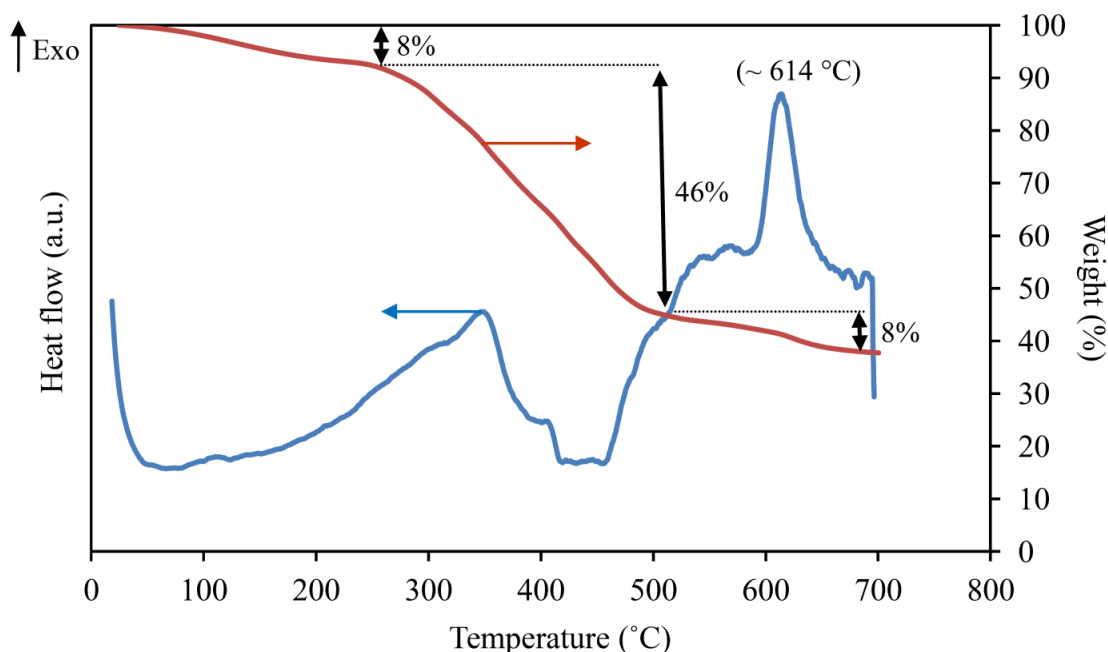
Fig. 3. 1. Results of DSC and TG analyses on the dried gel (nitrogen atmosphere, 5 °C/min.).

The stabilization process is performed in humid air using a tube furnace (Barnstead Thermolyne model 21100) and alumina crucibles. The dried gel is heated up to 550 °C with a heating rate of 0.4 °C/min and a dwell time of 3 hours, and then the furnace is shut down and left to cool to room temperature before removing the sample. The low heating rate and high humidity facilitate the oxidation and subsequent removal of the residual byproducts. Drying and stabilization of the gel under high humidity is also expected to provide a more homogenous product [36].

To evaluate the efficiency of the stabilization process, another TGA was performed on the stabilized powder (Fig. 3.2), confirming effective stabilization. The small weight loss in TGA of the stabilized powder, occurring at lower temperatures than 400 °C, can be attributed to the absorbed water. The weight loss may also be related to reactions between hydroxyl groups on the surface of the glass particles to produce water molecules [100].
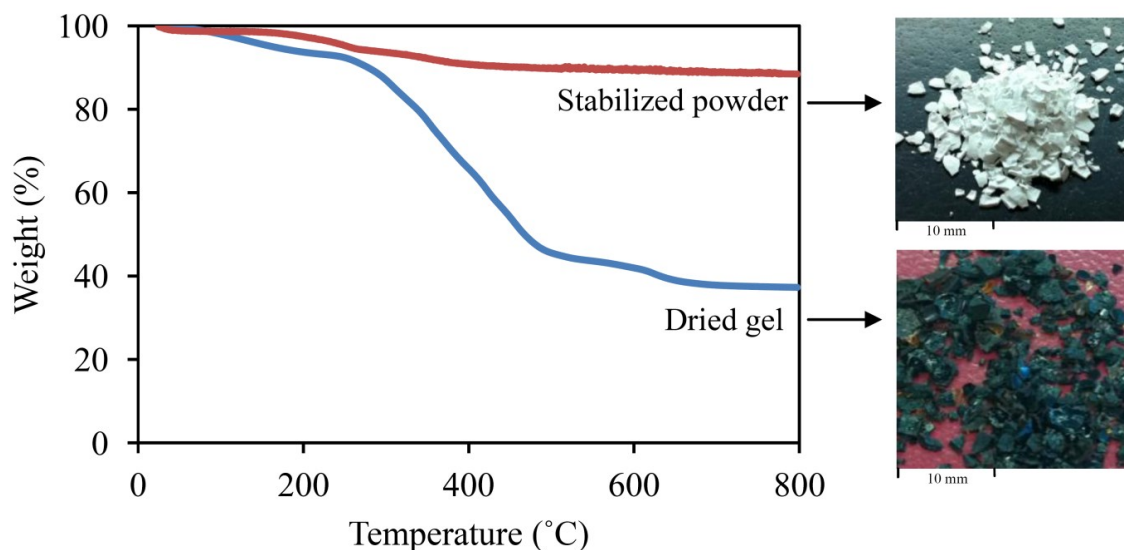
Fig. 3. 2. TGA results and physical appearance of the dried gel and the stabilized powder (nitrogen atmosphere, 5 °C/min.).

3.2.3. Characterization

After stabilization, the material was ground with an agate mortar and pestle and characterization tests were conducted on the resultant white powder. Morphology and composition were studied using a scanning electron microscope (SEM; HITACHI, S-3400N) equipped with energy-dispersive X-ray spectroscopy (EDS; Oxford Instruments; Wave Model). For this purpose, specimens were uncoated and consisted of powder spread on a carbon tape which was mounted on an aluminum sample holder. The imaging was carried out under high vacuum (< 1 Pa) with probe current, accelerating voltage and emission current set to 60 μA, 10 kV and 78 μA, respectively. The EDS analyzer was

calibrated using SiO_2, $NaAlSi_3O_8$, SiO_2, $CaSiO_3$, and GaP as standards in order to quantitatively detect the oxygen, sodium, silicon, calcium and phosphorous contents. Since the elements in the glass composition are heavier than carbon and there is no overlap in the X-ray spectra, EDS analysis is able to provide relatively accurate compositional results. To reveal the state of crystallinity of the powder, X-ray diffractometry analysis (XRD; X'Pert Pro, PANalytical) was carried out using Cu Kα radiation. Data were collected from 20 to 120 degrees (2θ), although only portions of the patterns containing useful information are reported ($20°<2\theta<70°$). A quantity of 15 mg of the powder was used for the Brunauer, Emmett and Teller N_2 adsorption–desorption test (BET; Tristar 3000 V6.07). The BET-specific surface area of the sample was thus measured by nitrogen adsorption at 77.3 K. Particle size distribution of the powder was determined via laser light scattering particle size distribution analysis (PSA; Horiba LA-920) using isopropyl alcohol as a dispersant. It should be noted that the analyzer measures the distance between the farthest points on each object and reports it as the particle diameter.

3.3. Results and discussion

The results of the EDS analysis on the stabilized powder for four different points are summarized in Table 3.1. The average EDS composition is very close to the nominal composition of melt-derived 45S5 Bioglass®. The small standard deviation values indicate that the material is homogenous. Under acidic conditions and prolonged reaction time as in our sol-gel process, the predominant growth mechanism is expected to be cluster-cluster rather than monomer-cluster, resulting in the formation of a polymeric gel [60, 69]. This type of gel is chemically more homogeneous than colloidal gels due to the possibility of better mixing at molecular scales [60]. Since all five expected elements are present in the composition of the material, we can conclude that the starting materials have undergone the expected hydrolysis and condensation reactions.

Table 3. 1.The results of EDS analysis

	O (wt.%)	Si (wt.%)	Na (wt.%)	Ca (wt.%)	P (wt.%)
EDS results	43.3 (2.46)[a]	21.2 (0.14)	16.4 (1.18)	17.0 (1.69)	2.1 (0.24)
Nominal composition	40.66	21.03	18.18	17.51	2.62

[a] The values in parentheses are standard deviations of four different measurements.

XRD patterns of the dried gel before and after various heat treatments are shown in 3.3. No peaks can be detected in the patterns of the dried gel and stabilized powder, although there is a broad band between 30° and 35° (2θ) in the latter pattern. This indicates that no crystallization occurs during the stabilization process. This observation combined with the results of the compositional analysis confirms that the white stabilized powder is fully amorphous sol-gel-derived 45S5 Bioglass®. The heat treatments at higher temperatures resulted in crystallization of $Na_2Ca_2Si_3O_9$, forming a glass-ceramic with ceramic content increasing with the heat treatment temperature. Fig. 3.3e shows the pattern of the glass sintered at 1000 °C, which is completely in agreement with the previous studies [11, 12, 50].

The BET results (2 repeats) are shown in Table 3.2. The BET-specific surface area of the powder is 11.75 m^2/g, which is on the order of ten times higher than that of a similar sized melt-derived 45S5 Bioglass® powder which is known to be dense rather than porous [17, 36, 42]. This characteristic is governed by the sol-gel process parameters, in particular the compositions of the starting materials and the gelation conditions. Each sol-gel system has its own gelation time, which is strongly dependent on the sol-gel process variables. The condensation reactions continue even after the gelation point due to the diffusion of small clusters through the network, increasing the chance of their bonding to the network. The 45-day processing period in our system aids this phenomenon, which may lead to a more compact network microstructure [21, 60, 69, 137]. The addition of a gelation catalyst accelerates the network formation, giving rise to a sparser, more heterogeneous network. Furthermore, it has been shown that inorganic sol-gel routes produce more porous glasses with less homogeneity in SiO_2-CaO-P_2O_5 systems, whereas glasses obtained from metalorganic routes have improved and more homogeneous textures [144]. Therefore, the smaller specific surface area in this study

compared to that of the common sol-gel-derived glasses can be mostly attributed to this new combination of organic starting materials and its slow gelation process.
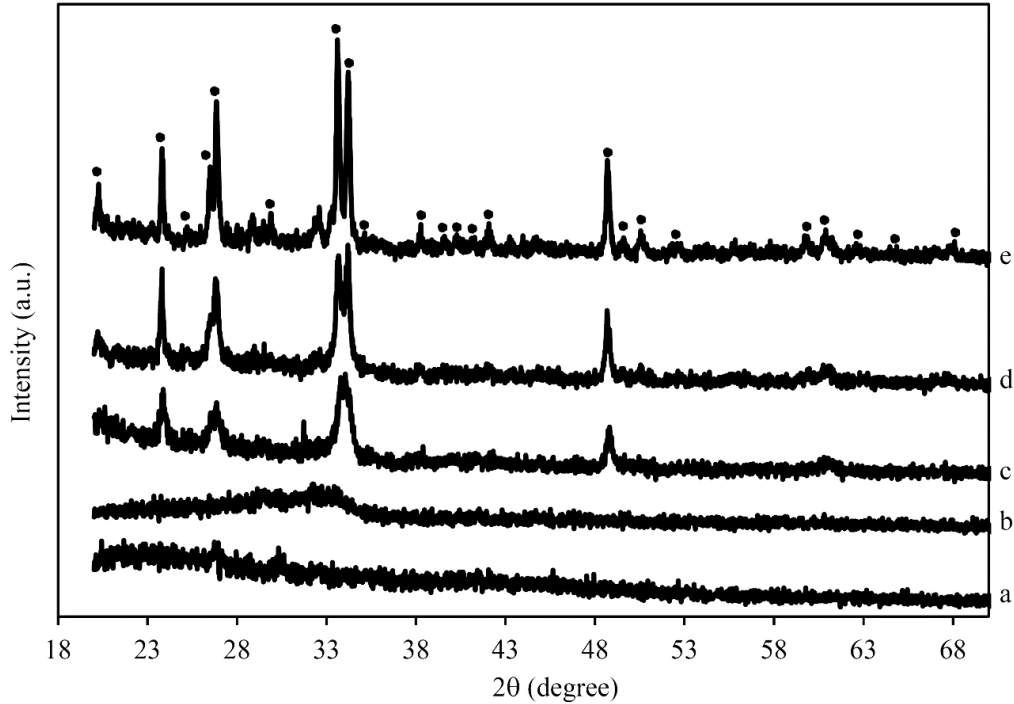
Fig. 3. 3. XRD patterns of the gel after a) drying (170 °C), b) stabilization (550 °C), heat treatment at c) 630 °C, d) 820 °C and e) sintering at 1000 °C (• Na$_2$Ca$_2$Si$_3$O$_9$).

Table 3. 2. Specific surface area of the stabilized powder

BET-specific surface area (m^2/g)	Total Pore Volume (cm^3/g)		Mean pore diameter (Å)	
11.75	In adsorption	0.065	In adsorption	276.21
	In desorption	0.076	In desorption	324.32

The particle size distribution of the powder is presented in Fig. 3.4. The refractive index of 45S5 Bioglass® and its suspension in isopropyl alcohol were considered to be 1.55 and 1.08, respectively. Two populations are distinguishable in this diagram: submicron and micron-sized. As explained previously, the predominant growth mechanism for our sol-gel system is cluster-cluster, leading to the formation of rather large secondary particles. The submicron-sized population follows a lognormal

distribution, and may be related to breakup of larger particles that occurs due to stirring prior to gelation [145]. The second larger diameter population likely consists of aggregates held together by hydrogen bonding of the surface hydroxyl groups as well as some particles held together by covalent bonds. Simple grinding by mortar and pestle leads to the upper limit of particle size of about 200 μm. According to the differential distribution, the powder includes approximately 43% submicron particles with the mean size of 600 nm, whereas the overall mean is 13.28 μm. Surface modification is a commonly used method to reduce the agglomeration [3, 21].
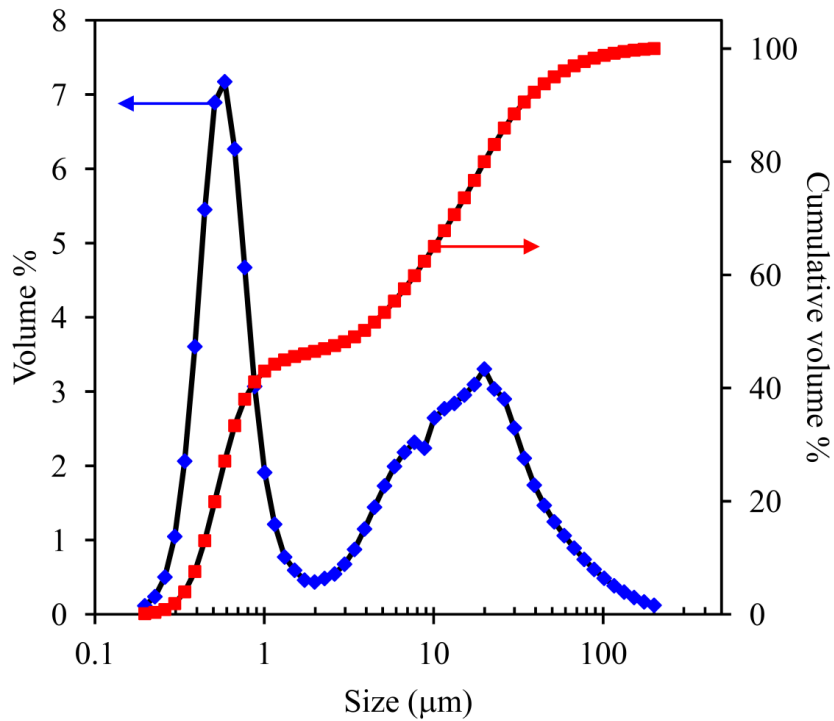
Fig. 3. 4. Particle size distribution of the stabilized powder, volume% and cumulative volume%.

Agglomeration is also obvious in the SEM images of the stabilized powder (Fig. 3.5). The morphology of the particles can be observed in Fig. 3.5d showing a rough surface as reported by Chen et al. [31] for their ternary system. They proposed a hypothesis claiming that the surface roughness and nanoscale morphology of the as-synthesized glass are attributed to the presence of lactic acid as catalyst. This feature can

result in higher bioactivity as well as improved interaction between particles and polymer matrix in composite scaffolds leading to better micro-mechanical interlocking.
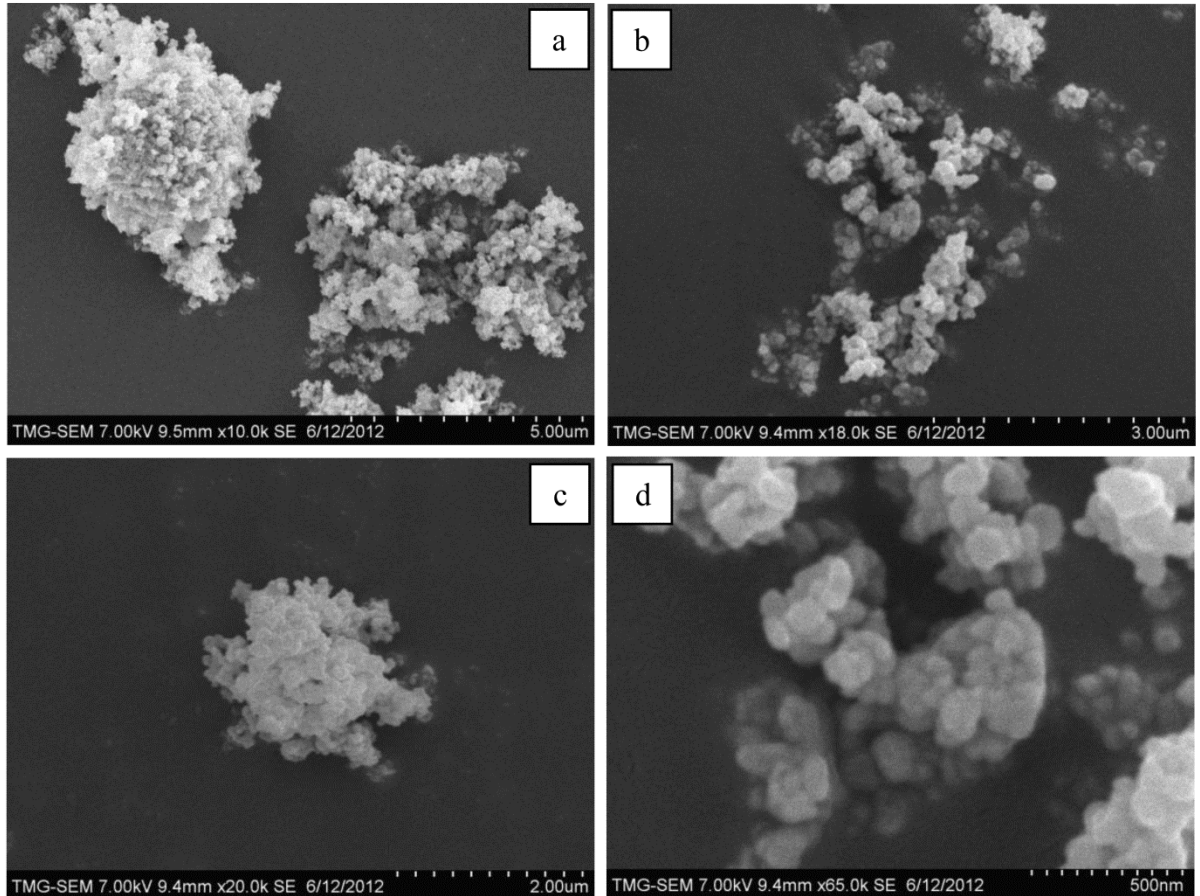
Fig. 3. 5. SEM morphologies of the stabilized powder in different magnifications:
a) ×10K, b) ×18K, c) ×20K, and d) ×65K.

3.4. Conclusion

Until now, clinical applications of 45S5 Bioglass® are limited only to the melt-derived type. Considering all the advantages of the sol-gel technique, 45S5 Bioglass® with improved properties, which can be synthesized at room temperature via a straightforward, flexible and inexpensive sol-gel route, is an excellent candidate for the current and future applications of this material. In this paper, the development of a novel

organic, nitrate-free, sol-gel route for the synthesis of 45S5 Bioglass® was presented. This process allows for the synthesis of fully amorphous, homogeneous, pure, submicron 45S5 Bioglass® powder with appropriately high specific surface area (11.75 m^2/g) for further processing. Since 45S5 is the most bioactive composition and sol-gel-derived bioactive glasses exhibit the highest rate of hydroxyapatite formation and bone bonding, this material is expected to display superior bioproperties, making it a good candidate as second phase in polymeric scaffolds, and/or a dental filler.

Chapter 4

Isothermal ternary phase diagram of the polylactic acid-dichloromethane-hexane system[1]

Ehsan Rezabeigi, Paula M. Wood-Adams and Robin A.L. Drew

Department of Mechanical and Industrial Engineering, Concordia University
Montreal, QC H3G 1M8, Canada

Abstract

The ternary phase diagram of polylactic acid, dichloromethane (solvent) and hexane (nonsolvent) is experimentally developed at room conditions based on naked-eye observations over 14-day periods. The experimental procedure is explained in detail, allowing it to be applied to similar ternary systems. Three regions are distinguishable in this diagram: single phase, liquid-liquid phase separated and solid-liquid phase separated. This diagram is then assessed based on the lever rule concept in ternary phase diagrams. Phase separation kinetics are also evaluated using turbidity studies to quantitatively monitor the cloudiness of the samples over time. The results show that, a small increase in polylactic acid concentration on the order of a few weight percent can drastically increase the phase separation rate. The application of polylactic acid in various fields has been increasing, and this work provides fundamental information essential for solvent-based processing (e.g., nonsolvent induced phase separation and immersion-precipitation) of this polymer in the system composed of dichloromethane and hexane.

Keywords: Phase diagram; Polylactic acid; Dichloromethane; Hexane; Nonsolvent; Phase separation; Turbidity

---

4.1. Introduction

Phase inversion and phase separation in polymer solutions are of interest mainly due to the subsequent applications such as the production of polymer fibers [74], porous membranes [119] and monolith foams [125] with controllable morphologies. Phase separation in a homogeneous polymer solution can occur by increasing the free energy of the system by changing the temperature (thermally induced phase separation; TIPS [146]) or adding an adequate amount of nonsolvent (nonsolvent induced phase separation; NIPS [125]).

The change in Gibbs free energy due to mixing, in a polymer-solvent system can be calculated by the Flory-Huggins equation (Eq. 4.1) [112, 131]

$$\Delta G = RT(n_1 \ln \phi_1 + n_2 \ln \phi_2 + n_1 \phi_2 \chi_{12}) \qquad \text{Eq. 4.1}$$

where R is the gas constant, and T is the absolute temperature. The subscripts 1 and 2 correspond to solvent and polymer, respectively. Also, n_i is the number of moles and ϕ_i represents the volume fraction. The Flory-Huggins interaction parameter (χ) between the two species is given by Eq. 4.2 [147]

$$\chi_{ij} = \frac{V_r}{RT}(\delta_i - \delta_j)^2 \qquad \text{Eq. 4.2}$$

where V_r represents reference molar volume, and δ is the solubility parameter, which can be calculated using "the group contribution method" via Eq. 4.3 [131, 147].

$$\delta = \frac{\rho \sum G}{M} \qquad \text{Eq. 4.3}$$

Here ρ is the density, G is the group molar attraction constant, and M is the molecular weight or mer molecular weight for a polymer [131, 147].

The addition of a nonsolvent to this binary system increases the ΔG of the mixture because of its interactions with the polymer and solvent as shown in Eq. 4.4 [112].

$$\Delta G = RT(n_1 \ln \phi_1 + n_2 \ln \phi_2 + n_3 \ln \phi_3 + g_{13}(u_1)n_3\phi_1 + \chi_{23}n_3\phi_2 + \chi_{12}n_1\phi_2) \qquad \text{Eq. 4.4}$$

In this equation, subscript 3 refers to the nonsolvent, and g_{13} is the solvent-nonsolvent parameter which is a function of $u_1 = \phi_1/(\phi_1+\phi_3)$ [112, 131].

Phase separation occurs when there is a two-phase system with a lower free energy level than the single phase at the current conditions [74, 131]. Depending on the free energy level of the system (Eq. 4.4), two types of nonsolvent induced phase separation may occur when adding a nonsolvent to a stable polymer solution: liquid-liquid phase separation and solid-liquid phase separation [125]. The former process results in polymer-rich and polymer-lean phases while the latter results in a polymer-lean liquid phase and pure polymer precipitate [125, 131]. Liquid-liquid phase separation is the principle of the NIPS foaming technique. Each polymer-solvent-nonsolvent system has its own phase separation behavior and kinetics, which are governed by the polymer concentration and molecular weight, nonsolvent to solvent ratio, and their nature [125]. A ternary phase diagram for such systems can provide useful information on the thermodynamic state of the system under certain conditions [113, 119, 148, 149].

Polylactic acid (PLA) is a thermoplastic which is classified as a saturated aliphatic polyester. Because of the asymmetric molecular structure, PLA is commonly used in different forms of L-PLA (PLLA), D-PLA (PDLA), and D,L-PLA (PDLLA) [74]. During the past few decades, PLA has been commercially produced and used in various fields such as biology, agriculture and packaging industries [75, 76, 81]. This biodegradable polymer is an interesting environmentally friendly replacement for the oil-based plastics. Also, since PLA has been approved by US Food and Drug Administration (FDA) for clinical applications, many biology-related studies have been conducted on this material; for example PLA-based bone scaffolds [74]. The facile synthesis of PLA, its availability, transparency, relatively high melting point, biodegradability, biocompatibility and mechanical properties, have attracted attention to this polymer both in terms of practical applications and research [76, 81].

Considering the increasing applications of PLA as well as the number of fabrication techniques based on phase separation and inversion phenomena for films, fibers, membranes and foams, the study of phase diagrams for PLA-based systems is important. Numerical calculations have been widely used to determine the binodal and spinodal boundaries and developing the phase diagram in polymer-solvent-nonsolvent ternary systems, whereas there are fewer experimental studies to identify different regions in the phase diagram [113-116]. In our work, an isothermal section of the PLA-dichloromethane (DCM)-hexane system is developed experimentally at room conditions and its potential for the production of highly porous monoliths is demonstrated. PLA is insoluble in hexane but soluble in DCM [75, 77]. Since hexane is miscible with DCM, this chemical was selected as the nonsolvent for the PLA-DCM solutions. Visual inspection is used to identify two-phase conditions.

For some compositions, phase separation rates are also studied and compared using turbidity measurements. There are various methods to monitor the phase separation process, amongst which turbidity is a convenient way to quantitatively measure the light transmission through the samples over time. In this technique, the turbidity of the samples which is measured in nephelometric turbidity units (NTU), is used as an indication of the progress of phase separation. The turbidity meter is much more sensitive than the naked eye to small changes in cloudiness and can more accurately detect the degree of phase separation.

4.2. Experimental procedure

4.2.1. Materials

PLA (NatureWorks LLC, Ingeo™ Biopolymer 4032D) with a high average molecular weight (M_n = 97000, M_w/M_n = 2) and 1.6 % D-lactide content, dichloromethane (DCM, Fisher Chemical; Stabilized/Certified ACS, ≥99.5) and hexanes (Fisher Chemicals; Certified ACS, ≥98.5 %) are used. The average molecular weights of the polymer are provided by the supplier based on the solution viscosity measurements

which have been specifically performed on the PLA batch we purchased. The relevant physical and chemical characteristics of these substances are presented in Table 4.1.

Table 4. 1. Some physical and chemical properties of the PLA, DCM and hexane

	PLA (as-received)		DCM		Hexane	
Chemical formula	$(C_3H_4O_2)n$		CH_2Cl_2		C_6H_{14}	
Chemical structure						
Thermal characteristics (˚C)	Melting point	168 [a]	Boiling point	40 [b]	Boiling point	69 [b]
	Glass transition temp.	65 [a]				
Density (g/cm³)	1.24 [c]		1.33 [c]		0.65 [c]	
Molecular weight (g/mol)	72.06 [d]		84.93		86.17	
Vapor pressure (mmHg)	-		376 (at 21 °C) [b]		128 (at 21 °C) [b]	
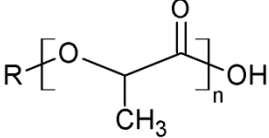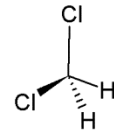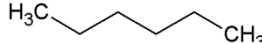
(a) From Fig. 4.1.
(b) From Ref. [150].
(c) Specified by supplier.
(d) Mer molecular weight.

4.2.2. Sample preparation and characterization

In order to facilitate the dissolution of PLA in DCM, the as-received PLA pellets are melted at 190 ˚C (20-30 min.) under nitrogen atmosphere, and then quenched by placing them in a freezer at -23 ˚C (60 min.) in order to remove all crystallinity. The DSC results (Fig. 4.1) reveal that a crystallization peak (~100 ˚C - 150 ˚C) appears in the curve of the PLA submitted to this thermal treatment, while no such peak exists for the as-received sample. The area beneath this peak (19.29 J/g) is close to the area of the melting peak (24.26 J/g, at ~168 ˚C) showing that the melted-quenched PLA is almost completely amorphous (~ 95%).

Since the phase separation process takes place at room temperature and atmospheric pressure, the only system variables are the concentrations of components of which there are only two independent variables: the concentration of PLA in DCM (first

stage in the solution preparation procedure) and the hexane/DCM (v/v) ratio. Experimental points were spaced with a resolution of 0.25 wt.% and 0.25 in these variables, respectively. In order to precisely locate the boundary of the liquid-liquid and solid-liquid regions of the phase diagram, experimental points in its vicinity were spaced more closely in terms of hexane/DCM with a resolution of 0.15. When needed additional points were evaluated close to the boundaries. It should be noted that, a sample containing the PLA in DCM concentration of "X" wt.% and hexane to DCM volume ratio of "Y" is referred to as (X wt.%, Y v/v) in the following.
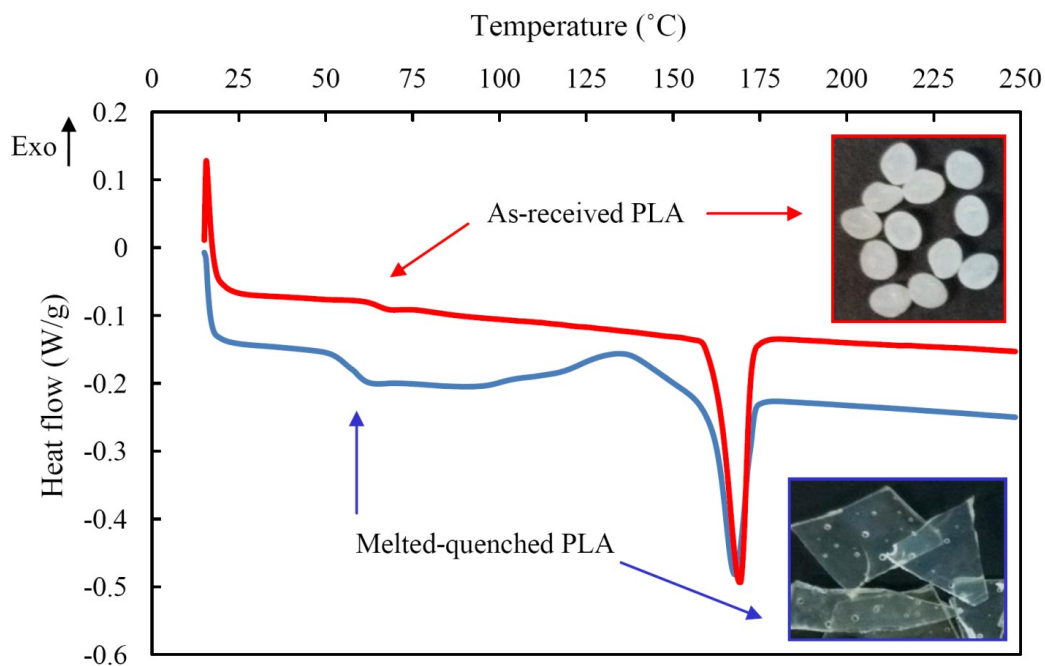
Fig. 4. 1. Results of DSC analysis, and physical appearance of as-received and melted-quenched PLA.

PLA-DCM solutions with different concentrations (0.25-30 wt.%) are prepared as required by weighing (± 0.01 g) the PLA and the mixture (amorphous pellets and DCM). To accelerate the dissolution process, the mixture is stirred at 30 ˚C until no solid is visible, adding DCM as needed. Finally, the solutions are once again weighed at room temperature and the evaporated DCM is replaced to produce the desired concentration.

Solutions prepared in this manner were stable, single phase systems at room temperature, and the saturation point was not reached.

Subsequently, the required volume of hexane (± 0.01 ml) is gradually added under vigorous stirring at room temperature. Instantaneous localized phase separation for higher PLA concentration solutions is avoided by adding the hexane in a dropwise manner. The final samples are tightly sealed and stored at room conditions. The samples are visually inspected several times a day for a maximum of 14 days. A visually noticeable increase in blurriness was taken to be the cloud-point or liquid-liquid phase separation. Precipitation was recorded as solid-liquid phase separation. These results are then used to develop the phase diagram.

A turbidity meter (MicroTPW, HF Scientific Inc.; 0<NTU<1100) is also used to monitor the phase separation rates for selected systems. The device is calibrated at least once a day using 0.02, 10 and 1000 NTU standards. Each reported turbidity value in this study is the average of three measurements.

In order to demonstrate the potential of the NIPS process, we also prepare and characterize one PLA monolith using a composition which undergoes liquid-liquid phase separation: (18 wt.%, 1 v/v). After the nonsolvent addition, the phase separation starts and proceeds until gelation. The gel is soaked in methanol in order to completely replace the solvent and nonsolvnet and then dried in air. The porosity% of the NIPS-derived foam is calculated based on apparent density and its morphology is examined by scanning electron microscopy (SEM; HITACHI, S-3400N).

4.3. Results and discussion

The morphology and porosity% of the PLA foam produced from the liquid-liquid phase separated system at 18 wt.%, 1 v/v is presented in Fig. 4.2. The interesting morphology and high porosity of the final monolith illustrate the potential of the NIPS process. The current fundamental study of the phase behavior of the PLA-DCM-hexane system is necessary in order to fully map the process space for the eventual production of highly porous PLA monoliths.

Before developing the phase diagram, the solubility parameters of each component of our system are calculated. By using Eq. 4.3, and the information provided in Table 4.1, the solubility parameters of PLA, DCM and hexane at 25˚C are determined to be 10.10, 10.54 and 7.24 $(cal/cm^3)^{1/2}$, respectively. From Eqs. 4.1 to 4.3, we can see that a larger difference in solubility parameters results in a larger value for ΔG of mixing, meaning a lower potential for dissolution. As expected, DCM is a good candidate as solvent for PLA since $\left|\delta_{PLA} - \delta_{DCM}\right|$ is very small. Hexane is also a good candidate for nonsolvent for PLA since $\left|\delta_{PLA} - \delta_{hexane}\right|$ is large. This indicates that, addition of this nonsolvent to a PLA-DCM solution will effectively increase the Gibbs free energy of the system according to Eq. 4.4, which may result in a phase separation.
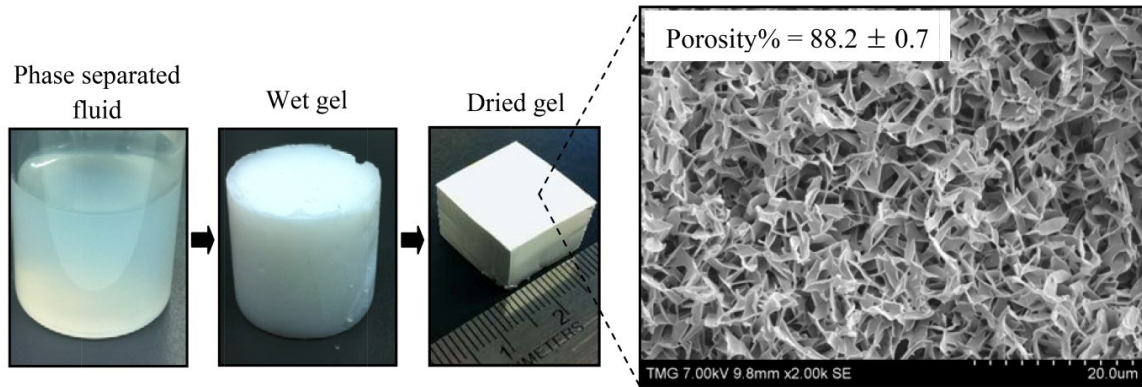
Fig. 4. 2. Overview of the production of a highly porous foam from a liquid-liquid phase separated PLA-DCM-hexane sample (18 wt.%, 1 v/v).

4.3.1. Developing the ternary phase diagram

The results of our 14-day study of the appearance of the various samples used to determine the phase boundaries are summarized in Table 4.2. The likelihood for phase separation increases as the concentration of PLA in DCM and/or the hexane/DCM volume ratio increases [111, 125]. For example, sample (6.5 wt.%, 1 v/v), undergoes liquid-liquid phase separation, thus for all the samples with higher concentration of PLA in DCM (6.75 to 30 wt.%) with hexane/DCM volume ratio of 1 or higher, phase

separation definitely occurs. As discussed previously, the system minimizes its free energy by phase separation and the resultant phase state (either liquid-liquid or solid-liquid) is stable, and is unaffected by mechanical stirring at room conditions (confirmed experimentally).

Table 4. 2. The results of 14-day observation of the samples

Hexane/DCM (v/v)	PLA in DCM concentration (wt.%)																																
	0.25	0.5	0.75	1	3	5	6	6.25	6.5	6.75	7	9	10	11	13	13.25	13.5	13.75	14	15	16	16.5	16.75	17	18	19	19.5	19.75	20	23	25	29	30
0.25												S		S			S									S		S	S	S	L	L	L	
0.5												S		S			S	S	S	S	S	S	S	S	L	L	L			L				
0.75				S	S				S	S		S	S	S	L	L	L		L			L		L	L	L								
1		S		S	S	S	S	S	S	L	L	L	L	L	L	L			L		L			L	L	L			L	L	L	L		
1.15		P		P		P						P																						
1.25	P	P	P	P																														P

(S) Single phase
(L) Liquid-liquid phase separation
(P) Precipitation, solid-liquid phase separation
☐ Indicates no measurement

Eqs. 4.5 and 4.6 are used to convert the points of Table 4.2 to the concentration of each component (wt.%), so that the results can be placed on the ternary phase diagram.

$$PLA(wt.\% \text{ in overall system}) = \frac{204.6(X_{PLA})}{204.6 + V_{H/D}(100 - X_{PLA})} \qquad \text{Eq. 4.5}$$

$$DCM(wt.\%) = \frac{204.6(100 - X_{PLA})}{204.6 + V_{H/D}(100 - X_{PLA})} \qquad \text{Eq. 4.6}$$

Here X_{PLA} and $V_{H/D}$ are the concentration of the PLA in DCM solution (wt.%) and the hexane/DCM volume ratio, respectively. Note that Eq. 4.5 gives the concentration of PLA in the final mixture, containing both solvent and nonsolvent. In Table 4.3, the compositions and their phase state, which are frequently used in this article, are shown in terms of both presentations.

In Fig. 4.3, the results of all experiments are shown on the PLA-DCM-hexane phase diagram where the phase boundaries are subsequently drawn by connecting the

experimental points. Since sample (0.5 wt.%, 1.15 v/v) exhibited solid-liquid phase separation (Table 4.2), all the compositions with higher hexane/DCM volume ratio and/or PLA in DCM concentration were assumed to show solid-liquid phase separation and the boundary, separating the solid-liquid region from the liquid-liquid region was simply drawn as a line representing this condition. The points which are very close to the boundaries may show metastability and/or very slow phase separation kinetics which are not captured within the 14 day timeframe.

Although PLA is reported to be soluble in DCM up to ~ 99 wt.% [77]; we did not carry out any experiments above 22 wt.% PLA line in the phase diagram, due to the high viscosity of the PLA-DCM solutions.

Table 4. 3. Key points from Table 4.2, converted to the compositions on the ternary phase diagram, using Eqs. 4.5 and 4.6

Nomenclature used in Table 4.2		State	Overall mixture composition		
PLA in DCM concentration (wt.%)	Hexane/DCM (v/v)		PLA (wt.%)	DCM (wt.%)	Hexane (wt.%)
1	1	Single phase	0.67	66.72	32.61
5	1		3.41	64.88	31.71
7	1	Liquid-liquid	4.81	63.94	31.25
10	1		6.94	62.51	30.55
13	1		9.12	61.04	29.84
1	1.25	Solid-liquid	0.62	61.69	37.69

In Fig. 4.3, the boundary separating the single phase and liquid-liquid phase separated regions is known as the binodal [111]. Since the composition region in the vicinity of this boundary is expected to exhibit metastability, it is possible that the true binodal falls slightly below the boundary that we have identified after 14 days of observation. As expected, the single phase region is wider, i.e. the binodal occurs at a higher PLA wt%, at low hexane/DCM volume ratios. Precipitation becomes more likely towards the hexane-rich portion of the phase diagram. The liquid-liquid and the solid-liquid phase separated regions include the compositions that may be useful for various

fabrication methods such as NIPS foaming [125] and immersion-precipitation techniques [111, 113].
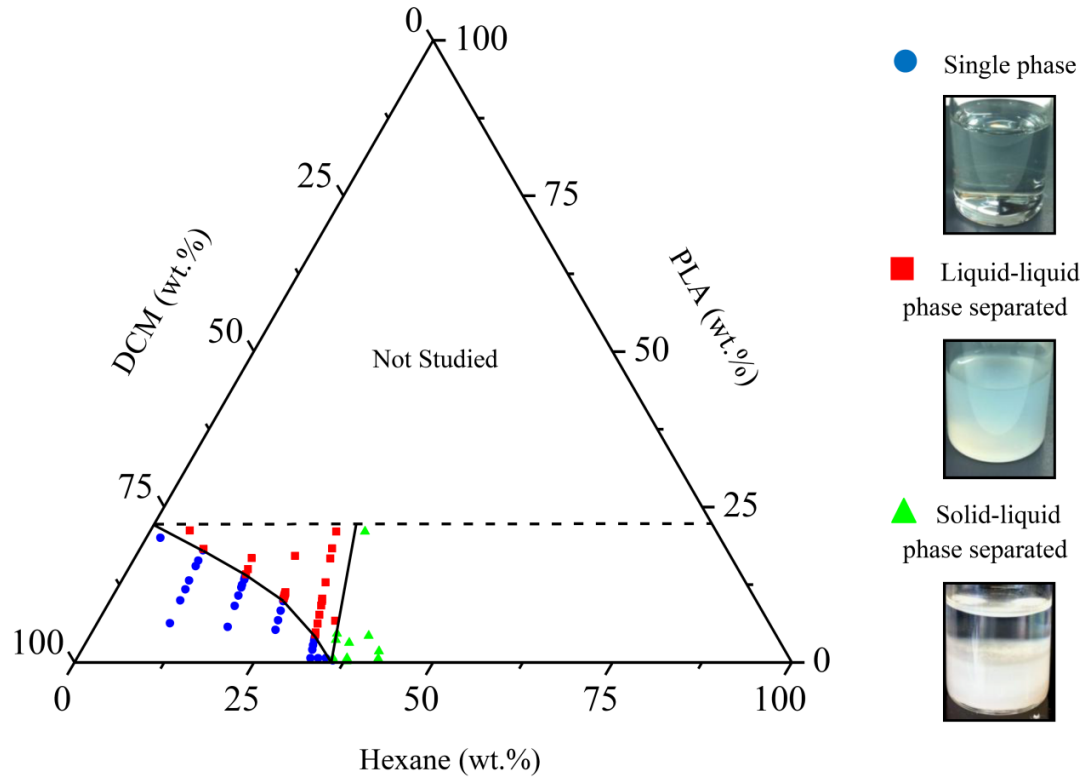
Fig. 4. 3. The results of all the experiments in the PLA-DCM-hexane ternary phase diagram.

The liquid–liquid phase separation process in our system is mainly governed by spinodal decomposition for moderate to high PLA concentration resulting from micro-scale concentration fluctuations. The fine, homogeneous, interconnected morphology of the monolith shown in Fig. 4.2 also indicates the occurrence of spinodal decomposition. Nucleation and growth is most likely the phase separation mechanism occurring for the low PLA concentration samples [122, 131]. Spinodal decomposition occurs spontaneously for unstable conditions where only a negligible energy barrier exists, whereas, nucleation and growth, is favored under metastability [131]. The liquid-liquid phase separation leads to a polymer-rich phase which eventually forms the backbone of the monolith and a polymer lean phase filling in the channels [131]. The solid-liquid phase separation is expected to occur by the spinodal decomposition at the lower polymer

concentrations and nucleation and growth at the highest concentration [127]. Both result ultimately in the formation of semi-crystalline particles of PLA [130, 131].

It has been observed that some compositions in the liquid-liquid phase separated region reach a gelation point over time after the initial phase separation. Initially the system retains fluidity and resembles an emulsion and after the gelation point the submerged monolith is no longer fluid. These compositions are located towards the PLA and hexane rich corner of the liquid-liquid phase separated region. Gelation in such ternary systems including a crystallizable polymer is attributed to the crystallization of the polymer which occurs during the later stages of phase separation as the solvent diffuses from the polymer-rich phase to the polymer-lean phase [127, 130].

4.3.2. Experimental verification of the phase diagram

Since the lever rule is applicable to ternary phase diagrams, it can be used to further test our phase diagram. This rule provides information about the position of a mixture of two known compositions in the phase diagram. The composition of the mixture is on the line connecting those two primary points, and its exact position depends on the mixing weight ratio [148]. Eqs. 4.7 and 4.8 give the composition (point C) of the mixture of the starting compositions (points A and B). These equations are obtained based on the lever rule and an adaptation of the ternary phase diagram to the Cartesian coordinate system.

$$PLA_C = PLA_B - \alpha(PLA_B - PLA_A)$$

Eq. 4.7

$$DCM_C = DCM_B + \alpha(PLA_B - PLA_A + Hexane_B - Hexane_A)$$

Eq. 4.8

Here PLA_i is the weight% of PLA in the mixture at point i, and α is the weight fraction of composition A in the final mixture (i.e., $\alpha = BC/AB$ and $0 < \alpha < 1$). Note that the above equations require that $PLA_B \geq PLA_A$.

In order to use the lever rule to verify our phase diagram, 3 points (A, B_1 and B_2 in Fig. 4.4) were selected from different regions and 3 binary combinations were prepared by mixing, and the position of the resultant points (C_1, C_2 and C_3) on the phase diagram were calculated using Eqs. 4.7 and 4.8. The compositions of the initial mixtures and their binary combinations are presented in Table 4.4. The phase states of points C_1, C_2 and C_3 were liquid-liquid phase separated, single phase and single phase, respectively in accordance with the phase diagram.
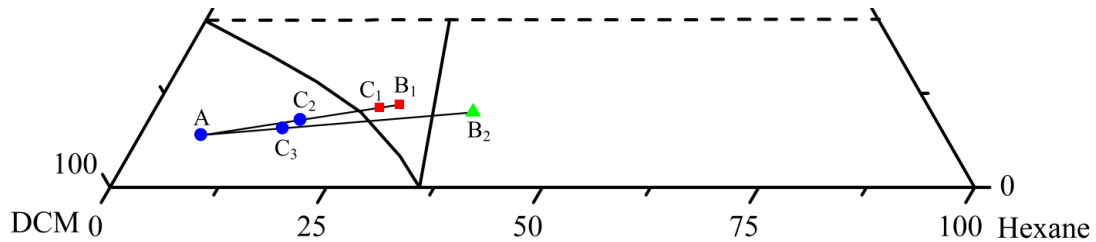
Fig. 4. 4. The compositions used in the lever rule tests.

Table 4. 4. Lever rule application for points in Fig. 4.4

Compositions of the starting points (wt.%)								
Point A (wt.%)			*Point B₁ (wt.%)*			*Point B₂ (wt.%)*		
PLA	DCM	Hexane	PLA	DCM	Hexane	PLA	DCM	Hexane
7	86	7	11	61	28	10	53	37
Lever rule; compositions of the mixtures (wt.%)								
Point C_1			Point C_2			Point C_3		
(mixture of A and B₁; α= 0.1)			(mixture of A and B₁; α= 0.5)			(mixture of A and B₂; α= 0.7)		
PLA	DCM	Hexane	PLA	DCM	Hexane	PLA	DCM	Hexane
10.6	63.5	25.9	9	73.5	17.5	7.9	76.1	16

Next, 3 new samples with compositions C_1, C_2 and C_3 were made by adding hexane to PLA-DCM solutions, and the turbidity of these samples as well as the samples which had been prepared via the lever rule, were measured every three hours over 24 hours, and the averages are presented in Fig. 4.5. The turbidities of samples with the same composition prepared in two routes are the same within experimental error, confirming that the lever rule is applicable to our phase diagram. These turbidity values

remain almost the same after 5 days, except for sample C_1 whose turbidity gradually increased up to ~ 450 NTU due to slow liquid-liquid phase separation.
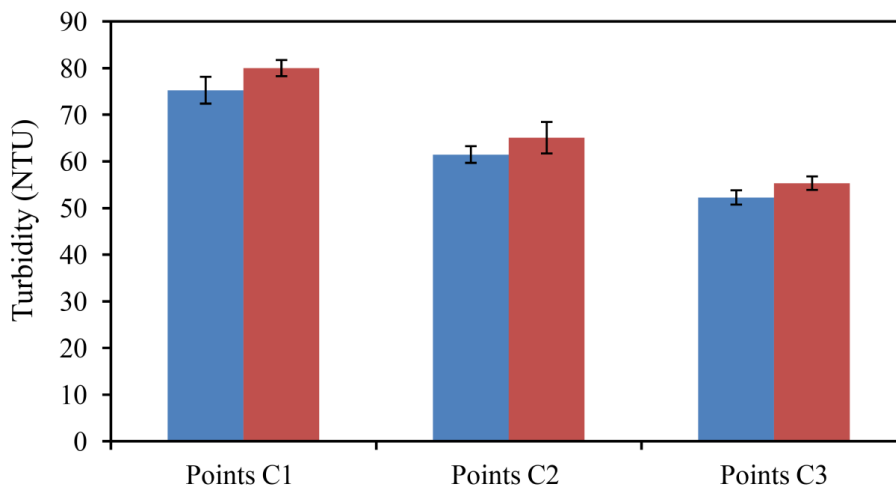
Fig. 4. 5. The turbidity measurements in average (8 measurements over 24 hours). Left columns: direct mixing of hexane with PLA-DCM solutions; right columns: the results of the lever rule.

4.3.3. Turbidity studies

Phase separation occurs for all compositions in the two-phase regions of the phase diagram, but the rate of phase separation varies significantly with composition. In Fig. 4.6, the turbidity versus time of 5 different systems is shown. The curves in this figure are the average of two sets of experiments. The sample with the highest PLA content (13 wt.%, 1 v/v) has the fastest phase separation kinetics, reaching 1100 NTU within 8 hours. In comparison, it takes 45 and 66 hours to reach the same turbidity for samples (10 wt.%, 1 v/v) and (7 wt.%, 1 v/v), respectively. Halving of the PLA concentration (13 wt.%, 1 v/v to 7 wt.%, 1 v/v), results in an ~ 8 times slower phase separation. This strong dependence of phase separation rate on PLA content means that the mass transfer between the polymer-rich and polymer-lean phases in sample (13 wt.%, 1 v/v) is faster during phase separation, most probably due to lower miscibility. Phase separation continues until the system reaches the viscous effect region [111] where the inter-phase mass transfer stops. After this point no further visible change is observed. This results in

the formation of a percolating polymer framework through the mixture. For the sample with lowest polymer concentration (1 wt.%, 1 v/v), essentially no change in turbidity was detected over 5 days, confirming that this sample is single phased. Sample (5 wt.%, 1v/v), which is very close to the experimentally determined binodal, shows a very small increase in turbidity after 5 days, indicating that the sample gradually undergoes phase separation at a very slow rate. The images of these five samples at different stages of the turbidity studies are shown in Fig. 4.7. In some cases, especially at turbidity less than 20 NTU, the naked eye cannot differentiate between the samples.
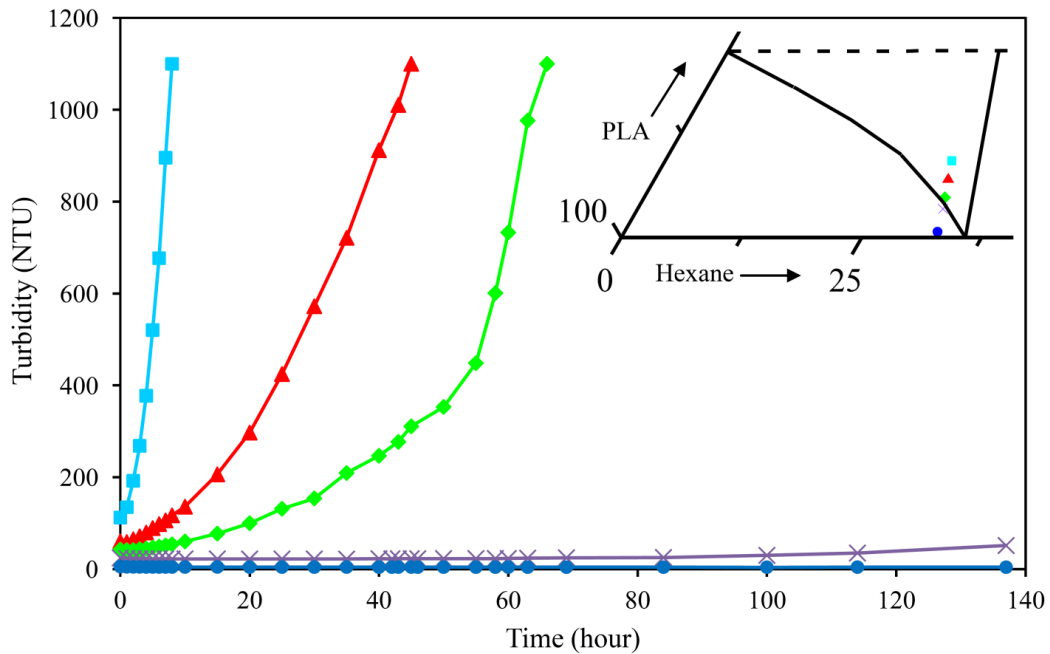
Fig. 4. 6. Kinetics studies using turbidity measurements. ■ (13 wt%, 1 v/v), ▲ (10 wt.%, 1 v/v), ◆ (7 wt.%, 1 v/v), ✕ (5 wt.%, 1 v/v) and ● (1 wt.%, 1 v/v). Standard deviation (SD) of all points < 5.

	1100 NTU	116.6 NTU	53.7 NTU	21.8 NTU	4.05 NTU
After 8 hours					
	>1100 NTU	1100 NTU	310.5 NTU	22.3 NTU	3.97 NTU
After 45 hours					
	>>1100 NTU	>1100 NTU	1100 NTU	23.8 NTU	3.95 NTU
After 66 hours					
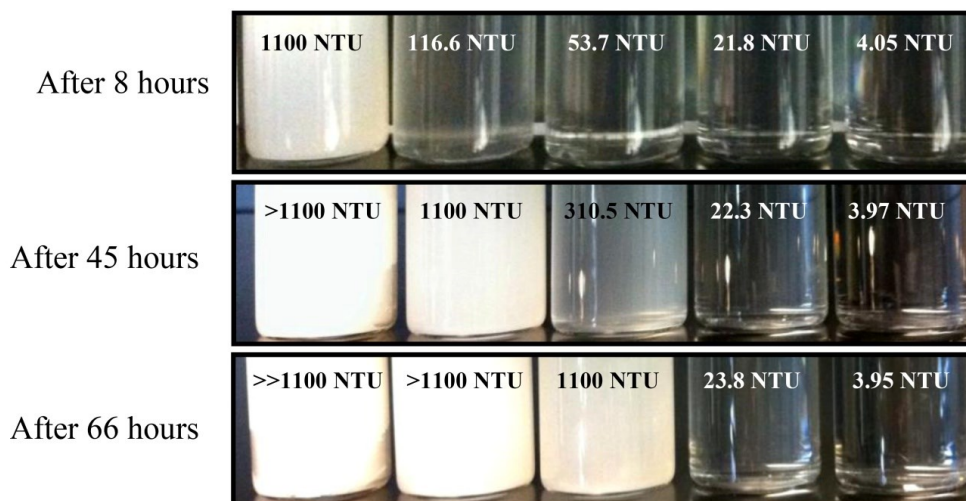
Fig. 4. 7. The physical appearance of the samples used for the turbidity studies at different stages. Left to Right: (13 wt.%, 1 v/v), (10 wt.%, 1 v/v), (7 wt.%, 1 v/v), (5 wt.%, 1 v/v) and (1 wt.%, 1 v/v). The background of the images is black to make a better contrast with the samples.

In order to be able to properly attribute turbidity changes after nonsolvent addition to phase separation, we must consider the linear increase in turbidity with polymer concentration in a single phase system (Fig. 4.8). The best fit line (Eq. 4.9) provides an accurate ($R^2 = 0.98$) relationship between the concentration of the PLA in DCM solutions and their turbidity values

$$T = 5.25 X_{PLA} + 2.07$$

Eq. 4.9

where T and X_{PLA} are turbidity (NTU) and the concentration (wt.%) of the PLA in DCM solution, respectively. Since no chemical reaction occurs between PLA and DCM, this line is expected to be valid for even higher concentrations.
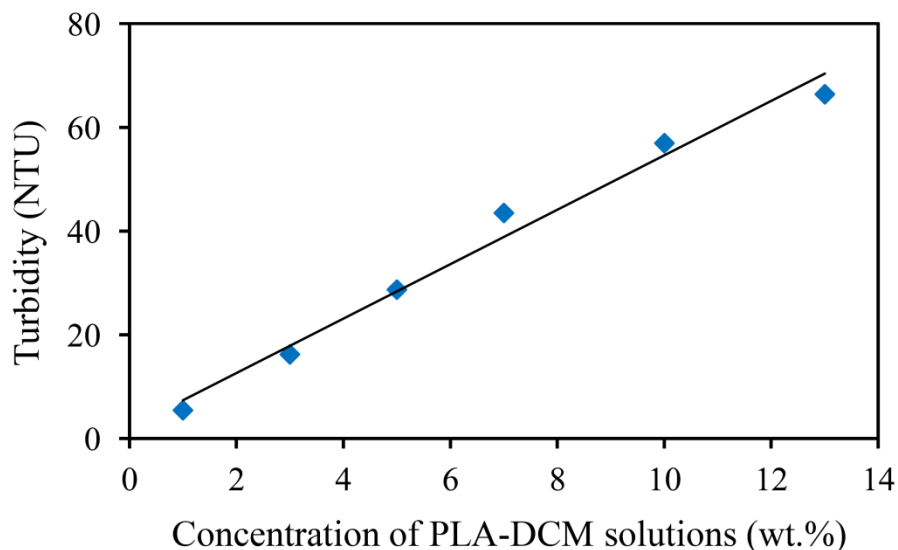
Fig. 4. 8. Turbidity vs. the concentration of PLA-DCM solutions. SD of all points < 2.

In Fig. 4.9, the turbidity of samples (1 wt.%, 1 v/v) and (1 wt.%, 1.25 v/v) are shown over 5 days. These compositions are in the single phase and solid-liquid phase separated regions of the phase diagram, respectively (Table 4.3). The turbidity of both samples decreases from ~ 7.3 NTU (Eq. 4.9) to ~ 4.5 NTU (Fig. 4.9) upon nonsolvent addition, due to the low turbidity of hexane (~ 0.08 NTU) and to the absence of liquid-liquid phase separation. The turbidity of sample (1 wt.%, 1.25 v/v) gradually drops over the first 40 hours due to precipitation, while the turbidity of sample (1 wt.%, 1 v/v) is essentially constant. After ~ 55 hours, the turbidity of sample (1 wt.%, 1.25 v/v) increases about 0.43 NTU over 14 hours, and plateaus. As shown in the image in Fig. 4.9, the precipitation of a very thin layer of PLA on the wall of the cuvette has resulted in the higher turbidity. The turbidity of the liquid phase after transferring to a clean cuvette was found to be 0.7 NTU, which is very close to that measured for a mixture of hexane and DCM at v/v = 1.25. This indicates that the precipitation of sample (1 wt.%, 1.25 v/v) is complete after ~ 70 hours. This is also in agreement with our visual inspection results (Table 4.2).

Di Luccio et al. [111] also showed that the precipitation rate in a similar ternary system is strongly related to the polymer concentration. In our system, we observe the

same phenomenon. For example, complete precipitation occurs within less than 10 seconds for sample (7 wt.%, 1.25 v/v).
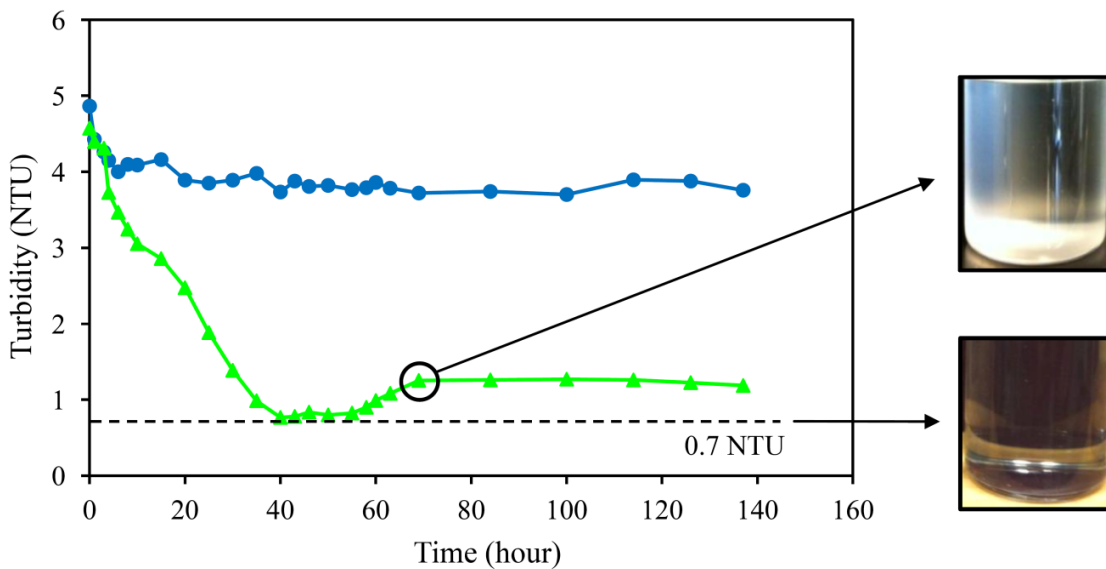
Fig. 4. 9. Kinetic studies on samples: ● (1 wt.%, 1 v/v) and ▲ (1 wt.%, 1.25 v/v). The turbidity of the liquid phase of sample (1 wt.%, 1.25 v/v) is 0.7 (dashed line). SD of all points < 0.06.

4.4. Conclusion

The ternary phase diagram for PLA-DCM-hexane system was developed experimentally by identifying the boundaries between single phase, liquid-liquid phase separated and solid-liquid phase separated regions. The detailed procedure developed here is general and can be used for similar systems. The validity of the phase diagram was verified by the lever rule. Kinetics studies using turbidity measurements showed that increasing PLA concentration significantly speeds up the phase separation kinetics. Considering the increasing applications of PLA in forms such as foam, fiber and membrane, identification of different phase regions in the PLA-DCM-hexane phase diagram, facilitates nonsolvent-involved fabrication processes such as NIPS and immersion-precipitation.

Chapter 5

Production of porous polylactic acid monoliths via nonsolvent induced phase separation[1]

Ehsan Rezabeigi, Paula M. Wood-Adams and Robin A.L. Drew

Department of Mechanical and Industrial Engineering, Concordia University
Montreal, QC H3G 1M8, Canada

Abstract

Polylactic acid (PLA) is one of the most promising polymers for use as the matrix of a bone scaffold. In this work, porous PLA monoliths are fabricated via nonsolvent induced phase separation using dichloromethane as a solvent and hexane as a nonsolvent. The PLA-dichloromethane-hexane compositions which undergo liquid-liquid phase separation followed by gelation are shown to allow for the production of high quality foams. Solvent exchange with methanol after aging the gel is found to substantially reduce shrinkage during drying. Using this simple, versatile and template-free method we produced PLA foams with porosities as high as ~90.8%, specific surface area up to 54.14 m^2/g, crystallinity up to 62.6% and compressive modulus ranging from 1.8 to 57 MPa. Depending on ternary mixture concentration and standing temperature a range of mesoporous and combined meso/macroporous morphologies suitable for use as a bone scaffold are produced.

Keywords: Polylactic acid, scaffold, foam

5.1. Introduction

Polymer foams are well-known for the ease of processing and high specific surface area [103]. Porous polymers in the form of particles, fibers, films, membranes and monoliths are used in many fields such as cushioning, packing, filtration, thermal and/or mechanical insulation, electronics, smart materials and biomedical applications [103, 104, 106, 117, 151]. Porous polymer monoliths are also widely used as the precursor template for the production of other porous materials [103]. Thus, many polymer foaming methods have been developed to meet the various requirements of each application [104].

Template-based foaming techniques [103] such as colloid crystal templating [117], "gas-based techniques" [106] such as those involving supercritical fluids (especially CO_2) [106, 107], and more recently, thermally induced phase separation (TIPS) and 3D printing [14, 122, 152] are commonly used for foaming of thermoplastics. In order to increase the process flexibility, some combinations of these techniques have also been developed such as combined injection molding/TIPS [153], and nonsolvent induced phase separation (NIPS)-based 3D printing of scaffolds with a maximum porosity of 75.8 ± 1.9 [154]. Dhandayuthapani et al. [14] thoroughly classified the fabrication techniques for polymer-based scaffolds.

Although nonsolvent-involved technologies have been used for almost 50 years for the fabrication of membranes, the production of porous monoliths via NIPS has only been studied in a limited way [103, 104, 125, 151, 155]. Advantages of NIPS such as versatility, simplicity and room temperature processing, make this technique very promising. Also, the shape of the final monolith can be determined with a mold wherein the phase separation and gelation occur [3, 125, 155]. NIPS-derived porous polymers are typically expected to be isotropic [117], highly porous and fully interconnected [105, 117, 125]. The phase separation mechanism and consequently the morphology and properties of the final porous products are strongly dependent on the phase separation standing temperature, polymer concentration and its molecular weight, the nonsolvent to solvent ratio as well as their nature [125, 155].

The NIPS process can be understood by the Flory-Huggins theory for the polymer-solvent-nonsolvent ternary systems [118, 155]. Addition of nonsolvent to a polymer solution increases the Gibbs free energy of the system which may consequently result in phase separation [118, 125, 155]. The phase separation continues until the combination of the two phases reaches a stable condition with the lowest free energy. Depending on the composition and temperature this condition can be liquid-liquid phase separated or solid-liquid phase separated. The solid-liquid phase separated system includes the polymer precipitate and a polymer-lean liquid phase with a clear boundary in between the two phases. Liquid-liquid phase separation leads to the formation of an interpenetrating network structure of a polymer-rich phase consisting of the polymer and a portion of the solvent, and a polymer-lean phase which contains the nonsolvent and the remaining solvent. At this stage the mixture simply appears cloudy even though two distinct phases coexist. The polymer-rich and polymer-lean phases will form the monolith skeleton and pores respectively after aging and drying [118, 125, 155]. Shrinkage and densification caused by pore collapse due to capillary forces are important challenges associated with the drying of gels obtained from the aged phase separated system [156, 157]. The Young-Laplace equation (Eq. 5.1) gives the pressure difference (Δp) between the liquid phase of the gel and its vapor, reflecting the capillary forces applied on the pores during drying.

$$\Delta p = \frac{2\gamma}{r}$$
Eq. 5.1

Here γ is the liquid-vapor (surface) tension and r is the mean pore radius [156, 157].

The use of higher than room temperature drying temperatures to facilitate evaporation of the solvent(s) is not possible in the case of many polymers such as polylactic acid (PLA) due to the low glass transition temperature [75, 88, 155, 158]. Supercritical drying can be used to transform gels into aerogels with almost no capillary forces involved [156]. In our NIPS process, the issue with the gel shrinkage is mitigated and the effect of drying is examined on shrinkage and the crystallinity of the monoliths.

PLA is an environmentally friendly thermoplastic with relatively high melting point as well as good biodegradability, biocompatibility and mechanical properties [75, 88, 155, 158]. Since lactic acid has asymmetric molecular structure, PLA can be found as L-PLA (PLLA), D-PLA (PDLA), and D,L-PLA (PDLLA) with different properties. Due to these properties along with the polymerization process which makes PLA inexpensive among the aliphatic polyesters, this polymer has been extensively studied, produced and used in many applications [88, 105, 151]. PLA has been approved by the US Food and Drug Administration (FDA) for clinical applications; for example, PLA bioresorbable sutures are used clinically [14, 75, 155]. PLA has been shown to have a low adverse body response when used as soft or hard tissue implants. Most research is currently focused on using this polymer as a matrix for bone scaffolds [3, 7, 105, 109].

An ideal polymer-based composite scaffold must be highly porous and consist of both interconnected mesopores and macropores (>100 μm) which are important for the attachment of bone cells (mesopores), and vascularization and bone ingrowth (macropores) respectively [3, 106]. Thus, a versatile polymer foaming technique is required to create the desirable morphology and properties for this application.

The great potential of NIPS for the production of porous polymer monoliths is the main motivation for the current study. In our previous work [155], the PLA - DCM (solvent) - hexane (nonsolvent) phase diagram was experimentally developed at room conditions. The liquid-liquid phase separated region of this diagram was identified and is used in this study to develop a NIPS procedure for producing PLA foams. The resultant foams are then characterized in terms of porosity, shrinkage, morphology, crystallinity and mechanical properties. The phase separation mechanism is identified for each composition and temperature by considering the morphology observations [122, 128, 155].

Although crystallization from melt and solution for PLA has been well studied [7, 88, 109, 159], there is still a lack of detailed information about crystallization during phase separation in a ternary system containing a nonsolvent [125]. PLA is a crystallizable polymer and depending on the D and L isomeric contents and its thermal/process history, it can be semi-crystalline (PLLA and PDLA) or amorphous (PDLLA) [88, 155]. In our study the effects of phase separation temperature, drying

87

conditions and the nonsolvent/solvent ratio on the crystallinity of the foams are also investigated elucidating the crystallization and phase separation processes.

We demonstrate that highly porous, semi-crystalline PLA foams with high specific surface area, unique morphologies and high mechanical properties can be produced by NIPS process which is a simple, flexible method.

5.2. Experimental procedure

5.2.1. Materials

High average molecular weight PLA (M_n = 97000, M_w/M_n = 2) with 1.6% D-lactide was obtained from NatureWorks LLC (Ingeo™ Biopolymer 4032D). This molecular weight is calculated based on solution viscosity measurements conducted on our PLA batch by the supplier. Dichloromethane (DCM, Fisher Chemical; Stabilized/Certified ACS, ≥99.5), hexanes (Fisher Chemicals; Certified ACS, ≥98.5 %), and methanol (Fisher Chemicals; Certified ACS, 99.9 %) are also used. The physical and chemical properties of these materials which may be useful for the results and discussion section are presented in Ref. [155].

5.2.2. Fabrication of PLA foams

PLA-DCM-hexane mixtures in liquid-liquid phase separated form are used to create PLA foams via the NIPS process [155]. The mixtures of appropriate ternary compositions are prepared as described in Ref. [155]. Then phase separation process occurs by storing the tightly sealed vials containing the mixtures under atmospheric pressure and one of 4 standing temperatures (-23 °C, 4 °C, 23 °C and 40 °C). The majority of experiments are performed under ambient conditions (23 °C) and selected system compositions are evaluated at the other phase separation standing temperatures. Note that when phase separation occurs at temperatures other than room temperature the process can be considered to be a combination of NIPS and TIPS techniques. Depending on the composition of the system and the standing temperature, some mixtures undergo

gelation as a result of phase separation. The gels are allowed to age at room temperature for an additional 10-30% of their gelation time. The gel point for these liquid-liquid phase separated systems is defined as the loss of fluid-like behavior [118]. The wet, aged gels are removed by breaking their glass vessels. Cubic specimens are carefully cut from the central portion of the gels, and immediately immersed in ~150 ml methanol (Fig. 5.1). The cubes are suspended on a mesh platform while the methanol is gently stirred in order to improve the solvent exchange process which lasts for 30 hours. The methanol is completely replaced once during this process.

After the solvent exchange stage, the methanol-soaked, cubic monoliths are obtained and their dimensions are measured using a caliper. The samples are then dried in air at room temperature on a mesh platform for up to 24 h. Drying is assumed to be complete when the weight of the monolith does not change when placed under vacuum for several hours (70 cmHg). These conditions were determined by exploring the effect of the lack of solvent exchange and vacuum drying on the crystallinity of the foam. The linear shrinkage is determined from the dimensions of the dry and wet monoliths. Cubes of $5 \times 5 \times 5$ mm^3 are precisely cut from the centre of the dry monoliths where they are more homogenous. The apparent densities of these cubes are determined from mass and volume. The monoliths are kept stored in a desiccator for further characterization.
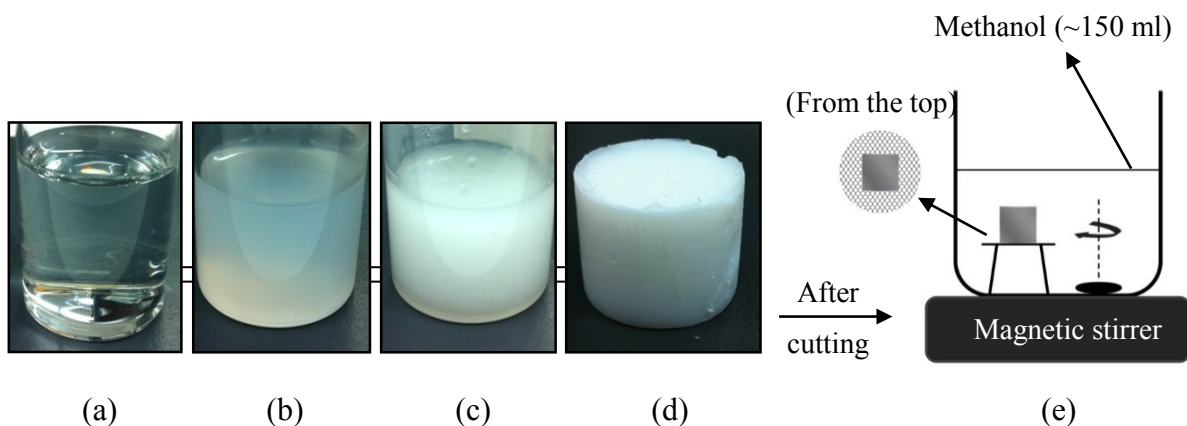
Fig. 5. 1. Steps involved in the NIPS process to create the monoliths: PLA in DCM solution (a), liquid-liquid phase separated system (b), aging gel (c), the wet, aged gel (d) and solvent exchange (e) which is followed by drying in air.

5.2.3. Characterization of the foams

The specific surface area and mean pore size of the monoliths are measured by Brunauer–Emmett–Teller (BET) N_2 adsorption–desorption test (Tristar 3000 V6.07) at 77.3 K, after a degassing step. Morphology of the monoliths are examined by scanning electron microscopy (SEM; HITACHI, S-3400N) using secondary electron mode under high vacuum. The foam specimens are coated with Au/Pd (70/30 wt.%) using a rotary-pumped sputter coater (Quorum, Q150R ES). Note that the best images were obtained from the fracture surface of the foams. Micro-CT analysis (SKYSCAN 1176) is used for obtaining three-dimensional images of the morphology. For this purpose, the cubic samples are used with no additional preparation.

Differential scanning calorimetry (DSC; TA Instruments, Q10) analysis was performed (5 °C/min, nitrogen atmosphere) using sealed aluminum pans in order to obtain the crystallinity of the foams.

Compression tests are performed on cubic foams (5×5×5 mm^3) using a DMA, TA Instruments, Q800 instrument. The load is applied by ramping from 0.05 N to a maximum of 15 N at a rate of 0.5 N/min. The modulus of the foams is then determined from the slope of the elastic portion of the stress-strain curves (only if $R^2 > 0.95$). The plates and the contacting faces of the samples must be completely parallel for accurate results.

5.3. Results and discussion

5.3.1. Porosity and morphology

In order to fabricate NIPS-derived foams, the starting ternary composition must undergo liquid-liquid phase separation and it also must form a gel. Compositions within the liquid-liquid phase separated region in the PLA-DCM-hexane phase diagram that undergo gelation within 20 days are shown in Fig. 5.2 (shaded area in figure). It is believed that crystallization in the polymer-rich phase leads to gelation [118, 155] where micro-crystallites act as crosslinks and result in the formation of a three-dimensional

percolating network-like structure [118]. The main focus of the current work is on the systems containing hexane/DCM = 1 (v/v) and various PLA contents within the gelation window because they are the most useful for the production of scaffolds. Systems with v/v < 1 exhibit much longer gelation times (8-20 days) compared to those of systems containing v/v = 1 (Table 5.1). Less hexane and more DCM (i.e., v/v < 1) in systems with the same PLA concentration result in a lower ΔG according to Eq. 4 of Ref. [155], causing a reduced likelihood for phase separation followed by crystallization and gelation.
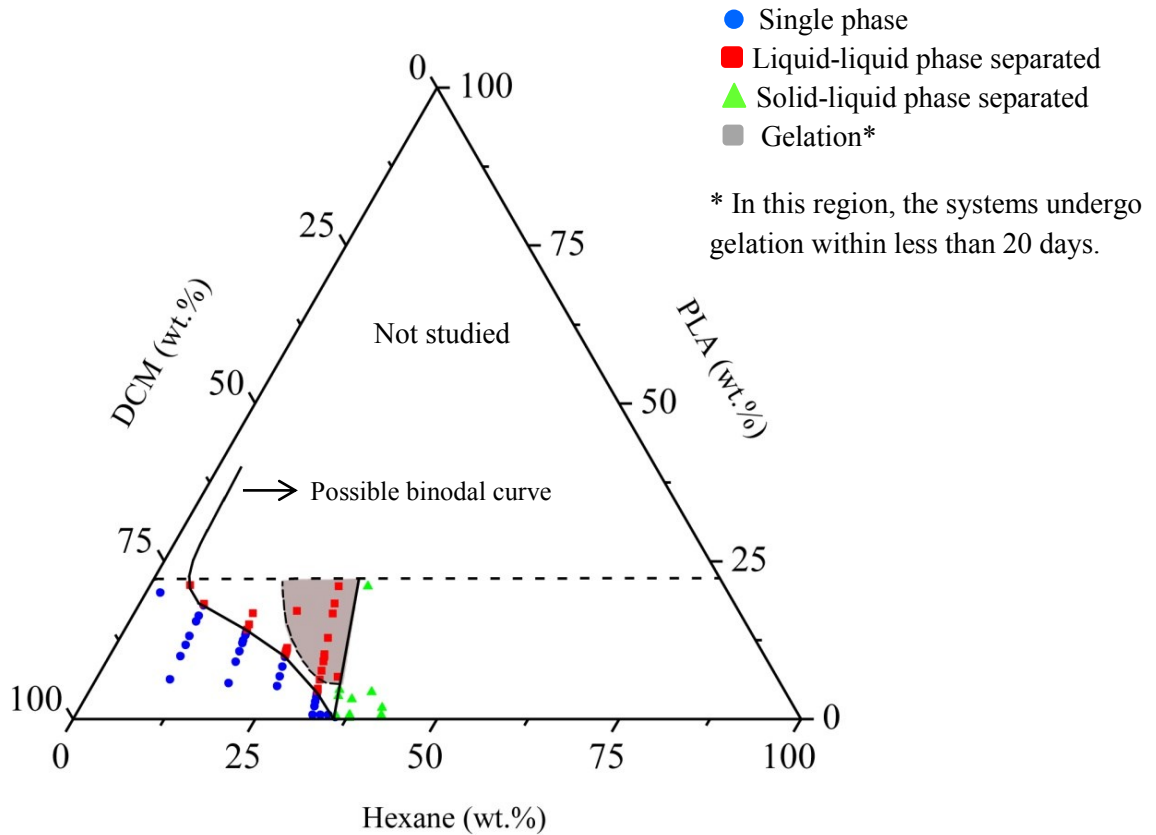
Fig. 5. 2. The phase diagram of the PLA-DCM-hexane system experimentally developed at room temperature (23 °C) based on a 14-day observation [155]. The binodal most likely curves up as indicated after the last liquid-liquid phase separated experimental point (■). Note that the sets of linearly arranged experimental points (■) represent hexane/DCM ratios 1, 0.75, 0.5 and 0.25 from right to left.

Table 5.1 presents the gelation time, apparent density and linear shrinkage of the foams prepared from mixtures with hexane/DCM = 1 v/v (Fig. 5.2) at phase separation standing temperatures of 23 °C and -23 °C. The linear shrinkage (Table 5.1) is isotropic except for the monolith with the lowest PLA concentration (10 wt.%, 1 v/v, 23 °C) where twisting also occurs (Fig. 5.3a). The samples that shrink isotropically are essentially crack-free even for high values of shrinkage [156, 157].

Table 5. 1. Gelation time, linear shrinkage and apparent density of monoliths containing hexane/DCM = 1 v/v presented as mean ± standard deviation (n = 4)

Systems[a]	Gelation time	Linear shrinkage in 3 directions (%)			Apparent density (g/cm^3)
		Width (W)	Length (L)	Thickness (T)	
(7 wt.%, 1 v/v, 23 °C)	N/A[b]	N/A	N/A	N/A	N/A
(10wt.%, 1 v/v, 23 °C)	15 ± 1.5 days	50.9 ± 3.0	48.6 ± 2.9	45.7 ± 5.5	0.63 ± 0.03
(13 wt.%, 1 v/v, 23 °C)	3 ± 0.5 days	46.7 ± 2.0	47.1 ± 1.5	46.5 ± 3.0	0.69 ± 0.03
(15 wt.%, 1 v/v, 23 °C)	24 ± 3 h	45.0 ± 1.0	43.5 ± 0.7	44.5 ± 0.7	0.75 ± 0.04
(17 wt.%, 1 v/v, 23 °C)	8 ± 2 h	27.6 ± 7.5	27.6 ± 8.0	27.3 ± 9.5	0.44 ± 0.18
(18 wt.%, 1 v/v, 23 °C)	6.5 ± 0.5 h	1.5 ± 0.5	1.8 ± 0.6	2.2 ± 0.7	0.14 ± 0.01
(20 wt.%, 1 v/v, 23 °C)	115 ± 15 min.	2.5 ± 0.5	2.0 ± 0.3	2.5 ± 0.2	0.15 ± 0.01
(23 wt.%, 1 v/v, 23 °C)	40 ± 6 min.	1.3 ± 0.2	1.6 ± 0.3	1.1 ± 0.3	0.19 ± 0.01
(25 wt.%, 1 v/v, 23 °C)	30 ± 5 min.	1.6 ± 0.3	2.0 ± 0.5	1.8 ± 0.5	0.20 ± 0.02
(13 wt.%, 1 v/v, -23 °C)	~ 4 h	3.6 ± 0.3	3.2 ± 0.3	3.8 ± 0.2	0.12 ± 0.02
(23 wt.%, 1 v/v, -23 °C)	~ 10 min.	3.5 ± 0.5	3.9 ± 0.4	4.2 ± 0.5	0.20 ± 0.01

(a) System (X wt.%, Y v/v, T °C) corresponds to a system of PLA-DCM solution (X wt.%) mixed with hexane at a nonsolvent to solvent volume ratio of Y (v/v) which is allowed to undergo phase separation at a temperature of T °C.
(b) No gelation occurs within 20 days.

(a)   (b)
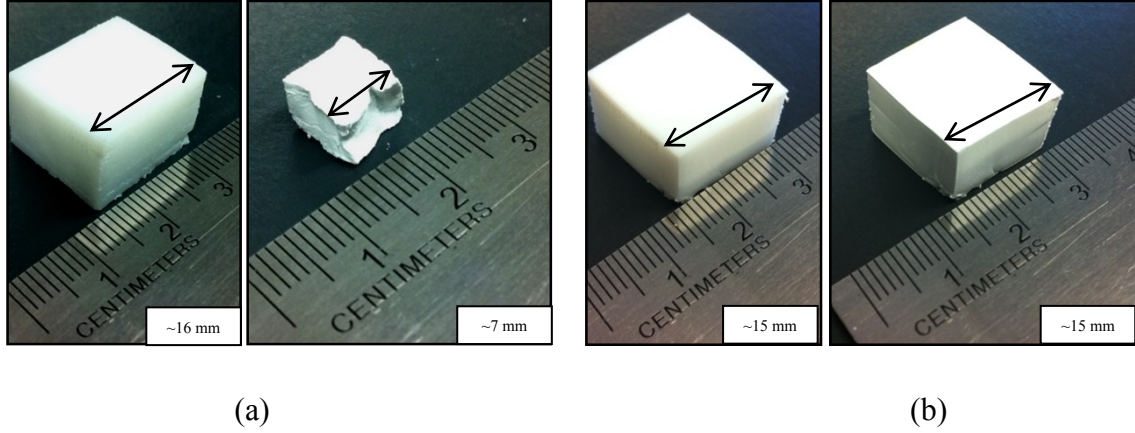
Fig. 5. 3. The physical appearance of methanol soaked gels (left images) and air dried gels (right images) corresponding to compositions of Table 5.1: (a) (10 wt.%, 1 v/v, 23 °C) and (b) (18 wt.%, 1 v/v, 23 °C).

Using the apparent density of the foams and Eq. 5.2, the porosity of the foams can be calculated [7, 104].

$$P = 1 - \frac{\rho}{\rho_\circ}$$
Eq. 5.2

Here P represents the foam porosity, ρ/ρ_o is the relative density [104] where ρ and ρ_o are respectively the foam apparent density (Table 5.1) and the density of the nonporous PLA [160] which can be calculated from Eq. 5.3 [161].

$$\rho_\circ = w_c(\rho_c - \rho_a) + \rho_a$$
Eq. 5.3

Here w_c is the crystalline volume fraction and ρ_a and ρ_c are respectively the density of fully amorphous (1.248 g/cm^3) and crystalline (1.290 g/cm^3) PLA [75, 161]. The porosity of the foams must be calculated based on the density of the nonporous PLA with the same degree of crystallinity. It will be shown in section 5.3.2 that all of the NIPS-derived foams are semi-crystalline and their crystallinity depends on the composition of the system and the preparation conditions such as phase separation standing temperature. The

corresponding mean crystallinity values are obtained from the results presented in section 5.3.2 in order to calculate the actual ρ_o values.

Fig. 5.4 illustrates the dependency of porosity and linear shrinkage on initial PLA in DCM concentration. Three regions can be distinguished in this figure: at low PLA concentrations we have a region of fragile gels and at high PLA concentrations we have a region of resilient gels with a transition zone in between. In the following paragraphs we will examine the porosity, shrinkage, microstructure and specific surface area in each of these three regions.
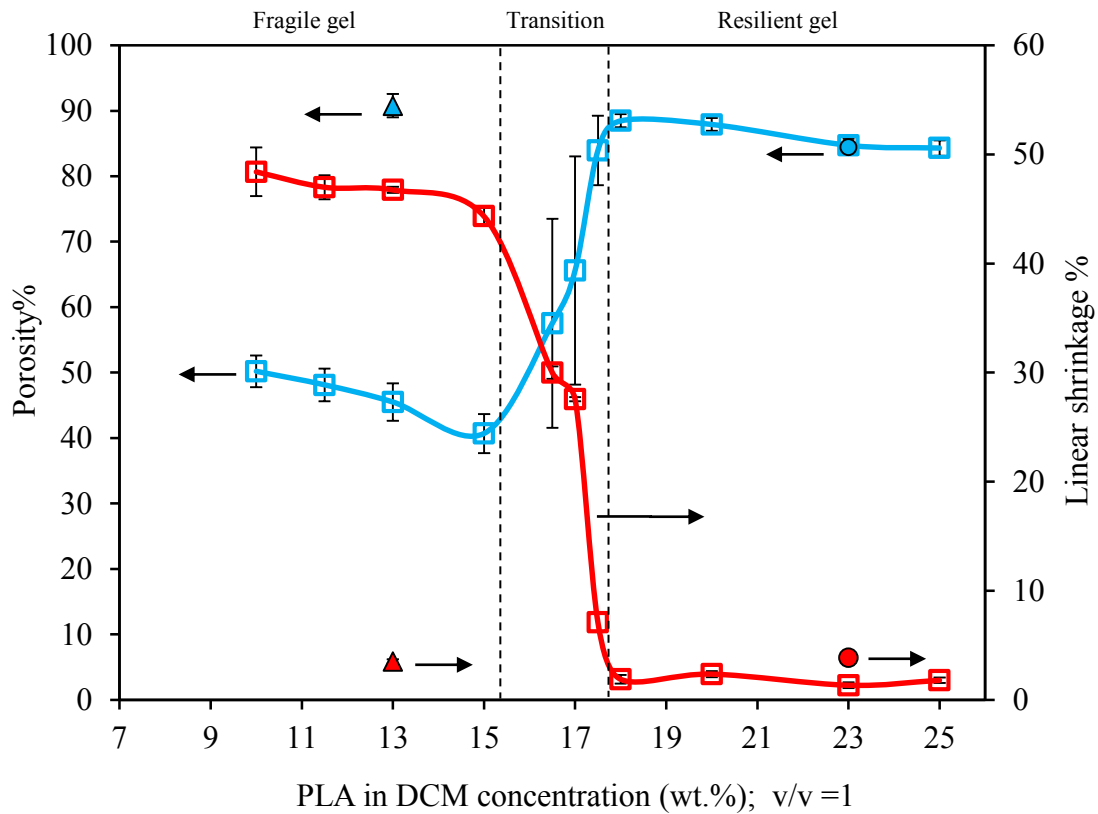
Fig. 5. 4. Porosity and average linear shrinkage versus PLA in DCM concentration of original mixture (n=4): □ shrinkage and □ porosity of the systems phase separated at ambient conditions (23 °C), ▲shrinkage and ▲porosity of (13 wt.%, 1 v/v, -23 °C), and ● shrinkage and ● porosity of (23 wt.%, 1 v/v, -23 °C).

At low PLA concentrations and ambient standing temperature, the phase separation and pore formation mechanism is most likely nucleation and growth [122, 155]. Since the gelation times are long for these compositions (1 to 16 days), large pores and high porosity might have been theoretically expected [122, 125, 155]. However, the thin skeleton of these monoliths are not strong enough to resist the capillary forces induced during drying leading to severe pore collapse [156, 157]. This results in high shrinkage and low porosity as can be seen in Fig. 5.4. The impact of substantial shrinkage on the morphology of these foams can be seen in SEM images (Fig. 5.5 a, b and c). The expected nucleation and growth microstructure is not observed because of severe pore distortion due to shrinkage. Crystallization of PLA immediately after the liquid-liquid phase separation process provides more strength for the PLA framework leading to the formation of final foams whose microstructures are presented in the following. The crystallization of PLA during the phase separation is discussed further in section 5.3.2.

In the case of low PLA concentration and low standing temperature (13 wt.%, 1 v/v, -23 °C) the system exhibits a very low shrinkage and the highest porosity of all the systems studied. The low shrinkage of this system is due to the presence of very large pores in its morphology (Fig. 5.6 a and c) which are less affected by capillary forces during drying according to Eq. 5.1. A bimodal pore size population, large spherical pores (Fig. 5.6 a and c) combined with much smaller pores (Fig. 5.6e), results in much higher porosity compared to that of the monolith of the same composition but phase separated at room temperature (Fig. 5.5b). The formation of this dual morphology can be understood by considering Eqs. 1-4 in Ref. [155]. According to these equations, the Gibbs free energy of a ternary system rapidly drops at lower temperatures combined with the presence of the nonsolvent hexane, facilitating the occurrence of phase separation. Under these conditions, the polymer lean nuclei grow quickly into large spheres [104] at -23 °C due to rapid DCM diffusion from the polymer-rich to polymer-lean phase as a result of lower solubility of PLA in DCM at such a low temperature. As a result, the polymer-rich phase becomes so concentrated in PLA and very lean in DCM and hexane that its composition is most likely located close to the PLA-rich corner of the phase diagram. The formation of the mesoporous, needle-like morphology (Fig. 5.6e) is likely a result of crystallization of PLA from this highly concentrated solution [118, 119, 122, 162].
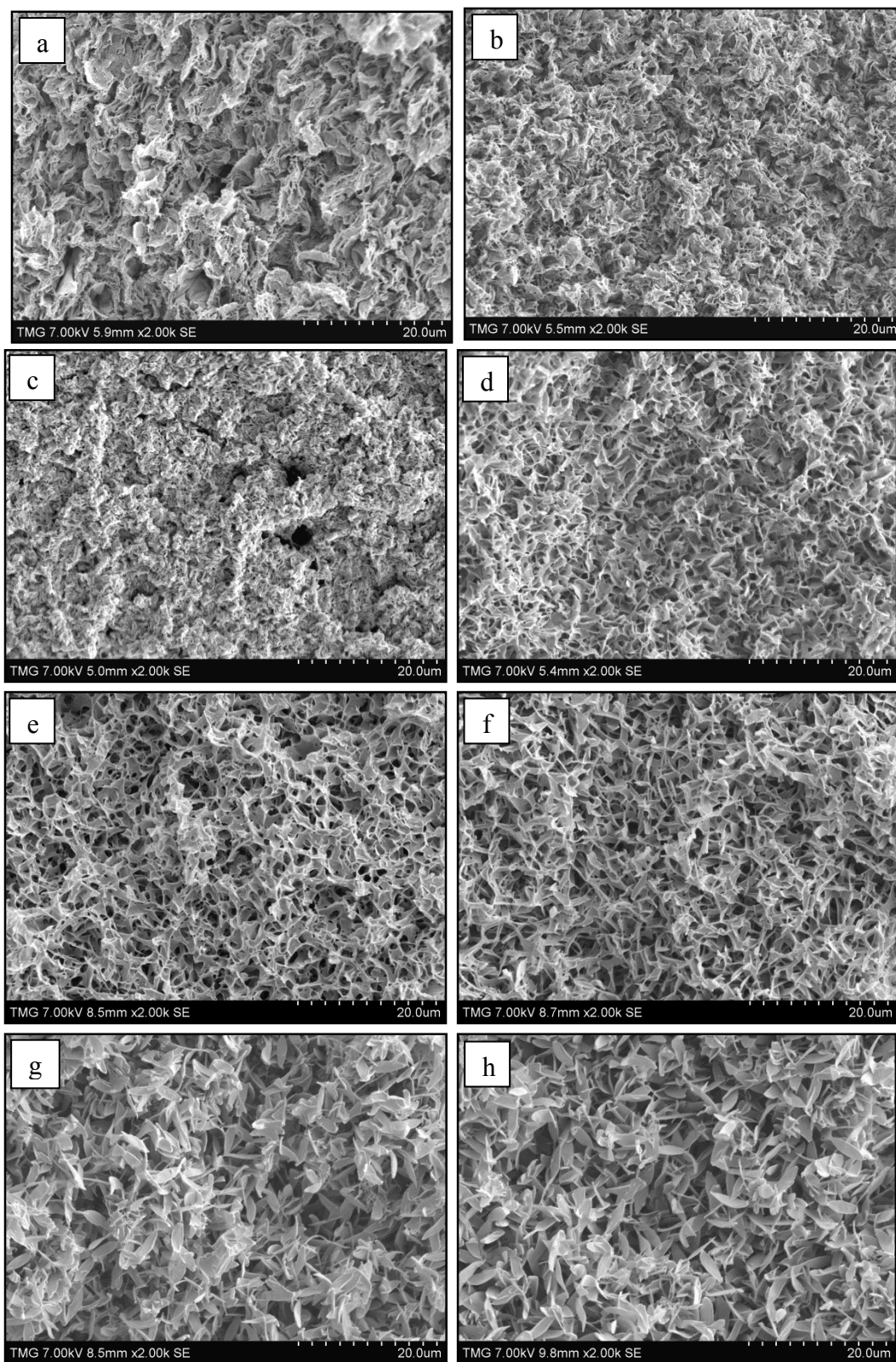
Fig. 5. 5. SEM images of the monoliths prepared at ambient conditions (23 °C); initial PLA in DCM concentrations (wt.%) of a) 10, b) 13, c) 15, d) 17, e) 18, f) 20, g) 23 and h) 25.
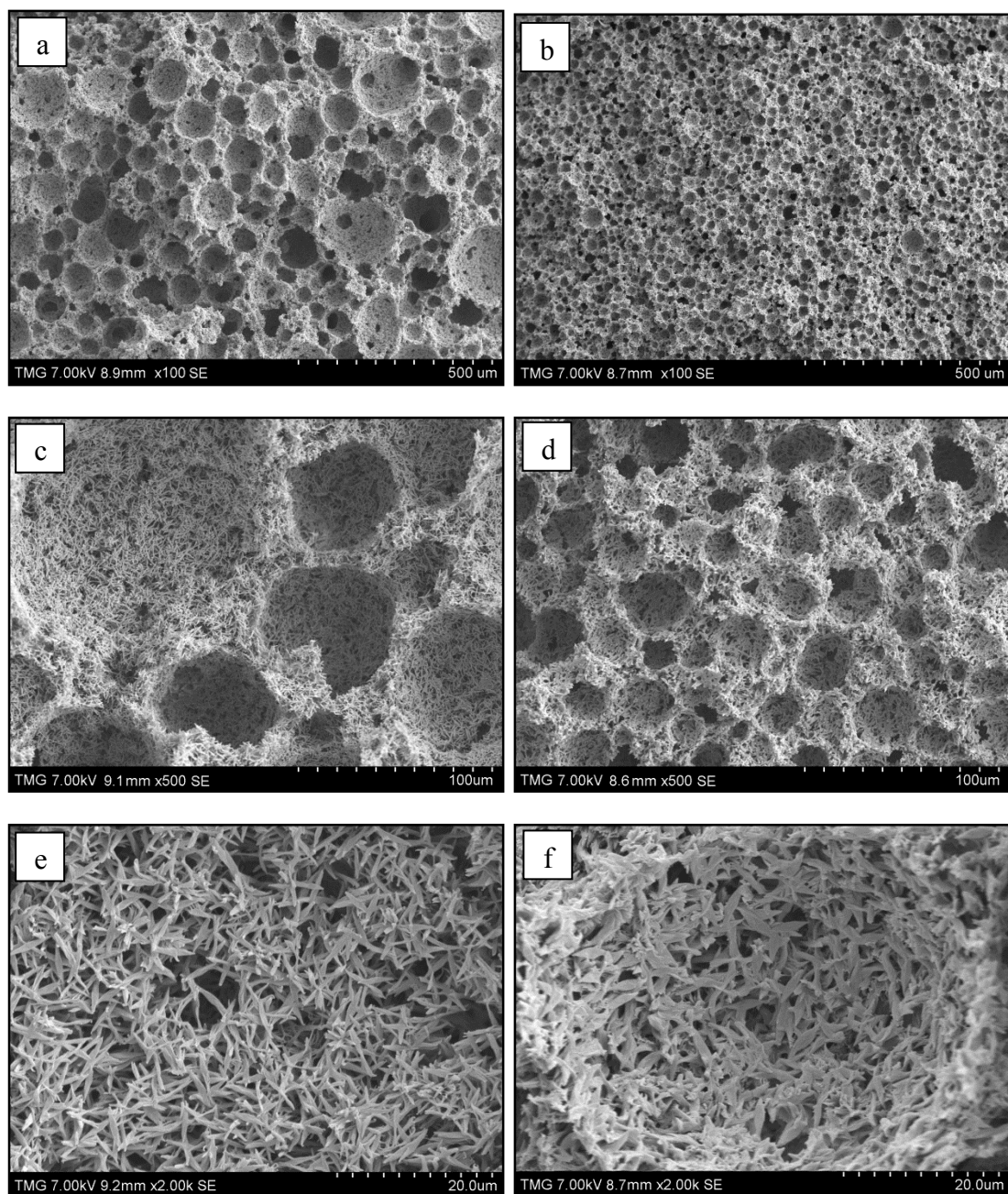
Fig. 5. 6. SEM images at various magnification of two systems of different composition which are phase separated at -23 °C: left: (13 wt.%, 1 v/v) and right: (23 wt.%, 1 v/v).

The BET results for the fragile gel systems (10 wt.%, 1 v/v, 23 °C) and (13 wt.%, 1 v/v, 23 °C) presented in Table 5.2 indicate that the former has some closed pores since its specific surface area is much less than that of the latter although its porosity is higher. The BET technique cannot detect closed pores while the porosity which is based on

apparent density clearly incorporates all pores. The closed pores are also visible in the SEM image of this sample (Fig. 5.5a).

Table 5. 2. The results of BET analysis

Systems	Specific surface area (m²/g)	Mean pore size (nm)	Region (Fig. 5.4)
(10 wt.%, 1 v/v, 23 °C)	29.33	12.1	Fragile gel
(13 wt.%, 1 v/v, 23 °C)	41.80	14.2	
(17 wt.%, 1 v/v, 23 °C)	45.75	10.1	Transition
(18 wt.%, 1 v/v, 23 °C)	54.14	10.3	Resilient gel
(25 wt.%, 1 v/v, 23 °C)	45.36	15.7	

By increasing PLA concentration above 15 wt.%, the skeleton of the foams becomes thicker and shrinkage decreases since a portion of the pores do not collapse in response to the capillary forces (transition region in Fig. 5.4). Since capillary forces and the strength of the skeleton balance each other, the transition occurs sharply over a narrow composition range (~ 15 – 18 wt.%, 1 v/v). This means that in this region even a small variation in composition and/or preparation procedure significantly affects the final shrinkage and porosity, as reflected in large standard deviations (Fig. 5.4). Note that the solvent and nonsolvent in this system are very volatile and such small compositional variations during preparation are likely [155]. The morphology in the transition region (Fig. 5.5d) is completely different from that in the fragile gel region: foam (17 wt.%, 1 v/v, 23 °C) has higher porosity and much less pore collapse and distortion. This also results in higher specific surface area for this foam (Table 5.2).

For the higher PLA in DCM concentrations (resilient gel region in Fig. 5.4), the foam skeleton is strong enough to resist the capillary forces leading to very small shrinkages (Fig. 5.3b) and high porosities. The SEM images (Fig. 5.5 e-h) show a noticeable difference in foam morphology in this region in comparison with those of the fragile gel foams, caused by different phase separation mechanisms and the occurrence or not of pore collapse. Considering that the spinodal is located above the binodal on the phase diagram (Fig. 5.2), these high PLA concentration compositions are expected to be in the unstable region where liquid-liquid phase separation is mainly driven by spinodal decomposition. Any small compositional fluctuation under this unstable condition can

result in localized liquid-liquid phase separation [122, 155]. Note that in our process we mix our nonsolvent with the polymer solution, thus the final ternary composition is immediately reached and can be located on the phase diagram where the phase separation occurs. Based on the spinodal decomposition mechanism, continuous, interconnected, homogeneous and fine morphologies which are formed from the polymer-rich phase are expected within these monoliths [117, 125, 153, 155]. Although these characteristics can be seen in the morphologies presented in Fig. 5.5 e and f corresponding to (18 wt.%, 1 v/v, 23 °C) and (20 wt.%, 1 v/v, 23 °C) respectively, for the higher PLA concentrations the morphology (Fig. 5.5 g and h) changes into a less homogeneous, flake-like structure which is not as continuous. This is probably due to faster crystallization of PLA leading to gelation [118] and higher viscosity which limits the spinodal decomposition [123].

According to Fig. 5.6, a similar spherical morphology as that observed and explained for the low PLA concentration system (13 wt.%, 1 v/v, -23 °C) is observed for higher PLA concentration (23 wt.%, 1 v/v, -23 °C). The spherical pores of the former foam are larger than those of the latter foam because of the larger volume of the liquid phase (combination of solvent and nonsolvent) and slower phase separation process for the system (13 wt.%, 1 v/v, -23 °C). Note that the formation of these large pores most probably occurs at the very early stage of the phase separation.

The specific surface area continues to increase to 54.14 m^2/g by moving from the transition to the resilient gel region (Table 5.2), where the maximum porosity is also observed for sample (18 wt.%, 1 v/v, 23 °C). High specific surface area is very important for the application of these foams to composite scaffolds, providing more contact surface for the bodily fluids to diffuse through and for the bone cells to attach to and proliferate and grow. It also increases the degradation rate of the scaffold *in vivo* [7, 14, 105, 106]. Above the PLA in DCM concentration of 20 wt.%, both porosity and specific surface area decrease. The reduction in porosity is simply due to the combination of higher PLA content but similar shrinkage to that of the previous foams in this region. The lower specific surface area can be attributed to the coarser structure which can be seen in Fig. 5.5 g and h as compared to Fig. 5.5e. It indicates that the foams with flake-like microstructure (Fig. 5.5 g and h) are not as interconnected as the foams with lower PLA content (Fig. 5.5 e and f) in the resilient gel region.

In general, the mean pore sizes measured by BET analysis (Table 5.2) reveal that these foams can be indeed considered as mesoporous (2-50 nm) foams according to the International Union of Pure and Applied Chemistry specifications [103, 163].

In Fig. 5.7, the micro-CT three-dimensional images of the two foams are presented: (18 wt.%, 1 v/v, 23 °C) and (13 wt.%, 1 v/v, -23 °C). The micro-CT images confirm the continuous, homogeneous and isotropic nature of the monoliths. Also the large spherical pores which are observed in Fig. 5.6 a and c, are also visible in the micro-CT images (Fig. 5.7b).

(a)   300 μm   (b)   400 μm
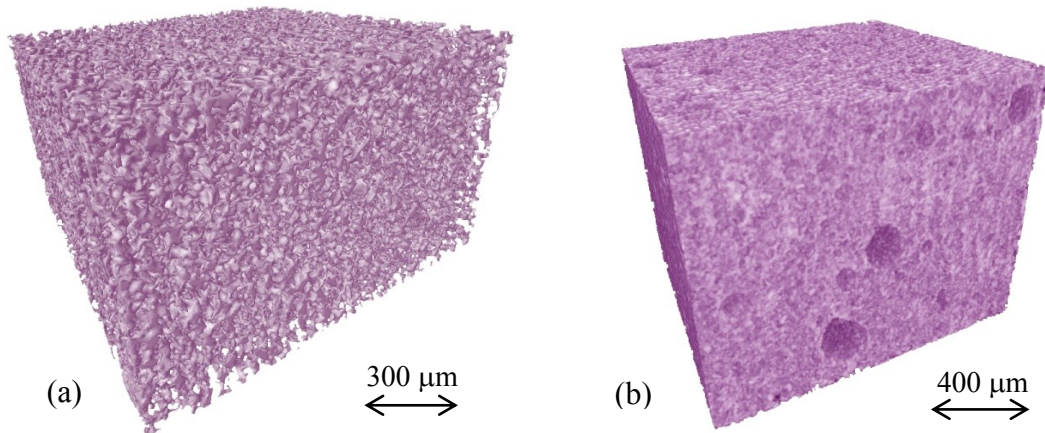
Fig. 5. 7. Micro-CT three-dimensional images of foam (18 wt.%, 1 v/v, 23 °C) (a) and foam (13 wt.%, 1 v/v, -23 °C) (b), and corresponding to SEM images in Fig. 5.5e and Fig. 5.6a respectively.

Producing an ideal morphology for bone scaffolds via phase separation is a challenge [109]. Even though the porosity of the foams prepared at room standing temperature can be as high as ~88.5%, their mesoporous morphologies (Fig. 5.5) are not ideal for bone scaffolds because of the lack of macropores [3]. In comparison, the morphology of the foams prepared at a standing temperature of -23 °C (Fig. 5.6) includes both meso- and macropores, demonstrating potential for such applications [105, 107, 164]. A simple permeability test is performed on foam (13 wt.%, 1 v/v, -23 °C) indicating that the pores are interconnected. The result and discussion on this test are presented in Appendix A.

PLA scaffolds with similar morphologies to those in Fig. 5.6 have been previously fabricated by other techniques: solution casting with sacrificial paraffin spheres as templates [105], supercritical gel drying combined with particulate leaching [107] and "phase inversion using supercritical CO_2 as a nonsolvent in the presence of ammonium bicarbonate particles" [164]. Hua et al. [123, 124] have studied PLGA and PLLA scaffolds with similar morphologies to ours (Fig. 5.6) fabricated via a TIPS method incorporating small amounts of nonsolvent (nonsolvent/solvent = 0.15 – 0.2 v/v). They found that the nonsolvent content, even at low contents, has the greatest effect on the cloud-point temperature. They have also showed that by quenching the systems to low temperatures, crystallization prevents the liquid-liquid phase separation process by substantially increasing the viscosity of the system. Unlike these techniques, our approach does not require templates or freeze drying, or any other complicated methods. Furthermore, because of the versatility and simplicity of our method, foams with various pore sizes can be produced by selecting the polymer concentration and/or the phase separation temperature as explained above.

5.3.2. Crystallinity

NIPS-derived foams have been shown to be semi-crystalline for crystallizable polymers as a result of crystallization during phase separation [125]. The low D content of our PLA allows for significant crystallinity in the final monoliths [7, 88].

Crystallization during phase separation and the gel aging in such systems is a type of crystallization from solution, in which the solvent diffuses from the polymer-rich to polymer-lean phase (instead of evaporating from a polymer solution) providing the opportunity for the chains to form crystalline lamellae (on the order of 10 nm thick) [125, 165]. The phase separation rate and the final degree of crystallinity have an inverse relationship. At higher phase separation rates, the solvent extraction from the polymer-rich phase is faster meaning the polymer chains have less time to form lamellae, which eventually results in lower overall crystallinity [118, 128, 155]. The kinetics of the liquid-liquid phase separation in this ternary system have been previously studied [155].

The degradation rate of polymer-based scaffolds strongly depends on its degree of crystallinity: a polymer with higher crystallinity requires longer time to degrade *in vivo* [7, 158]. Thus, measuring the crystallinity of the foams is important. Crystallinity of the foams (X_C in percent) is calculated from the DSC results using Eq. 5.4.

$$X_C = \frac{\Delta H_m - \Delta H_C}{\Delta H_0} \times 100$$

Eq. 5.4

where ΔH_m, ΔH_c and ΔH_0 are enthalpy of fusion, enthalpy of crystallization and the enthalpy of fusion of fully crystalline PLA (106 J/g [159]), respectively [159]. Based on this, the crystallinity of our as-received PLA is ~32.5%.

The crystallinity of the foams (Fig. 5.8), decreases on the order of a few percent with increasing PLA in DCM concentration until it essentially plateaus in the resilient gel region. The (10 wt.%, 1 v/v, 23 °C) system which has the lowest PLA concentration among these samples has the highest crystallinity. This can be explained by the slower phase separation process providing more time for the polymer chains to form crystalline lamellae. Crystallization from a solution with higher polymer concentration increases the chance of the formation of multi-lamellae aggregations resulting in amorphous polymer trapped in between of the crystalline lamellae [122, 165]. This results in lower overall crystallinity for the corresponding foams (Fig. 5.8).
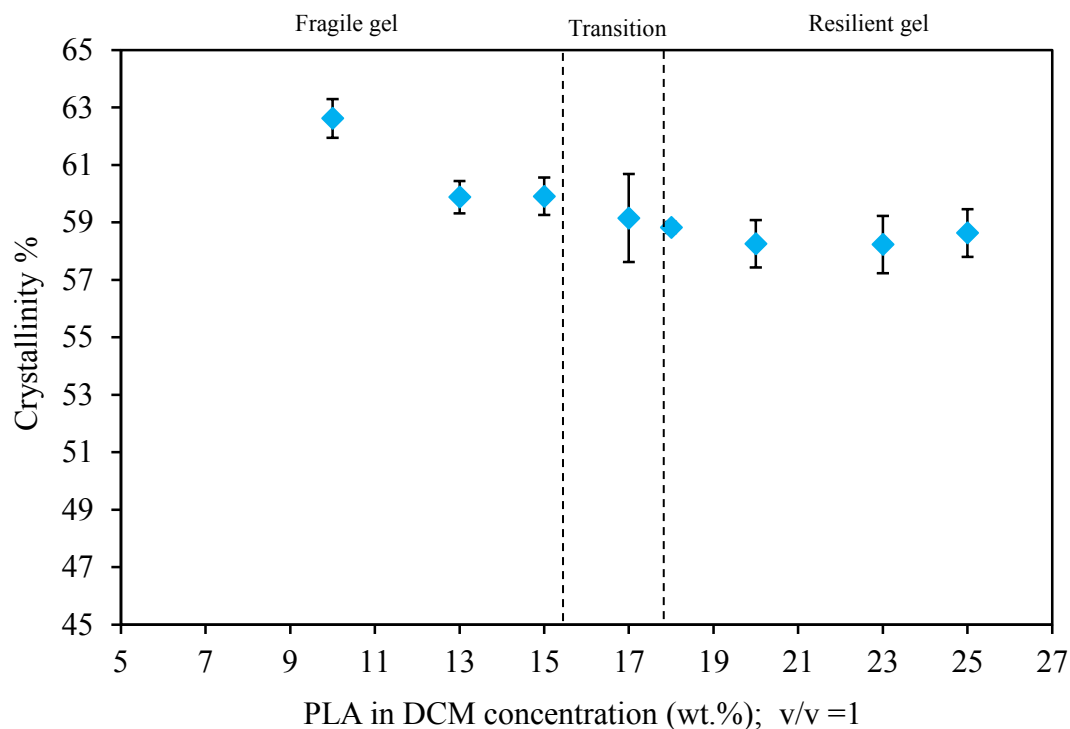
Fig. 5. 8. The effect of PLA in DCM concentration on the crystallinity of the final monoliths (solvent exchange, air drying, room temperature); (n= 4).

Fig. 5.9 shows the impact of the solvent exchange and the subsequent drying step on the crystallinity of the foams. Using vacuum (70 cmHg) compared to simply drying the gel in the air results in a slightly lower crystallinity due to the faster removal of the liquid phase from the monolith. The effect of solvent exchange is much more significant. During this step, the remaining DCM in the polymer-rich phase of the gel is gradually replaced by methanol providing additional time for crystallization. This effect is more noticeable for (13 wt.%, 1 v/v, 23 °C) because of the higher remaining DCM content in its polymer-rich phase of the gel.
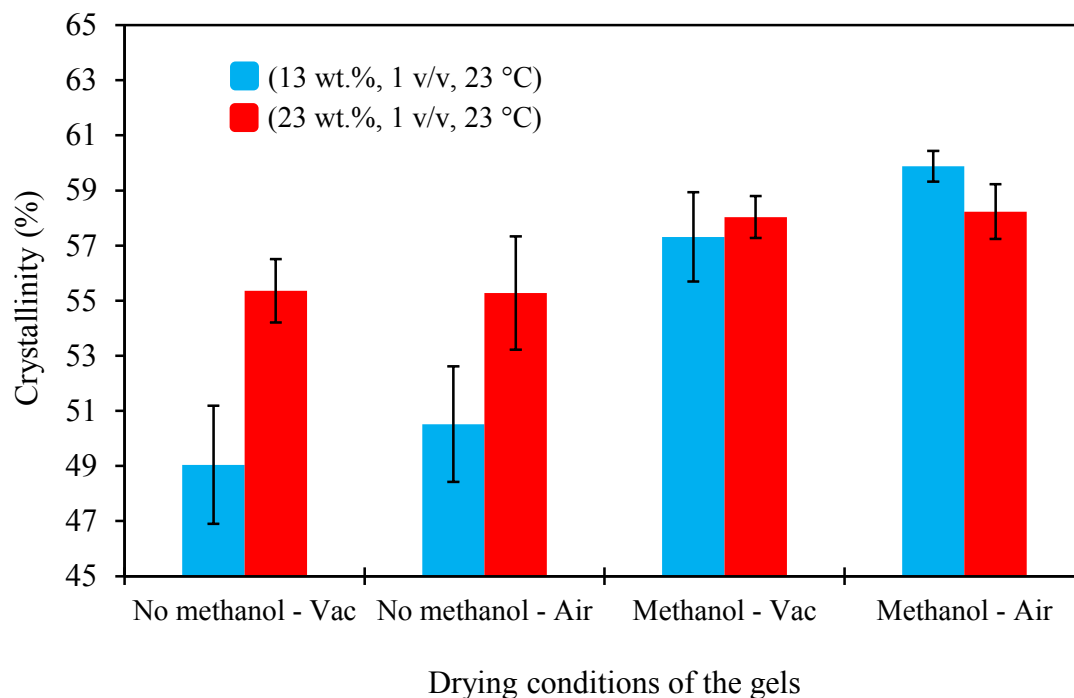
Fig. 5. 9. The effect of solvent exchange using methanol, and the subsequent drying step (using vacuum or simple air drying) on crystallinity of the monoliths (n= 3).

The effect of phase separation standing temperature on crystallinity is shown in Fig. 5.10. At the lowest standing temperature, -23 °C, phase separation is faster due to a reduction in solubility of the polymer in the solvent according to Eqs. 1-3 in Ref. [155], and a lower polymer chain mobility [125, 155]. This results in a higher rate of solvent diffusion from the polymer-rich to the polymer-lean phase, whereas the miscibility of the solvent and nonsolvent is independent of temperature [155]. Under such conditions the polymer chains are less able to form the crystalline lamellae. Crystallinity increases by increasing the phase separation standing temperature to room temperature and drops again at 40 °C. At this temperature, the phase separation rate is lower because of the higher solubility of PLA in the DCM and the greater mobility of the polymer chains [125, 155]. Thus, the phase separation stops while there is slightly more DCM in the polymer-rich phase of the gel compared to that of the same system at room temperature. This results in the slightly lower crystallinity in the final monoliths (Fig. 5.10).

The final crystallinity of the (13 wt.%, 1 v/v) system is higher at all standing temperatures due to its slower phase separation process as compared to that of the (23 wt.%, 1 v/v) system.
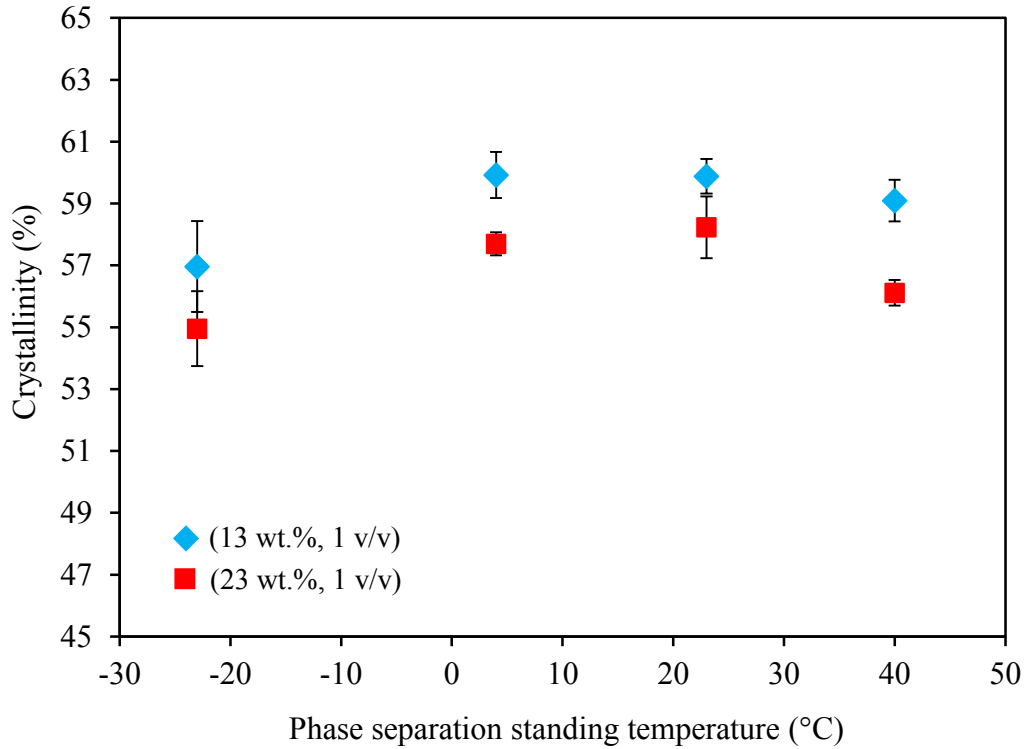
Fig. 5. 10. The effect of phase separation standing temperature on crystallinity of the monoliths (n= 3).

5.3.3. Mechanical properties

An ideal bone scaffold must have mechanical properties close to those of the defective bone. Also, it should not collapse during handling and placement, or as a result of normal activities when in the body, and it must sustain mechanical support as the new bone is regenerating. Thus the accurate measurement of mechanical properties using compression testing is extremely important. The mechanical properties of the foams are related to the porosity, final crystallinity, and morphology of the monoliths which are

determined by both processing conditions and basic characteristics of the polymer [3, 7, 14, 109].

An example of the two types of stress-strain behavior that we observed is shown in Fig. 5.11. For all samples except for (13 wt.%, 1 v/v, -23 °C), simple linear elastic behavior was observed and neither yielding nor fracture were reached within the experimental force range. Foam (13 wt.%, 1 v/v, -23 °C) has the lowest modulus (Fig. 5.12) and is the only foam to exhibit a yielding point at ~0.2 MPa (Fig. 5.11) within the range of stresses experimentally accessible. This foam yields because of the presence of the large spherical pores in its morphology (Fig. 5.6a) along with its lower crystallinity.
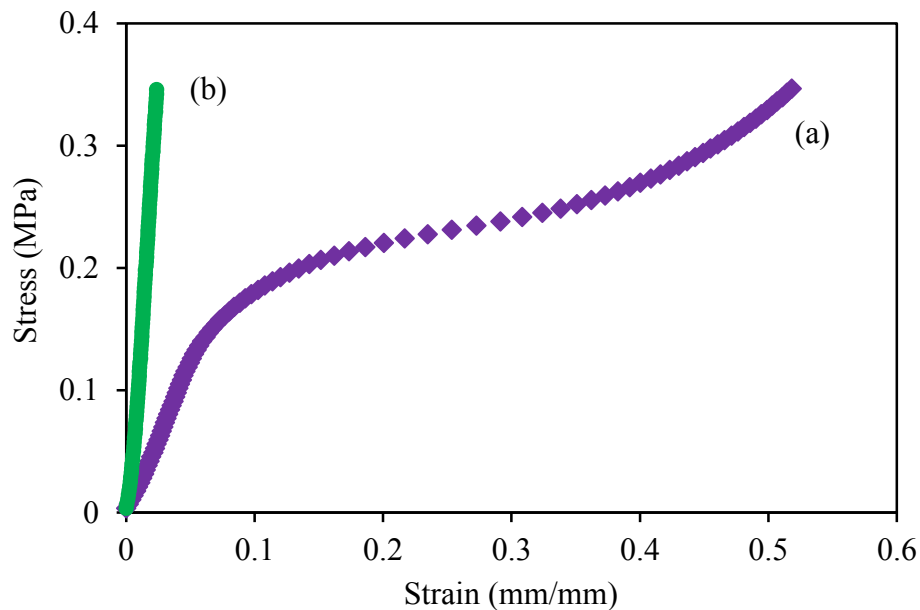
Fig. 5. 11. Stress-strain curves of foams (13 wt.%, 1 v/v, -23 °C) (a) and (23 wt.%, 1 v/v, -23 °C) (b).

The results of compression testing are summarized in Fig. 5.12 in terms of compressive modulus of the foams versus the PLA in DCM concentration used to prepare the foams. The foams from the fragile gel region have the highest modulus due to their higher crystallinity and lower porosity as compared to the foams in the other regions. In this region, modulus is mainly governed by the crystallinity of the foams rather than their

106

porosity or morphology, because many of the original pores within the skeleton collapsed due to capillary forces during drying.
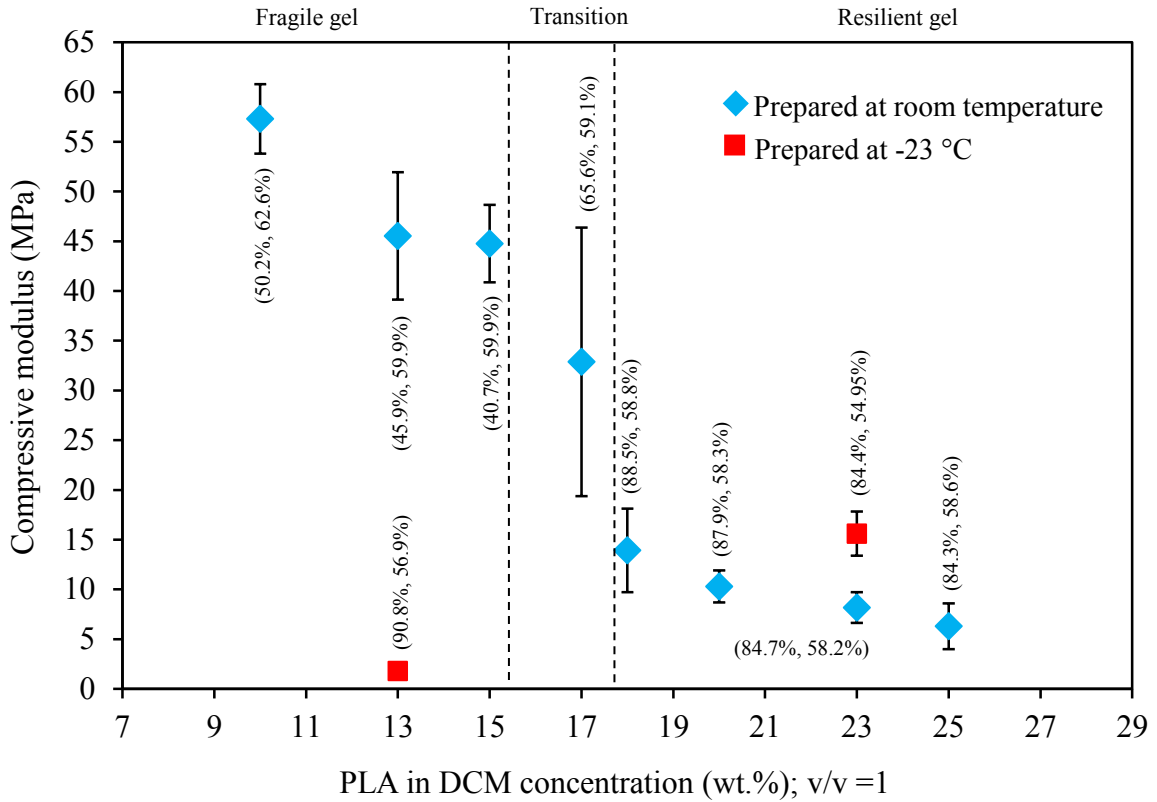
Fig. 5. 12. Compressive modulus of the foams versus their PLA in DCM concentration. The values in parentheses are (mean porosity in %, mean crystallinity in %) corresponding to each experimental point (n= 3 or 4).

In the resilient gel region, the modulus decreases with decreasing porosity and their crystallinities are essentially the same, revealing that morphology is the determining factor for these foams. For example, foam (18 wt.%, 1 v/v, 23 °C), with the highest porosity has also a high modulus due to its continuous, homogenous, mesoporous morphology (Fig. 5.5e) that allows stress to be transferred and distributed equally throughout the entire framework. For this reason, this particular foam has a higher modulus than other highly porous PLA bone substitutes described in the literature [7, 107, 121, 154, 160]. Foams (23 and 25 wt.%, 1 v/v, 23 °C) with the flake-like

morphology (Fig. 5.5 g and h) exhibit a slightly lower modulus due to their less continuous morphology. This effect of morphology is also clear in the behavior of foam (23 wt.%, 1 v/v, - 23 °C). The modulus of this foam is higher than that of the foam (23 wt.%, 1 v/v) prepared at room temperature.

5.4. Conclusion

A straightforward procedure was designed for the fabrication of PLA foams via a template-free, versatile method: nonsolvent induced phase separation (NIPS). The compositions which undergo gelation within the liquid-liquid phase separated region of the PLA-DCM-hexane phase diagram were identified and used to produce the foams. A parametric study of the effect of system composition on shrinkage and porosity was performed allowing for the minimization of shrinkage. We demonstrate that NIPS is able to produce PLA foams with high specific surface area up to 54.14 m^2/g and porosity ranging from 40.7% to 90.8%. All of our NIPS-derived foams were found to be semi-crystalline with crystallinity decreasing as the initial PLA in DCM concentration increases. Interesting pore morphologies, including homogeneous mesoporous and combined meso/macroporous structures, are obtained depending on composition and the phase separation standing temperature. The compressive modulus of the foams ranges from 1.8 – 57 MPa. In particular, the compressive modulus of the mesoporous foam with the highest porosity (~88.5%) is as high as 13.9 MPa. It was shown that the modulus of the foams is governed by both crystallinity and morphology. Given the relatively high modulus and porosity, the combined meso/macroporous morphology which is a good candidate as bone scaffolds, is identified. Considering the good mechanical properties, high porosity and combined meso/macroporous morphology of the foams as well as the simplicity and versatility of the process, NIPS is a very promising technique for the fabrication of polymer foams with unique properties.

Chapter 6

The incorporation of surface modified sol-gel-derived 45S5 Bioglass® in highly porous polylactic acid monoliths[1]

Ehsan Rezabeigi, Paula M. Wood-Adams and Robin A.L. Drew

Department of Mechanical and Industrial Engineering, Concordia University
Montreal, QC H3G 1M8, Canada

Abstract

Composite scaffolds consisting of a biodegradable polymeric matrix and well-dispersed bioactive glass particles (Class A) are one of the most promising bone substitutes. In this study, sol-gel-derived 45S5 Bioglass® is surface modified with the silane coupling agent, 3-methacryloxypropyltriethoxysilane. The surface modification process effectively diminishes the agglomeration between glass particles and improves their dispersibility in polylactic acid (PLA) solutions. The surface modified particles are incorporated (2 wt.%) in PLA via a nonsolvent induced phase separation process to produce highly porous, (up to ~91%) bioactive, composite scaffolds. The PLA-dichloromethane (solvent)-hexane (nonsolvent) systems are allowed to phase separate at -23 ºC which results in a meso/macroporous morphology with no sacrificial phases involved. Interestingly, the incorporation route of particles (via solvent or nonsolvent) with the foaming process has the greatest impact on porosity, crystallinity and morphology of the resulting scaffolds. SEM images showed that the embedded surface modified particles are interlocked within the mesoporous structure of the monoliths but not completely covered by PLA such that they can be in contact with physiological fluids. *Keywords*: Bioglass, Polylactic acid, scaffold

---

1. This Chapter *will be published shortly*: Ehsan Rezabeigi, Paula M. Wood-Adams and Robin A.L. Drew, "The incorporation of surface modified sol-gel-derived 45S5 Bioglass® in highly porous polylactic acid monoliths".

6.1. Introduction

Highly porous, polymer-based monoliths containing submicron bioactive particles are one of the most promising systems for the fabrication of the ideal scaffold for bone regeneration. Such composite scaffolds may exhibit homogeneous degradation rate, improved cell attachment and desirable mechanical properties to support the defective bone over the healing process. Composites of 45S5 Bioglass$^{®}$ and polylactic acid (PLA) have been extensively studied for this application due to their excellent bioproperties as well as the complementarity of their properties [3, 15, 16, 134, 160, 166].

45S5 Bioglass$^{®}$ (45% SiO_2, 24.5% CaO, 24.5% Na_2O and 6% P_2O_5 (wt.%)) is the most bioactive composition which can be used for both soft and hard tissue regeneration. This glass exhibits Class A bioactivity as well as osteogenic and angiogenesis properties which accelerate the healing process [3, 7, 166].

Polylactic acid (PLA) is a biodegradable, synthetic polymer which is classified as a saturated aliphatic polyester. PLA has been widely used for biomedical applications especially bone regeneration due to its good mechanical properties, bioresorbability and biocompatibility [7] and good processability [15].

Although these composite scaffolds have the potential to be desirable in terms of composition and morphology, their overall bioactivity, mechanical properties and degradation behavior are adversely affected by incompatibility between the organic and inorganic phases [7]. In general, (bio-)glasses are hydrophilic and polymers are hydrophobic. The hydrophilic nature of the glasses is attributed to their surface hydroxyl groups and the hydrophobicity of the polymers is due to the nonpolar hydrocarbon groups in their molecular structure [3, 7, 15, 166].

Physical or chemical surface modification can improve the interfacial adhesion between the organic and inorganic phases. Chemical routes including the deposition of specific polymers or coupling agents onto the glass surface, result in a tougher and more effective surface functionalization compared to those of the physical methods [15, 92]. Silane coupling agents are well-known adhesion promoters which are able to covalently bond the organic and inorganic phases. This is due to their molecular structure consisting of both polar and nonpolar portions which are normally linked by a alkyl bridge (n =

$0,1,2,\ldots$): $R-(CH_2)_n-Si-X_3$. The polar end capped with the hydrolysable group (X) which may be acyloxy, amine or halogens, is able to covalently bond to the inorganic phase via its surface OH groups. The nonpolar portion of the molecule includes an organofunctional group (R) which may be amino, methacryl or glycidoxy. The alkyl groups of the coupling agent increase its compatibility with the organic phase and its reactive organofunctional group may directly form a covalent bond with the organic phase [92]. The most commonly used silanes are well summarized in Refs. [15, 33, 91].

There are two routes for grafting silanes onto a glass surface: anhydrous and hydrolytic deposition. There is no catalyst involved in anhydrous deposition and the water content is minimized. This procedure requires high temperatures and long reaction times and is not applicable for all silanes. In hydrolytic deposition, the silane molecules are hydrolyzed and then attached to the surface hydroxyl groups via secondary bonds. Strong covalent bonds subsequently form during refluxing and/or drying, as a result of water elimination (Fig. 6.1) [15, 16, 98, 99].
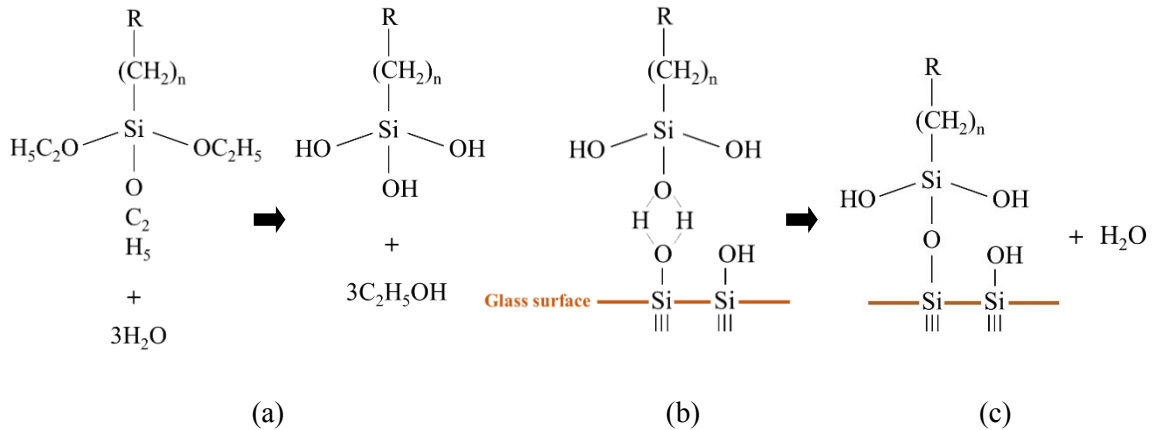
Fig. 6. 1. The steps in the hydrolytic deposition of a triethoxysilane onto the surface of a silica-based glass: hydrolysis of the silane (a), hydrogen bonding of the silane molecule to the glass surface (b) and the formation of the covalent bond after the elimination of water (c) [98].

The silane is hydrolyzed in the presence of water and typically a catalyst. In this method, obtaining a monolayer and minimizing the silane self-polymerization is more difficult than in the anhydrous method. The water content and the pH govern the

111

hydrolysis and condensation rates which if properly balanced encourage the formation of a monolayer [3, 15, 98-100].

Surface modification of 45S5 Bioglass® has been mainly limited to its melt-derived type which is known to be dense with low specific surface area (≤ 1 m^2/g) [7, 166]. In this study, we are attempting to surface modify a sol-gel-derived 45S5 Bioglass® which we have previously described [166]. The sol-gel route is one of most well-known methods for the direct production of submicron glass particles with a high specific surface area and a surface densely functionalized with OH groups. These two characteristics can improve the efficiency of the surface modification by increasing the available reactive sites on the glass particles [3, 15, 16].

The production of scaffolds via modified TIPS which contains a small amount of nonsolvent has been previously studied [122, 123, 126, 134, 167, 168]. The incorporation of the nonsolvent encourages the liquid-liquid phase separation at low temperature. Chen et al. [122], showed that the addition of nonsolvent can change the typical anisotropic morphology of the TIPS-derived scaffolds to an isotropic morphology consisting of (semi-)spherical macropores. In our previous study [169], we showed that the isotropic mesoporous structure of NIPS-derived PLA foams can be changed into an isotropic macro/mesoporous morphology by lowering the phase separation standing temperature with no freeze drying involved. Previous biological studies with foams of similar morphologies [122, 123, 126, 134, 167, 168] have indicated great potential for bone scaffold applications. This combined with the excellent bioactivity of 45S5 Bioglass®, is the main motivation for the current study. Here, we investigate the effect of incorporation of surface modified 45S5 Bioglass® particles on morphology, porosity and crystallinity of the NIPS-derived PLA foams at phase separation standing temperature of - 23 ℃.

6.2. Experimental procedure

6.2.1. Materials

Our previously synthesized sol-gel-derived 45S5 Bioglass® powder [166] is used after grinding. 3-methacryloxypropyltriethoxysilane (MPTES; Gelest Inc, >95%) is used

as the silane coupling agent. The surface modification process includes the following materials: anhydrous ethanol (RICCA Chemical Company, ACS Reagent Grade) as dispersing medium for the glass powder and solvent for MPTES, ammonium hydroxide (Fisher, Certified ACS PLUS, 28.5 wt.%) as catalyst and deionized water (DI water; Fisher, Deionized Ultra Filtered Water).

PLA (M_n = 97000, M_w/M_n = 2) with 1.6% D-lactide was obtained from NatureWorks LLC (Ingeo™ Biopolymer 4032D). The molecular weight information is provided by the supplier based on solution viscosity measurements conducted on our batch. Dichloromethane (DCM; Fisher Chemical; Stabilized/Certified ACS, >95.5) and hexane (Fisher Chemicals, Certified ACS, > 95 %) are used as solvent and nonsolvent for PLA, respectively. Methanol (Fisher Chemicals; Certified ACS, 99.9 %) is also used during the solvent exchange process.

6.2.2. Surface modification process

The 45S5 Bioglass® powder is degassed (90 kPa vacuum, 150 ºC, 10 – 12 hours) to eliminate adsorbed water and other contaminants. The powder is then exposed to a humid environment at 60 ºC for 5 – 6 hours in order to equilibrate the surface hydroxyl groups [98-100]. The powder is again dehydrated (90 kPa vacuum, 150 ºC, 5 hours) to remove physisorbed water molecules and leave only active hydroxyl groups on the glass surface.

The powder (0.2 g) is then dispersed in 10 ml of absolute ethanol using an ultrasonication bath (VWR, model 250T) for 1 hour. All following steps are carried out immediately to avoid agglomeration: The silane (0.7 ml) is added to the suspension while stirring (400 – 600 rpm). Ammonium hydroxide is then added to adjust the pH between 9 and 10. Considering the amount of water in the ammonium hydroxide, DI water can be added (if needed) to reach an overall water content of 0.13 ml. This water molar content is 3 times that of silane, which is the stoichiometric amount for complete silane hydrolysis. The powder is collected by centrifuge (VWR, 12000 rpm, 10 min.) after stirring for 12 hours and refluxing for 1 hour at 85 – 90 ºC. The powder is then dispersed in 50 ml ethanol to remove any physisorbed silane and followed by centrifugation. The

sample is rinsed in this manner twice more and then dried in a Teflon container under vacuum (90 kPa) at 150 ºC for 8 – 10 hours.

6.2.3. Foam production

A template-free foaming method which is a combination of the NIPS and TIPS techniques is used [169] in order to produce the pure PLA foams from PLA-DCM-hexane systems phase separated at -23 ºC which gives the desired morphology. Here we produce two new PLA foams (16 wt.%, 1 v/v, -23 ºC) and (19 wt.%, 1 v/v, -23 ºC) in addition to those previously studied [169]: (13 wt.%, 1 v/v, -23 ºC) and (23 wt.%, 1 v/v, -23 ºC). The characterization results of the two last systems including SEM images, porosity and crystallinity which are presented here are adapted from Ref. [169]. Note that (X wt.%, Y v/v, T ºC) corresponds to a system of PLA-DCM solution (X wt.%) mixed with hexane at a nonsolvent to solvent volume ratio of Y (v/v) which is allowed to undergo phase separation at a temperature of T ºC [169]. Since Y and T in this study are 1 v/v and -23 ºC for all systems, each foam is denoted only by its PLA in DCM concentration, (X wt.%), in the following sections.

The 4 systems (13, 16, 19 and 23 wt.%, 1 v/v, -23 ºC) are also used for producing the composite foams. PLA-based foams containing 2 wt.% glass particles (surface modified or unmodified), are produced by incorporating the particles into the foaming technique via two methods based on preliminary incorporation in either the PLA-DCM solution or the hexane. In route i) the glass particles are ultrasonically dispersed in DCM (~ 0.5 ml) and added to the PLA-DCM solution while stirring at 30 ºC until homogeneous followed by evaporation of excess DCM. Hexane is subsequently added to the suspension at room temperature. In route ii) the glass particles are ultrasonically dispersed in the hexane (v/v = 1) and then added gradually to the PLA-DCM solution while mixing at room temperature. In both cases the composite ternary systems are placed in a freezer at -23 ºC for phase separation and gelation. After aging the gel at -23 ºC for at least 24 hours, the gel is rinsed with methanol 3 times before removing from the mold. Next solvent exchange and air drying are performed as in Ref. [169]. Note that most of the samples are produced via DCM (route i) with surface modified powder. The

effect of the addition of unmodified glass particles as well as route ii preparation have been investigated on one system (13 wt.%, 1 v/v, -23 ºC).

6.2.4. Characterization

The glass powder is characterized in terms of composition, sedimentation and particle size before and after the surface modification to evaluate the efficiency of the silane deposition process. The glass powders (10 mg) are characterized by Fourier transform infrared spectroscopy (FTIR, NEXUS 670 FT-IR) over wavenumber range 600 to 4000 cm^{-1}. Sedimentation studies in hexane and PLA-DCM solution (5 wt.%) are performed by ultrasonically dispersing 15 mg glass powder in 2 ml of liquid. The time required for the powder to collect at the bottom and leave behind a relatively clear liquid is reported as the sedimentation time [16]. Laser light scattering particle size analysis (PSA; Horiba LA-920, isopropyl alcohol dispersant) is used to determine the particle size distributions [166].

The pure PLA foams as well as the composite foams are characterized in terms of apparent density, porosity, PLA crystallinity and morphology (fracture surface). A detailed description of sample preparation and test conditions for these analyses is presented in Ref. [169].

6.3. Results and discussion

6.3.1. Bioglass® powders

6.3.1.1. FTIR analysis

The FTIR spectra (600-3100 cm^{-1}) of sol-gel-derived 45S5 Bioglass® before and after surface modification as well as melt-derived 45S5 Bioglass®, used as a reference[1], are shown in Fig. 6.2. The peaks at 950-1200 cm^{-1} and 930 cm^{-1} correspond primarily to

---

1. The melt-derived Bioglass® was kindly provided by Professor Robert Hill from Queen Mary University of London.

the Si-O-Si groups of the glass network [9, 99]. It is likely that the weak peak of the P-O bonds at 1045 cm^{-1} slightly intensifies the strong peak of Si-O-Si at 950-1200 cm^{-1} [99]. The peak at 810-930 cm^{-1} is attributed to the Si-OH bonds which are the surface hydroxyl groups [170]. This peak is not detected in the spectrum of the melt-derived glass indicating a lower density of surface hydroxyl groups compared to that of the sol-gel-derived glass [3, 7, 16, 166].
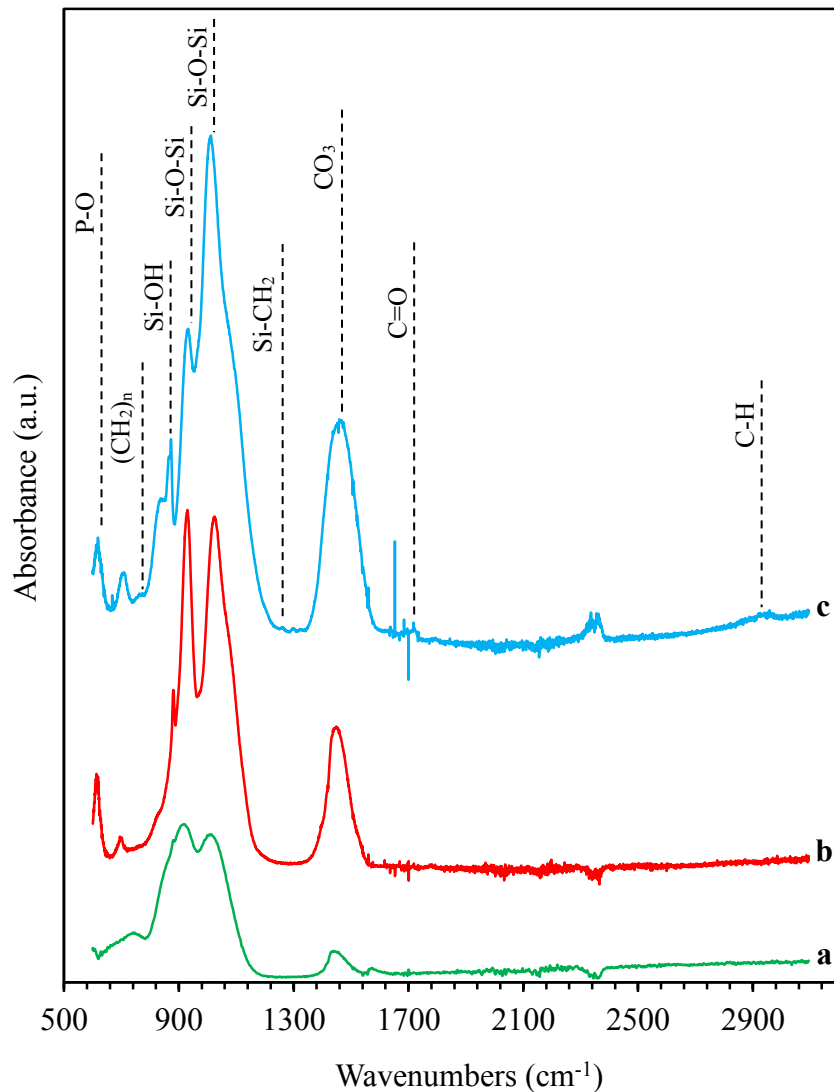
Fig. 6. 2. FTIR spectra of the melt-derived 45S5 Bioglass® (a); the sol-gel-derived 45S5 Bioglass® before (b) and after (c) surface modification.

New low intensity peaks appear in the glass spectrum after surface modification. The peak at 1720 cm^{-1} corresponds to the C=O stretching band of the ester functional group of the silane coupling agent [170, 171]. The peaks at 785 cm^{-1}, 1250 cm^{-1} and 2930 cm^{-1} are attributed to $(CH_2)_n$ deformation vibration [33], Si-CH$_2$ [170] and C-H stretching modes [16, 33] respectively, all related to the alkyl bridge of the silane molecules. The anticipated molecular structure of the grafted MPTES is shown in Fig. 6.4b. These peaks indicate that the silane molecules are successfully grafted onto the glass particles during the surface modification process.

The small peak at 627 cm^{-1} and the broad peak at 1450-1550 cm^{-1} correspond to the P-O bond of crystalline phosphate [9, 33, 99] and the CO$_3$ symmetric vibrational mode [172] respectively, suggesting the formation of crystalline hydroxycarbonate apatite (HCA) on the glass particles [33, 99, 172]. The formation of crystalline HCA is induced by H$_2$O and CO$_2$ in the environment during storage [33, 99, 172]. As part of the surface modification process the glass is exposed to a high humidity environment for several hours. This leads to more HCA being formed on the surface modified particles compared to that of the unmodified particles as confirmed by the intensity of these peaks. More HCA is formed on the sol-gel-derived bioglass (before and after surface modification) compared to the melt-derived bioglass showing our glass has a higher bioactivity as expected [3, 166].

6.3.1.2. Sedimentation studies

The results of sedimentation studies are presented in Table 6.1 indicating that surface modified glass particles are more compatible with hydrophobic fluids (PLA solution and hexane) than the unmodified particles. The grafting of silane coupling agents on the glass particles results in an increase in settling time of about a factor of 10. A longer settling time indicates a more stable suspension and better dispersibility of particles within the liquids used in our foaming process.

Table 6. 1. Results of sedimentation studies

Medium	Settling time (seconds)	
	Unmodified glass	Surface modified glass
PLA in DCM solution (5 wt.%)	15	120
Hexane	10	50

6.3.1.3. Particle size analysis (PSA)

The particle size distributions of the glass particles before and after surface modification are shown in Fig. 6.3. Both particle size distributions include two distinct populations: submicron and micron-sized particles [166]. Chen et al. [9], also observed a similar bimodal particle size distribution for sol-gel-derived 45S5 bioactive glass. According to these results, the severe agglomeration between particles in the original bioglass is effectively diminished after surface modification. Before surface modification, only 43% of the particles are submicron whereas afterwards 78% of the particles are submicron (Table 6.2). The mean particle size of the surface modified particles is also significantly decreased for both populations, especially the micron-sized, and overall as compared to those of the unmodified glass particles.

Table 6. 2. Particle size distribution characteristics

45S5 Bioglass®	Volume fraction of submicron particles	Mean particle size (μm)		
		Submicron population	Micron-sized population	overall
Unmodified	43%	0.61	23.69	13.28
Surface modified	78%	0.47	6.63	1.82
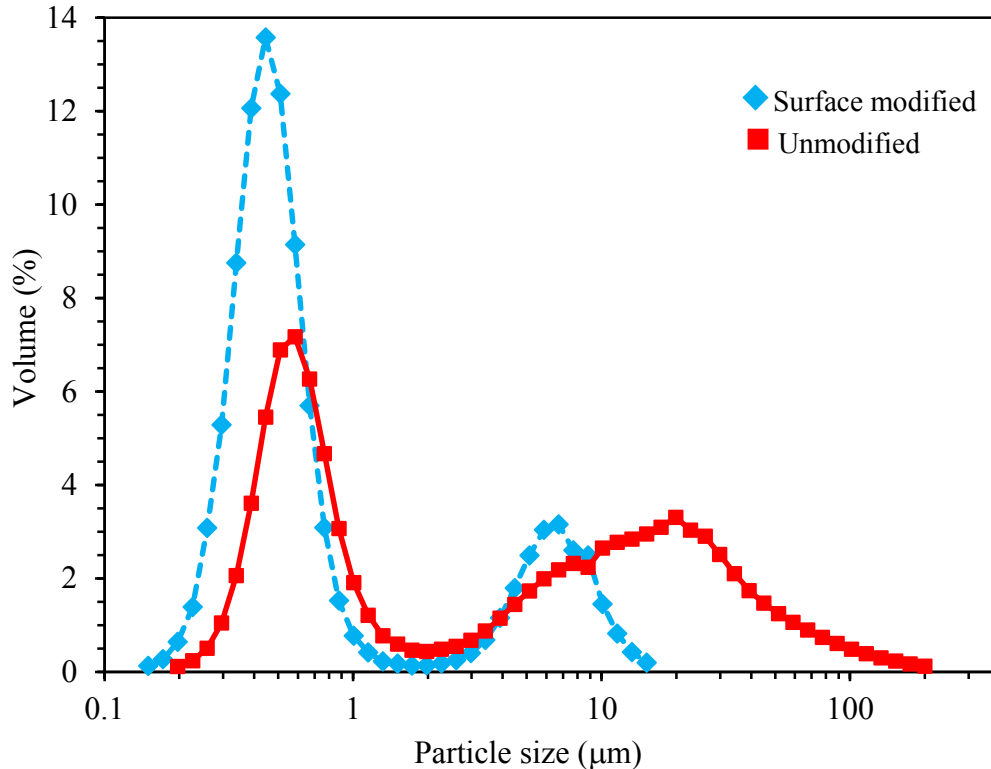
Fig. 6. 3. Particle size distribution of sol-gel-derived 45S5 Bioglass® before and after surface modification. The curve corresponding to the unmodified glass powder is adapted from Ref. [166].

Inorganic particles have a great tendency to agglomerate in organic solutions due to colloid stability [16]. Surface OH groups (Si-OH), which make the sol-gel-derived glass particles extremely hydrophilic, link the glass particles together via hydrogen bonding in a process called agglomeration (Fig. 6.4a) [15]. During the sol-gel process some primary particles also are fused together via covalent bonds forming aggregates [7, 15, 37, 166]. Ultrasonication of particle suspensions can be used to break apart some of the agglomerates but will not affect the aggregates. More intensive physical methods such as mechanical milling may be used to break apart aggregates to some extent [7, 15, 16, 37,166]. For surface modified particles, close inter-particle contact of the grafted molecules results in a decrease in configurational entropy and consequently a reduction in the tendency to agglomerate (Fig. 6.4b) [16]. The micron-sized population of the surface modified particles mostly contains the larger secondary particles formed via aggregation.

Some of the glass particles which form larger agglomerates immediately after ultrasonication and before surface modification (Fig. 6.4a) are also among the micron-sized population of the surface modified particles.

The better dispersibility of surface modified glass particles in a PLA-DCM solution combined with a smaller mean particle size and narrower particle size distribution (Fig. 6.3) allow for the production of higher quality PLA-based composite scaffolds as compared to unmodified glass. This is an important issue in particular for highly porous scaffolds with thin skeletons where large particles act as stress concentrators resulting in failure of the framework [16]. In some cases the mechanical properties of scaffolds made of pure polymer are higher than those containing large micron-sized particles in which mechanical failure occurs prematurely near to the particle/polymer interface [16, 91]. This issue and other physical characteristics of our composite foams will be discussed in the following sections.

(a)

(b)
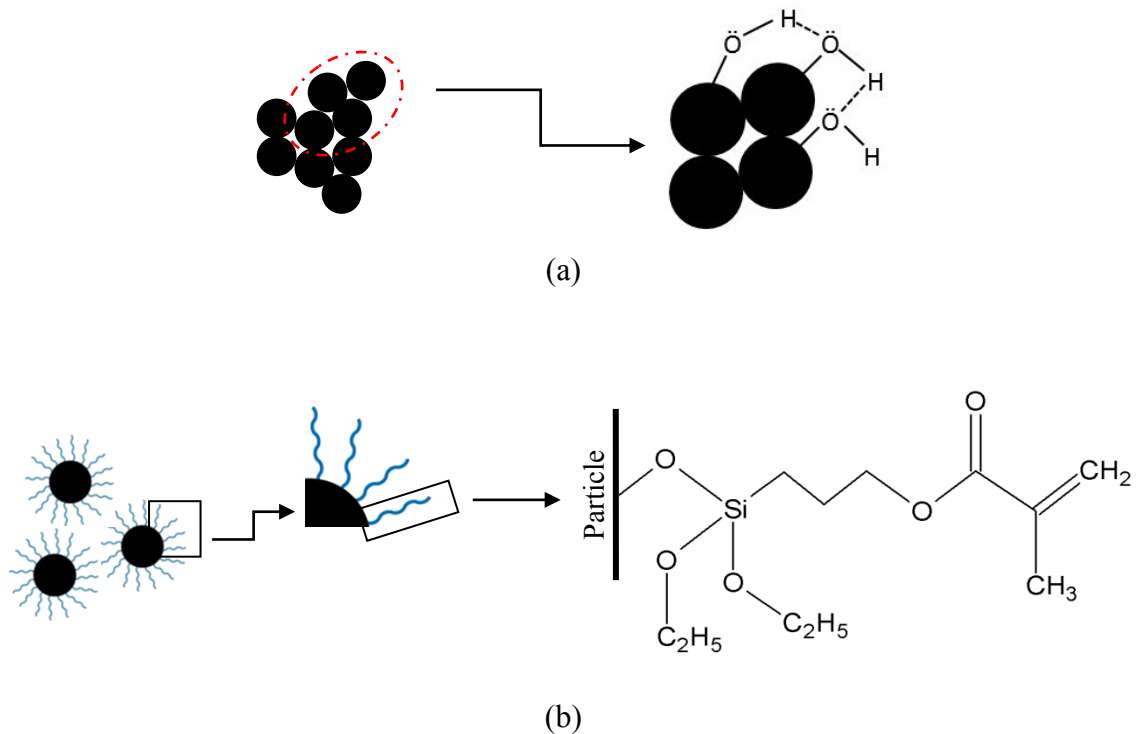
Fig. 6. 4. Hydrogen bonding between glass particles resulting in agglomeration (a) adapted from Ref. [15]; and silane molecules grafted onto the glass particles preventing agglomeration (b). The silane presented in this figure is grafted MPTES [98].

6.3.2. Foams

6.3.2.1. Apparent density, porosity and crystallinity

According to Fig. 6.5, the apparent density of the composite foam decreases slightly when prepared via DCM (route i) compared to that of the pure PLA foam. Considering the variation in the data we can conclude that this decrease is not significant. The apparent density of system (13 wt.%) significantly increases if the composite foam is prepared via hexane (route ii). This indicates that the phase separation of such ternary systems is highly sensitive to the incorporation route of the particles although the entire system is mechanically mixed. The trend observed in apparent density of the foams (Fig. 6.5) can be explained based on their morphologies (section 6.3.2.2).
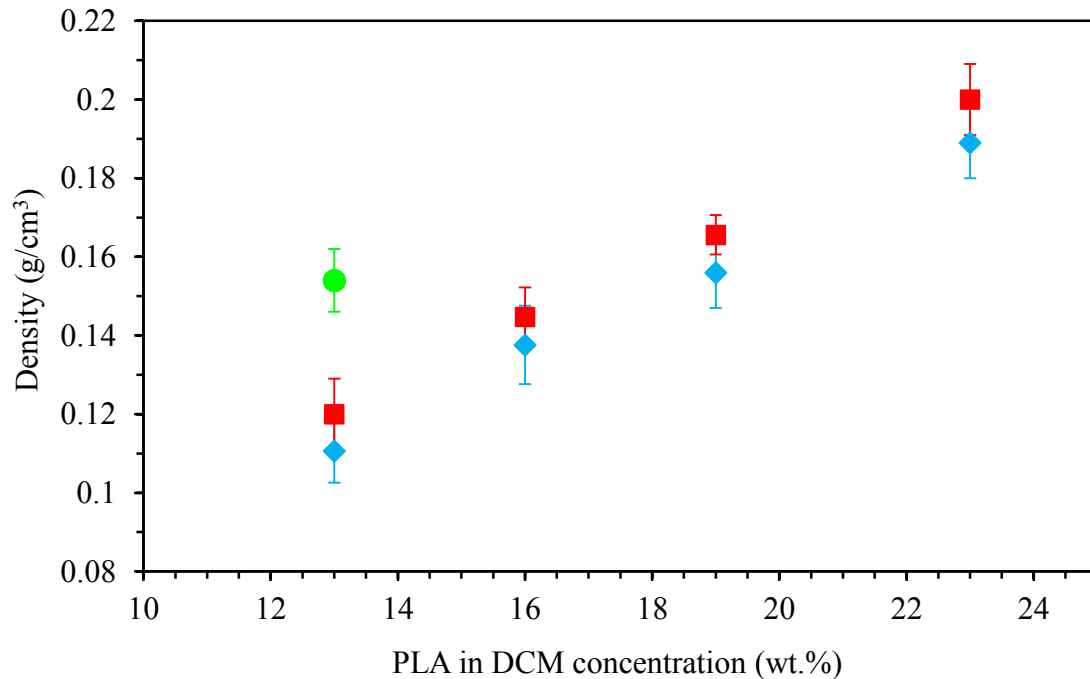
Fig. 6. 5. Apparent density of the NIPS-derived foams as a function of PLA in DCM concentration (n = 3 or 4): pure PLA (■); and composite systems wherein the surface modified glass particles are incorporated via DCM (route i ◆) and hexane (route ii ●).

The porosity of the foams can be calculated from Eq. 6.1 which is obtained by combining Eqs. 2 and 3 of Ref. [169] and the rule of mixtures for composites [160].

$$P = \left[1 - \rho \left(\frac{W_g}{\rho_g} + \frac{W_{PLA}}{w_C(\rho_C - \rho_a) + \rho_a} \right) \right]$$

Eq. 6.1

Here P and ρ represent the porosity and the apparent density of the foam, W_g and W_{PLA} are the weight fraction of the glass and PLA respectively, w_C is the crystalline volume fraction of the PLA matrix, ρ_g, ρ_a and ρ_c are the density of the glass (45S5 Bioglass®, 2.825 g/cm^3 [160]), fully amorphous PLA (1.248 g/cm^3 [75]) and fully crystalline PLA (1.290 g/cm^3 [75]). The apparent density (ρ) and the degree of crystallinity (w_C) of the foams are presented in Fig. 6.5 and Fig. 6.7, respectively. The porosity of the foams calculated using this approach is plotted as a function of their original PLA in DCM concentration (Fig. 6.6).

The porosity of PLA foams produced by phase separation at room temperature [169] depends very differently on PLA in DCM concentration than it does when phase separated at -23 ºC. As shown in Fig. 6.6, for both pure and composite foams of systems phase separated at -23 ºC, the porosity decreases linearly with increasing PLA content. This is because the phase separation mechanism is the same for all these systems and the large pores in their morphology result in minimal gel shrinkage during drying. The capillary force, which is responsible for the shrinkage of gels, is inversely correlated to the mean pore radius as shown by Eq. 1 of Ref. [169].

The incorporation of surface modified glass particles via DCM (route i) slightly increases the porosity of the foams compared to that of the corresponding pure system (Fig. 6.6). This is consistent with the work of Hong et al. [121] who showed that the addition of up to 20 wt.% of bioactive particles does not significantly affect the porosity of the PLLA foams produced via TIPS. According to Fig. 6.6, incorporation of 2 wt.% surface modified glass particles via hexane (route ii) significantly decreases the porosity of the foams of system (13 wt.%). This issue is discussed in section 6.3.2.2 in relation to the morphology examination.

Fig. 6. 6. Porosity of the NIPS-derived foams as a function of PLA in DCM concentration (n = 3 or 4): pure PLA (■); and composite systems wherein the surface modified glass particles are incorporated via DCM (route i ◆) and hexane (route ii ●).

The crystallinity of the PLA component is calculated based on Eq. 3 in Ref. [169] and shown in Fig. 6.7 as a function of original PLA in DCM concentration. The degree of crystallinity of the PLA matrix is not affected by the incorporation of 2 wt.% via DCM (route i). Although the particles are expected to induce crystallization, they also increase the viscosity of the system which accelerates gelation [123, 165, 169]. These two phenomena cancel each other resulting in a null effect. The degree of crystallinity of the PLA matrix of system (13 wt.%) wherein glass particles are incorporated via hexane (route ii) is significantly lower than that of the corresponding system prepared via route i (DCM). This issue will be discussed further in section 6.3.2.2 when we consider the foam morphology.
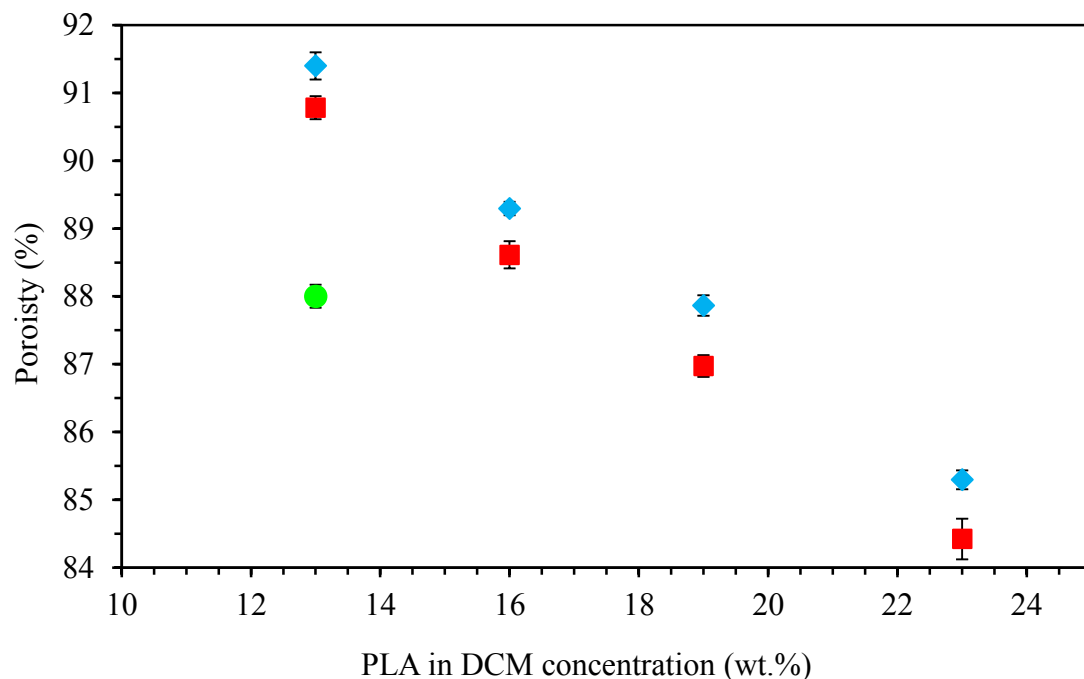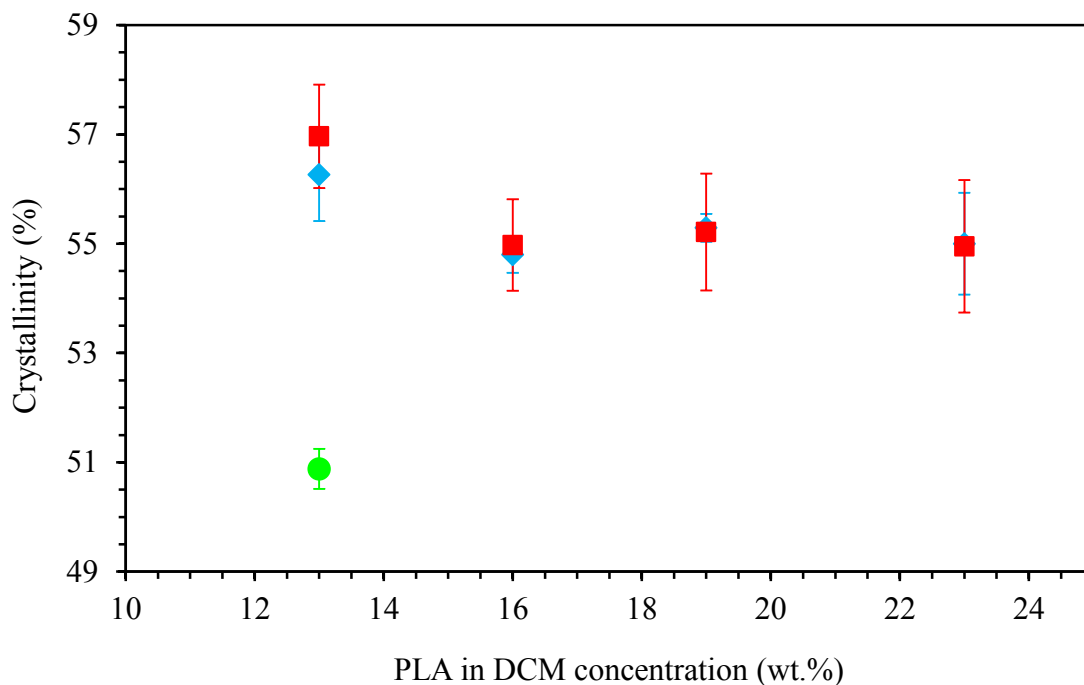
Fig. 6. 7. Crystallinity of the NIPS-derived foams as a function of PLA in DCM concentration (n = 3 or 4): pure PLA (■); and composite systems wherein the surface modified glass particles are incorporated via DCM (route i ◆) and hexane (route ii ●).

6.3.2.2. Foam morphology

The impact of incorporation of 2 wt.% surface modified glass particles via DCM (route i) on the foam morphology is striking (Fig. 6.8). In particular the spherical macropores are larger in the composite systems than in the equivalent pure PLA systems while the mesoporous structure is essentially unchanged. SEM images with higher magnifications showing the mesoporous morphology of both systems are presented in Appendix B. The size distribution is captured by selecting 70 macropores in the SEM images of each system. The results of this image analysis are presented in Fig. 6.9 showing that the macropores of the composite foams are significantly larger and their size distribution is narrower compared to those of the pure PLA foams. This change in macropore morphology is most likely due to the homogeneously distributed glass particles inducing the nucleation and growth phase separation mechanism [169]. We note that the formation of the meso-structure is driven by PLA crystallization [169] and that

neither the final crystallinity nor the meso-structure are significantly affected by the addition of glass particles via DCM (route i).

PLA foams with similar morphologies are produced by two-step quenching TIPS of the PLA-1,4 dioxane-water system followed by freeze drying [126]. The size distribution of the macropores is very wide due to the two-step quenching. The development PLA foams with similar morphologies are briefly reviewed in Ref. [169].

Pore morphology plays an important role on the performance of scaffolds *in vivo* [3, 169]. As interconnected macropores (> 100 μm) are necessary for vascularization and bone ingrowth, the topography of the surface of the scaffold in contact with cells has a significant impact on their behavior. The needle-like mesoporous morphology in our foams may enhance protein absorption and cell adhesion and growth as has been observed for similar nanostructured morphologies [107, 134].

Reverchon et al. [134], produced PLA/hydroxyapatite nanocomposite scaffolds from PLA-dioxane-ethanol system with similar macropores and a fibrous mesostructure. They used fructose particles (250 – 500 μm) as a porogen, a sacrificial phase, to create the macropores. A supercritical CO_2 assisted route is used for drying the gels. The same authors found that due to the interesting fibrous nanostructure combined with macropores, the human mesenchymal stem cells can efficiently differentiate onto the scaffold [107].
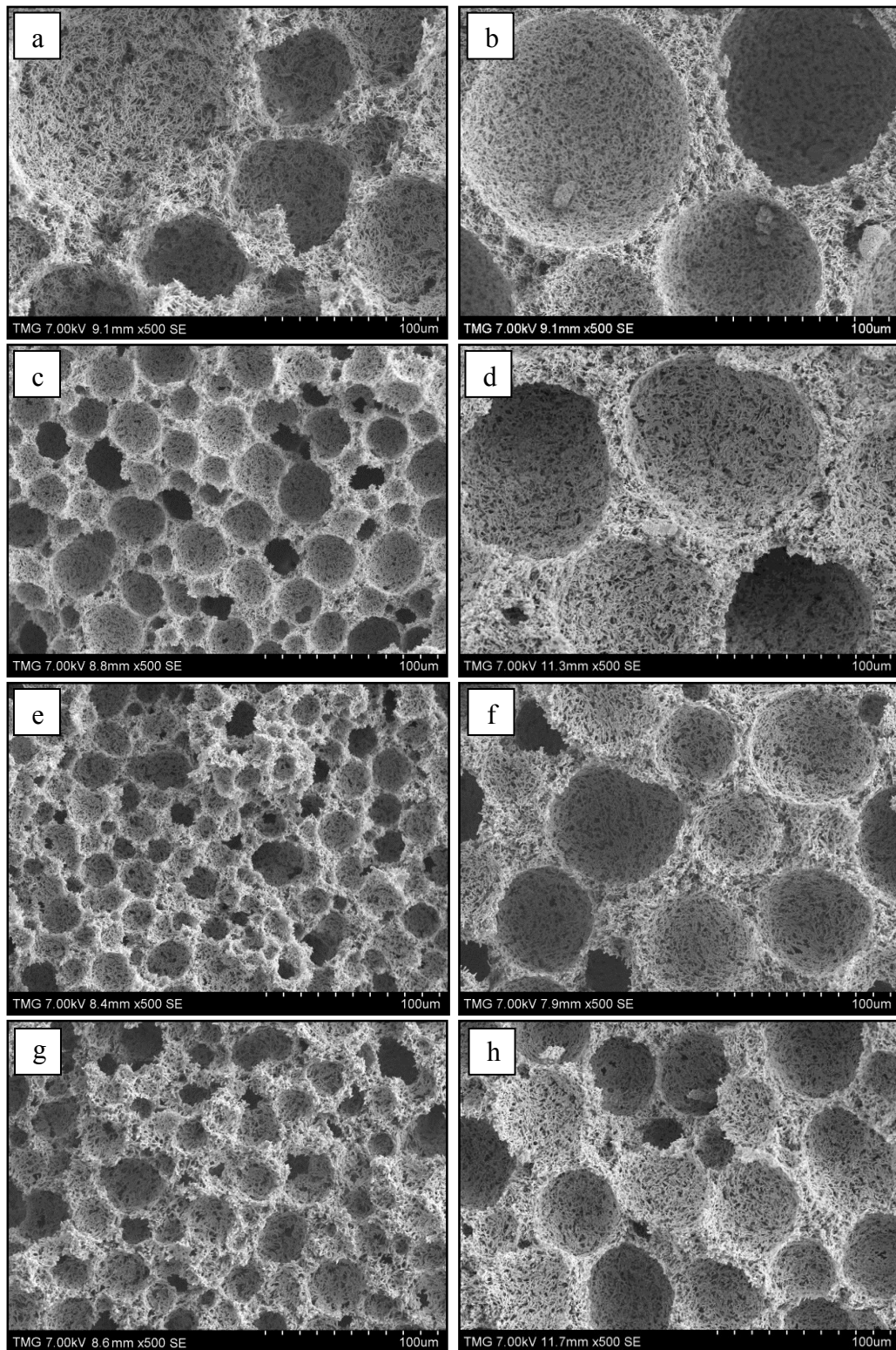
Fig. 6. 8. SEM images (× 500) of the foams with various PLA in DCM concentrations (wt.%): a and b) 13, c and d) 16, e and f) 19, g and h) 23. The left and right images are corresponding to pure PLA and composite systems respectively. These composite foams are produced via route i (DCM).
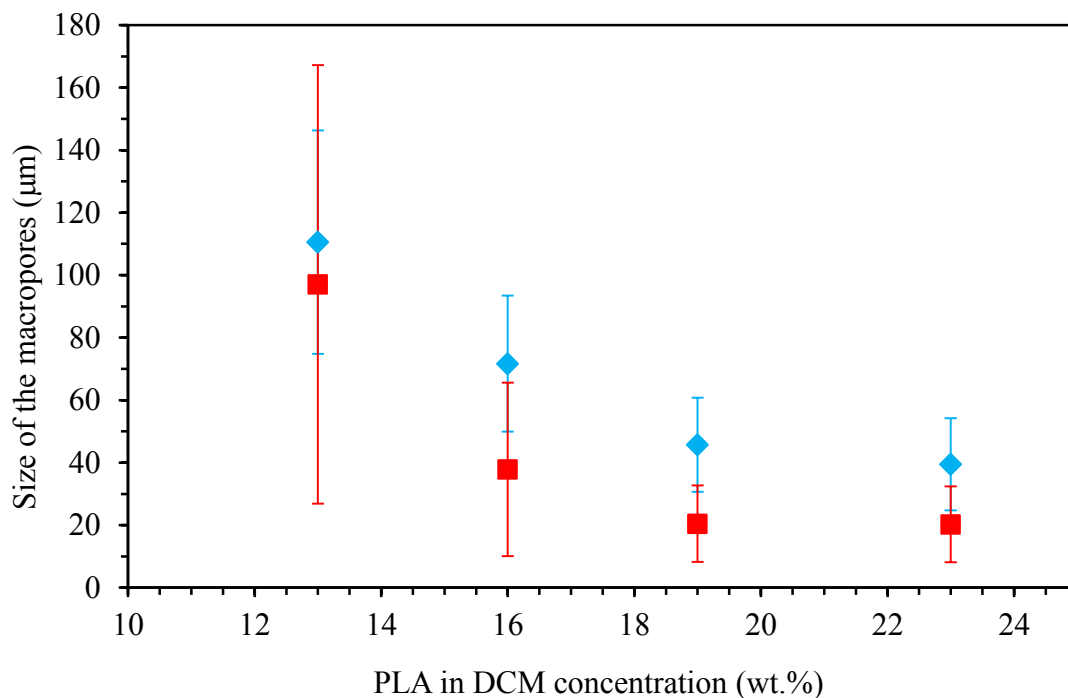
Fig. 6. 9. The results of image analysis on the size of the macropores of the foams (n = 70): pure PLA (■) and composite systems produced via DCM (route i ◆). The size of one macropore is considered as its diameter which itself can be the average of up to 4 diameters.

The effect of different incorporation routes of bioactive particles has not previously been studied in (modified) TIPS processes [107, 134, 160, 173, 174]. In the modified TIPS process the polymer is typically dissolved directly in a suspension of the particles in a solution of solvent and nonsolvent [122, 123, 167], a process that works only at low nonsolvent concentrations or high temperatures. In our study, because we mix the nonsolvent hexane with the polymer solution (PLA-DCM) we have two possible routes for incorporating the particles as explained previously: route i (via DCM) and route ii (via hexane). The incorporation of surface modified glass particles via hexane (route ii) significantly changes the morphology of the foam (Fig. 6.10) obtained from system (13 wt.%) compared to that of the corresponding pure system (Fig. 6.8a) and the composite system prepared via route i (DCM) (Fig. 6.8b). The spherical macropores are not perfectly formed when the modified glass particles are incorporated via hexane (Fig. 6.10c) which is most likely related to the longer gelation time for this system (24 to 30 hours) as compared to the same composition (13 wt.%) wherein the glass particles are

incorporated via DCM (~ 3.5 h) or the pure system without any glass particles (~ 4 h) [169]. It seems that the modified particles reduced the nonsolvent nature of the hexane in this case.

Fig. 6. 10. SEM images with various magnifications of the composite foam obtained from system (13 wt.%) containing 2 wt.% surface modified glass particles incorporated via hexane (route ii). Dashed circles are to guide the eye.

The crystallinity of the PLA matrix is also significantly lower for this system (Fig. 6.7) confirming that the crystallization process is hindered either kinetically or thermodynamically in the mixture during phase separation. Due to the disturbed mass transfer, a relatively large amount of liquid (polymer-lean phase) is rejected out of the gel during the phase separation and can be seen on top of the gel at the end of gelation. This

leads to a more compact structure with deformed macropores and a lower porosity (Fig. 6.6).

6.3.2.3. Particle spacial distribution

Next we consider the distribution of the surface modified glass particles of various sizes in the foams produced via route i (DCM). In the SEM images (Fig. 6.11) we can see both submicron (Fig. 6.11 a and b) and micron-sized (Fig. 6.11 c to f), incorporated in the PLA foam of system (13 wt.%) representing the two populations of these particles (Fig. 6.3 ---◆---). The submicron particles (Fig. 6.11 a and b) are attached to individual needles of the mesoporous structure. The micron-sized particles are embedded within (Fig. 6.11 c and d) or attached to (Fig. 6.11 e and f) the mesoporous structure. The embedded particles are interlocked in the mesoporous structure, while simultaneously can be in direct contact with physiological fluids due to the open-pore structure. This is not normally the case in composite scaffolds produced by other common methods where the bioactive particles are completely surrounded by the polymeric matrix (causing lower bioactivity) or located only on the surface (susceptible to being washed away) [7, 79, 121].

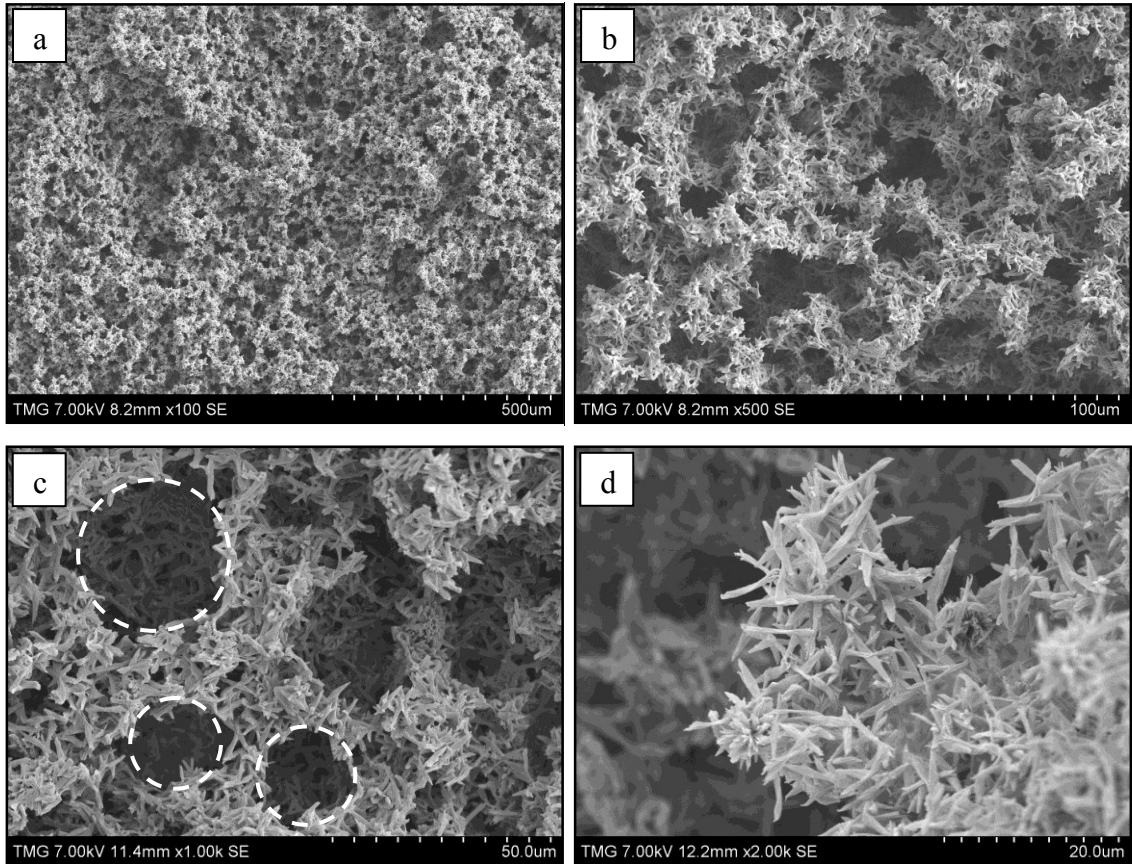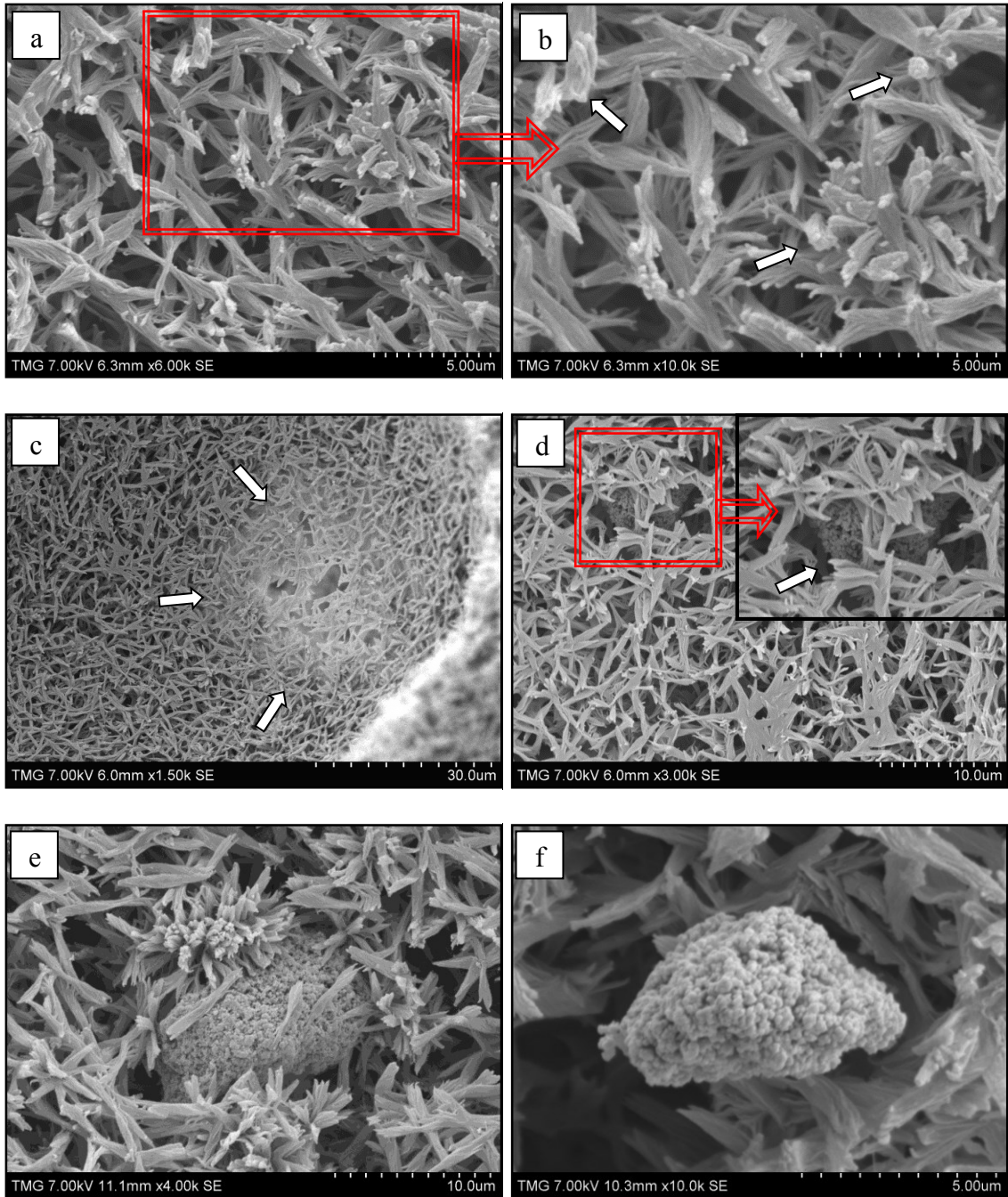Fig. 6. 11. SEM images with various magnifications of composite foams obtained from system (13 wt.%) containing 2 wt.% surface modified glass particles incorporated via DCM (route i). Submicron (a and b) and micron-sized (c – f) particles are seen in these images where the small arrows denote some of them.

In the case of the unmodified glass we do not see such a beneficial particle placement because of the significantly larger particles (up to ~ 200 μm) in this glass compared to a maximum of ~ 30 μm in the surface modified glass (Fig. 6.3). The large particles of the unmodified glass (Fig. 6.12) act as stress concentrators causing cracks in the matrix structure (Fig. 6.12b) potentially leading to a lower strength for the final monolith as previously observed with other scaffolds [16, 79, 91].
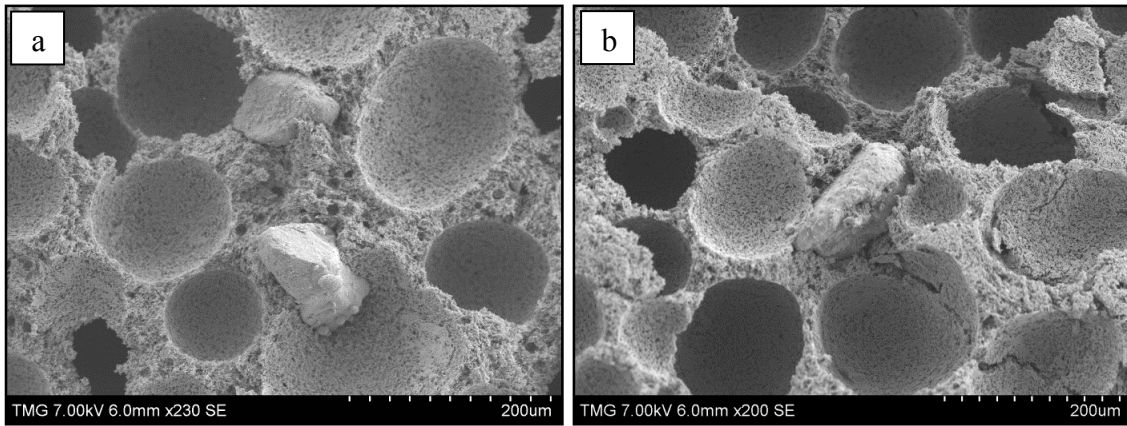
Fig. 6. 12. SEM images of the composite foam obtained from system (13 wt.%) containing 2 wt.% unmodified glass particles incorporated via DCM (route i).

6.4. Conclusion

A sol-gel-derived 45S5 Bioglass® was successfully surface modified using a silane coupling agent (3-methacryloxypropyltriethoxysilane) under basic conditions (pH = 9 – 10). The deposition of the silane onto the glass particles was confirmed by FTIR. It was shown that the tendency of glass particles to agglomerate is effectively diminished by surface modification. The surface modified bioglass contains 78% submicron particles and has a mean particle size of 1.82 μm while the unmodified bioglass has a mean particle size of 13.28 μm and 43% submicron particles.

Highly porous (up to ~ 91%) PLA-based scaffolds containing 2 wt.% surface modified 45S5 Bioglass® with an interesting meso/macroporous morphology were produced via liquid-liquid phase separation of the PLA-DCM-hexane system at -23 ºC. It

was shown that that the particle incorporation route, via solvent (DCM) or nonsolvent (hexane), has the greatest impact on porosity, crystallinity and morphology of the foams.

The incorporation of 2 wt.% glass via DCM slightly increased the porosity of the foams and did not affect the crystallinity of their PLA matrices. The spherical macropores of the composite systems are larger on average with a narrower size distribution compared to those of the corresponding pure PLA systems. The mesoporous morphology remains almost the same for both pure and composite scaffolds. The incorporation of glass particles (2 wt.%) via hexane significantly changed the pore morphology and decreased the porosity and crystallinity of the PLA foams.

For foams produced by the addition of particles via DCM, SEM images revealed that the surface modified particles are embedded within the mesoporous structure of the composite scaffolds. In this manner, the bioactive glass particles can be in contact with physiological fluids, while they are interlocked by the mesoporous PLA matrix. These composite monoliths have a great potential for bone scaffold applications.

Chapter 7

Conclusions, contributions and future work

7.1. Summary of conclusions

In this study, highly porous PLA-based monoliths with meso/macroporous morphology containing 2 wt.% surface modified sol-gel-derived 45S5 Bioglass®, were produced via liquid-liquid nonsolvent induced phase separation at a standing temperature of - 23 ºC.

Fully amorphous 45S5 Bioglass® with an appropriately high specific surface area (11.75 m^2/g) was synthesized via an organic, nitrate-free sol-gel route. The process was straightforward and did not require any specialized equipment such as glove box, freeze-drying, or refluxing. The selected combination of organic precursors required a stabilization temperature of ~550 ºC which was below the crystallization temperature of 614 ºC. This resulted in a fully amorphous product after stabilization. Although 43% of the glass particles were submicron with a mean particle size of ~ 600 nm, because of large micron-sized aggregates and agglomerates, the overall mean particle size was much higher (13.28 μm). Due to high bioactivity of the 45S5 composition and the advantages of the sol-gel method, our 45S5 Bioglass® is expected to exhibit excellent bioactivity and great potential for hard and soft tissue healing.

The ternary phase diagram of PLA-DCM-hexane system was experimentally developed based on the visual observations over a 14-day test periods. The single and two-phase regions were differentiated determining the binodal curve. The boundary between the liquid-liquid and solid-liquid phase separated regions was also identified. The validity of the phase diagram was verified by the lever rule. Phase separation kinetics based on turbidity measurements showed that an increase the initial PLA in DCM concentration significantly increased the rate of phase separation. These results are essential for the fabrication of PLA foams and membrane using the PLA-DCM-hexane system.

Compositions from the liquid-liquid phase separated region which underwent gelation were selected and used for producing PLA foams via NIPS. For the systems (hexane/DCM = 1 v/v) which were phase separated at room temperature, the foam porosity as a function of initial PLA in DCM concentration showed three regions, namely: the fragile gel, transition, and the resilient gel. At low PLA in DCM concentration (fragile gel) the foam porosity was low due to capillary forces induced shrinkage of the gels during drying. The porosity sharply increased over the transition region with increasing PLA in DCM concentration. After a maximum of about 88.5%, porosity slightly dropped in the resilient gel region where gels were stiff enough to resist capillary forces. This resulted in a lower shrinkage and higher porosity compared to those of the previous regions. The porosity and specific surface area of these foams were in the range of 40.7% to 88.5% and 29.3 to 54.1 m^2/g respectively.

Based on the phase diagram and SEM examination, the phase separation mechanism for the systems of the fragile and resilient gel regions was determined to be nucleation and growth and spinodal decomposition, respectively. The morphology of the foams in the fragile gel region was distorted due to the high shrinkage. The isotropic mesoporous morphology of the foams of the resilient gel region confirmed spinodal decomposition in these systems.

For the same systems but when phase separated at - 23 °C, the morphology is very different; a combination of large spherical macropores and a needle-like meso-structure which were formed via nucleation and growth and PLA crystallization, respectively. Gel shrinkage was minimal in these systems due to the large macropores, resulting in high porosities up to 90.8%.

DSC studies showed that the PLA foams are semi-crystalline (up to 62.6%) and their crystallinity decreases with increasing initial PLA-DCM concentration. Crystallinity also decreases with decreasing phase separation standing temperature. The compressive Young's modulus of the foams (1.8 to 57 MPa) was affected by their crystallinity and morphology such that systems with the highest crystallinity exhibit the highest compressive modulus. The potential of foams with meso/macroporous morphology for scaffold applications was discussed and these systems were selected for producing highly porous scaffolds in the next stage of the work.

The sol-gel-derived 45S5 Bioglass® was surface modified with a silane coupling agent (3-methacryloxypropyltriethoxysilane) under basic conditions (pH = 9-10) using ammonium hydroxide as a catalyst. The stoichiometric amount of water for a complete hydrolysis of silane was used. This is believed to minimize self-polymerization and encourage single-layer deposition of silane. FTIR spectroscopy results confirmed the deposition of silane molecules onto the glass particles. These results also revealed that crystalline hydroxycarbonate apatite formed on the glass particles due to exposure to humidity prior to surface modification, indicating the high bioactivity of our glass. Sedimentation studies showed that the surface modified particles exhibits better dispersibility and stability in PLA-DCM solutions due to increased hydrophobicity of particles compared to that of unmodified particles. Surface modification effectively diminished the agglomeration of the glass particles. The unmodified bioglass with an overall mean particle size of 13.28 μm contained 43% submicron particles whereas the surface modified bioglass contained 78% submicron particles with a much smaller overall mean particle size of 1.82 μm. The surface modified glass particles were incorporated into PLA foams with high porosity (up to ~ 91%) and a meso/macroporous morphology. The porosity of these foams (pure PLA and composite systems) decreased linearly with increasing initial PLA in DCM concentration. This was a completely different trend from that observed with the PLA foams prepared by liquid-liquid phase separation at room temperature. Interestingly, the incorporation route of particles (via DCM or via hexane) into the PLA foaming process had the greatest impact on the properties of the final foams. The incorporation of surface modified particles (2 wt.%) via DCM slightly increased the porosity and had no impact on the crystallinity of the PLA foams. The SEM images showed that these composite foams had larger macropores on average and a narrower size distribution compared to those of the pure PLA foams. The needle-like mesoporous morphology was essentially the same for both composite and pure systems. The incorporation of surface modified particles (2 wt.%) via hexane significantly decreased the porosity (~3%) and crystallinity (~6%) of the PLA foam. Also, the morphology of the foam was significantly changed such that the macropores were distorted and not perfectly spherical. This was most likely due to the much longer

135

gelation time of these systems compared to that of the composite systems prepared via DCM route.

SEM images revealed that large particles of unmodified glass (up to ~ 200 μm) acted as a stress concentrators causing cracks in the structure of foams leading to poorer mechanical properties. On the other hand, surface modified glass particles were perfectly incorporated in the foams such that even the largest micron-sized particles were embedded within the mesoporous structure. In this manner, the particles can be in contact with physiological fluids while they are interlocked by the mesoporous PLA matrix. Such composite scaffolds are expected to have good bioactivity and performance *in vitro* and *in vivo*.

7.2. Contributions

Each stage of this study has produced contributions to knowledge which all combine to allow for the production of highly porous PLA/Bioglass® scaffolds with remarkable morphologies and potential for bone regeneration.

For the first time, it was demonstrated that fully amorphous 45S5 Bioglass® with appropriately high specific surface area can be produced via the sol-gel method. A process based on a novel combination of organic, nitrate-free precursors was developed that required no specialized equipment. A high level of bioactivity is expected from our bioglass due to the high bioactivity of the 45S5 composition and the advantages of sol-gel-derived bioglasses.

The ternary phase diagram of the PLA-DCM-hexane system was experimentally developed and the single phase, liquid-liquid phase separated and solid-liquid phase separated regions of this system were identified. The detailed experimental methodology designed for studying the phase separation behavior and kinetics of this system can be used for similar polymer-solvent-nonsolvent systems. These results also provide general information for the production of porous PLA structures such as membranes and monoliths.

Highly porous, semi-crystalline PLA foams with good compressive modulus and interesting morphologies were produced from PLA-DCM-hexane system via a template-

free nonsolvent induced liquid-liquid phase separation route. The trend of shrinkage and porosity of PLA foams as a function of initial PLA-DCM concentration were presented allowing to select foams with low shrinkage and high porosity. The effect of composition, phase separation standing temperature and drying route on crystallinity of PLA foams was also described. These results improve the understanding of crystallization during phase separation in such processes. The theoretical and empirical knowledge required for the production of a range of mesoporous and meso/macroporous morphologies were also developed in this stage of the study.

For the first time, fully amorphous sol-gel-derived 45S5 Bioglass® was surface modified with a silane coupling agent. It was demonstrated that surface modification of glass particles can significantly diminish their agglomeration. Also, highly porous PLA-based composite scaffolds were produced by incorporation of surface modified bioglass particles into the system. It was found that the particle incorporation route (via DCM or hexane) had the greatest impact on porosity, crystallinity and morphology of the foams, even though in both cases the whole system is mechanically mixed prior to gelation. It was demonstrated that unlike most scaffolds produced by other techniques, the particles in our scaffold were fully-incorporated with the mesoporous structure of the PLA matrix. The great advantage of this meso/macroporous morphology is that the particles would be in contact with physiological fluids while they are still locked into this mesoporous structure preventing them from being washed off.

7.3. Recommendations for future work

Some suggestions for future work to expand this study are summarized in the following.

➢ The bioactivity of the sol-gel-derived 45S5 Bioglass® particles should be evaluated *in vitro* using simulated body fluid (SBF).
➢ The PLA-DCM-hexane ternary phase diagram can also be further developed, theoretically, based on Flory-Huggins equations. The theoretical binodal and spinodal should be located on the phase diagram and compared with our experimental results.

- Morphology of the foams prepared from systems which are phase separated at room temperature or - 23 °C were observed by SEM. It would be interesting to also examine the morphology of the foams prepared at other phase separation standing temperatures (4 °C and 40 °C) as well as foams obtained from other compositions (e.g., hexane/DCM = 0.75).

- It would be worth examining the original morphology of the fragile gels before shrinkage. For this purpose, the structure of the gels must be preserved by freezing or replacing the polymer-lean phase by a fluid which can diffuse through the structure and solidify. The results of such a study would help to better understand the phase separation mechanism in those systems.

- Further investigation on the interconnectivity of PLA foams with meso/macroporous morphology is recommended, although they are believed to be interconnected based on the SEM observations and the permeability test using graphite flakes. The incorporation of some surfactants and/or porogens in order to modify the morphology and improve interconnectivity of the foams can be also evaluated.

- The density of grafted silane (molecule/nm^2) after surface modification of the glass particles might be measured precisely using TGA.

- Incorporation of more than 2 wt.% surface modified glass particles (e.g., 5, 10 and 15 wt.%) with PLA foams of various systems should be investigated in order to produce composite scaffolds with higher bioglass contents. The properties of these composite scaffolds could be also evaluated as a function of bioglass content (wt.%).

- The composite scaffolds might be also characterized in terms of interconnectivity, mechanical properties and degradation rate *in vitro* and the results compared to those of the corresponding pure PLA foams.

- The production of foams from other types of PLA, PDLLA and PDLA, via the same NIPS process should also be investigated.

- The highly porous PLA foams with mesoporous or macro/mesoporous morphology might be considered for other applications such as acoustic insulation.

REFERENCES

[1]   S.M. Best, A.E. Porter, E.S. Thian, J. Huang, "Bioceramics: Past, present and for the future," *Journal of the European Ceramic Society,* vol. 28, p. 1319–1327, 2008.

[2]   George Stylios, Taoyu Wan, Peter Giannoudis, "Present status and future potential of enhancing bone healing using nanotechnology," *Injury, Int. J. Care Injured,* vol. 38, pp. 63-74, 2007.

[3]   J. Jones, "New trends in bioactive scaffolds: The importance of nanostructure," *Journal of the European Ceramic Society,* vol. 29, p. 1275–1281, 2009.

[4]   D. F. Williams, The Williams dictionary of biomaterials, Liverpool University Press, 1999.

[5]   L. Hench, "The story of Bioglass®," *J Mater Sci: Mater Med,* vol. 17, p. 967–978, 2006.

[6]   E. Gentleman and J. Polak, "Historic and current strategies in bone tissue engineering: Do we have a hope in Hench?," *J Mater Sci: Mater Med,* vol. 17, p. 1029–1035, 2006.

[7]   K. Rezwan, Q. Chen, J. Blaker and A. Boccaccini, "Biodegradable and bioactive porous polymer/inorganic composite scaffolds for bone tissue engineering," *Biomaterials,* vol. 27, p. 3413–3431, 2006.

[8]   R. Li, A. Clark and L. L. Hench, "An Investigation of bioactive glass powders by sol-gel processing," *Journal of Applied Biomaterials,* vol. 2, pp. 231-239, 1991.

[9]   Q.-Z. Chen, Y. Li, L.-Y. Jin, J. M. Quinn and P. A. Komesaroff, "A new sol–gel process for producing Na_2O-containing bioactive glass ceramics," *Acta Biomaterialia,* vol. 6, p. 4143–4153, 2010.

[10]   R. L. Siqueira, O. Peitl and E. D. Zanotto, "Gel-derived SiO_2–CaO–Na_2O–P_2O_5 bioactive powders: Synthesis and in vitro bioactivity," *Materials Science and Engineering C,* vol. 31, p. 983–991, 2011.

[11]   J. Qian, Y. Kang, Z. Wei and W. Zhang, "Fabrication and characterization of biomorphic 45S5 bioglass scaffold from sugarcane," *Materials Science and Engineering C,* vol. 29, p. 1361–1364, 2009.

[12]   Q. Chen and G. Thouas, "Fabrication and characterization of sol–gel derived 45S5 Bioglass®–ceramic scaffolds," *Acta Biomater.,* vol. 7, p. 3616–3626, 2011.

[13]   C. Gualandi, Porous Polymeric Bioresorbable Scaffolds for Tissue Engineering, London New York: Springer, 2011.

139

[14] B. Dhandayuthapani, Y. Yoshida, T. Maekawa and D. S. Kumar, "Polymeric Scaffolds in Tissue Engineering Application: A Review," *Int. J. Polym. Sci.,* vol. 2011, p. doi:10.1155/2011/290602, 2011.

[15] H. Zou, S. Wu and a. J. Shen, "Polymer/Silica Nanocomposites: Preparation, Characterization, Properties, and Applications," *Chem. Rev.,* vol. 108, p. 3893–3957, 2008.

[16] Y. Gao and J. Chang, "Surface Modification of Bioactive Glasses and Preparation of PDLLA/Bioactive Glass Composite Films," *Journal of Biomaterials Applications,* vol. 24, pp. 119-138, 2009.

[17] P. Sepulveda, J. Jones and L. Hench, "Characterization of melt-derived 45S5 and sol-gel–derived 58S bioactive glasses," *J Biomed Mater Res (Appl Biomater),* vol. 58, p. 734–740, 2001.

[18] M. Cerruti, D. Greenspan and K. Powers, "Effect of pH and ionic strength on the reactivity of Bioglass® 45S5," *Biomaterials,* vol. 26, p. 1665–1674, 2005.

[19] E. Neel, T. Mizoguchi, M. Ito, M. Bitar, V. Salih and J. Knowles, "In vitro bioactivity and gene expression by cells cultured on titanium dioxide doped phosphate-based glasses," *Biomaterials,* vol. 28, p. 2967–2977, 2007.

[20] J. Zhong and D. Greenspan, "Processing and Properties of Sol–Gel Bioactive Glasses," *J. Biomed. Mater. Res.,* vol. 53, p. 694–701, 2000.

[21] M. V.-R. D. Arcos, "Sol–gel silica-based biomaterials and bone tissue regeneration," *Acta Biomaterialia,* vol. 6, p. 2874–2888, 2010.

[22] L. Hench, "Genetic design of bioactive glass," *Journal of the European Ceramic Society,* vol. 29, p. 1257–1265, 2009.

[23] L. Hench, "Bioceramics: From Concept to Clinic," *Journal of the American Ceramic Society,* vol. 74, no. 7, pp. 1487-1510, 1991.

[24] L. Hench, D. Wheeler and D. Greenspan, "Molecular Control of Bioactivity in Sol-Gel Glasses , 13, 1998,," *Journal of Sol-Gel Science and Technology,* vol. 13, p. 245–250, 1998.

[25] V. Rajendran, A. Begum, M. Azooz and F. E. Batal, "Microstructural dependence on relevant physical–mechanical properties on SiO_2–Na_2O–CaO–P_2O_5 biological glasses," *Biomaterials,* vol. 23, p. 4263–4275, 2002.

[26] W. Vogel and W. Holand, "The development of bioglass ceramics for medical applications," *Angew Chem Inf Ed. Engl.,* vol. 26, pp. 527-544, 1987.

[27] N. Bovo, Structure-properties relationships in bioactive glasses for PAA based polyalkenate cements, Doctoral Dissertations: University of Padova, 2011.

[28] V. Aina, A. Perardi, L. Bergandi, G. Malavasi, L. Menabue, C. Morterra and D. Ghigo, "Cytotoxicity of zinc-containing bioactive glasses in contact with human osteoblasts," *Chemico-Biological Interactions,* vol. 167, p. 207–218, 2007.

[29] X. Chen, Y. Meng, Y. Li and N. Zhao, "Investigation on bio-mineralization of melt and sol–gel derived bioactive glasses," *Applied Surface Science,* vol. 255, p. 562–564, 2008.

[30] W. Xia and J. Chang, "Preparation and characterization of nano-bioactive-glasses (NBG) by a quick alkali-mediated sol–gel method," *Materials Letters,* vol. 2007, p. 3251–3253, 2007.

[31] X. Chen, B. Lei, Y. Wang and N. Zhao, "Morphological control and in vitro bioactivity of nanoscale bioactive glasses," *Journal of Non-Crystalline Solids,* vol. 355, p. 791–796, 2009.

[32] Z. Hong, A. Liu, L. Chen, X. Chen and X. Jing, "Preparation of bioactive glass ceramic nanoparticles by combination of sol–gel and coprecipitation method," *Journal of Non-Crystalline Solids,* vol. 355, p. 368–372, 2009.

[33] X. Chen, C. Guo and N. Zhao, "Preparation and characterization of the sol–gel nano-bioactive glasses modified by the coupling agent gamma-aminopropyltriethoxysilane," *Applied Surface Science,* vol. 255, p. 466–468, 2008.

[34] P. Sepulveda, J. R. Jones and L. L. Hench, "In vitro dissolution of melt-derived 45S5 and sol-gel derived 58S bioactive glasses," *J. Biomed. Mater. Res.,* vol. 61, p. 301–311, 2002.

[35] D. Bellucci, V. Cannillo, A. Sola, F. Chiellini, M. Gazzarri and C. Migone, "Macroporous Bioglass®-derived scaffolds for bone tissue regeneration," *Ceramics International,* vol. 37, p. 1575–1585, 2011.

[36] D. Arcos, D. Greenspan and M. Vallet-Regı, "A new quantitative method to evaluate the in vitro bioactivity of melt and sol-gel-derived silicate glasses," *J. Biomed. Mater. Res.,* vol. 65A, p. 344–351, 2003.

[37] A. R. Boccaccini, M. Erol, W. J. Stark, D. Mohn, Z. Hong and J. F. Mano, "Polymer/bioactive glass nanocomposites for biomedical applications: A review," *Composites Science and Technology,* vol. 70, p. 1764–1776, 2010.

[38] P. Saravanapavan, J. R. Jones, R. S. Pryce and L. L. Hench, "Bioactivity of gel− glass powders in the CaO-SiO$_2$ system: A comparison with ternary (CaO-P$_2$O$_5$-SiO$_2$) and

quaternary glasses (SiO$_2$-CaO-P$_2$O$_5$-Na$_2$O)," *J. Biomed. Mater. Res.,* vol. 66A, p. 110–119, 2003.

[39] K. Lobel and L. Hench, "Zn-Vitro Protein Interactions with a Bioactive Gel-Glass," *Journal of Sol-Gel Science and TechnoIogy,* vol. 7, pp. 69-76, 1996.

[40] V. Maquet, A. Boccaccini, L. Pravata, I. Notingher and R. Jerome, "Porous poly(α-hydroxyacid)/Bioglass® composite scaffolds for bone tissue engineering. I: preparation and in vitro characterisation," *Biomaterials,* vol. 25, p. 4185–4194, 2004.

[41] J. Jones and L. Hench, "Biomedical materials for new millennium: perspective on the future," *Materials Science and Technology,* vol. 17, pp. 891-900, 2001.

[42] T. Waltimo, T. Brunner, M. Vollenweider, W. Stark and M. Zehnder, "Antimicrobial Effect of Nanometric Bioactive Glass 45S5," *J. Dent. Res.,* vol. 86, pp. 754-757, 2007.

[43] A. Balamurugan, G. Balossier, D. Laurent-Maquin, S. Pina, A. Rebelo, J. Faure and J. Ferreira, "An in vitro biological and anti-bacterial study on a sol–gel derived silver-incorporated bioglass system," *Dental Materials,* vol. 24, p. 1343–1351, 2008.

[44] Z. Hong, R. L. Reis and J. F. Mano, "Preparation and in vitro characterization of novel bioactive glass ceramic nanoparticles," *J. Biomed. Mater. Res.,* vol. 88A, p. 304–313, 2009.

[45] Q. Chen and A. R. Boccaccini, "Coupling Mechanical Competence and Bioresorbability in Bioglass®-Derived Tissue Engineering Scaffolds," *Advanced Engineering Materials,* vol. 8, no. 4, pp. 285-289, 2006.

[46] Q. Z. Chen, I. D. Thompson and A. R. Boccaccinia, "45S5 Bioglass®-derived glass–ceramic scaffolds for bone tissue engineering," *Biomaterials,* vol. 27, p. 2414–2425, 2006.

[47] G. E. Vargas, R. V. Mesones, O. Bretcanu, J. M. P. Lo´pez, A. R. Boccaccini and A. Gorustovich, "Biocompatibility and bone mineralization potential of 45S5 Bioglass®-derived glass–ceramic scaffolds in chick embryos," *Acta Biomaterialia,* vol. 5, p. 374–380, 2009.

[48] [Online]. Available: http://www.ucl.ac.uk/~uccaati/bioglasses.html.

[49] L. Lefebvre, J. Chevalier, L. Gremillard, R. Zenati, G. Thollet, D. Bernache-Assolant and A. Govin, "Structural transformations of bioactive glass 45S5 with thermal treatments," *Acta Materialia,* vol. 55, p. 3305–3313, 2007.

[50] O. Bretcanu, X. Chatzistavrou, K. Paraskevopoulos, R. Conradt, I. Thompson and A. R. Boccaccini, "Sintering and crystallisation of 45S5 Bioglass® powder," *Journal of the European Ceramic Society,* vol. 29, p. 3299–3306, 2009.

[51] A. R. Boccaccini, Q. Chen, L. Lefebvre, L. Gremillard and J. Chevalierb, "Sintering, crystallisation and biodegradation behaviour of Bioglass®-derived glass–ceramics," *The Royal Society of Chemistry,* vol. 136, p. 27–44, 2007.

[52] L. Hench, "Innovative ceramic technologies to transform the world," in *37th International Conference & Exposition on Advanced Ceramics and Composites (ICACC'13)*, Daytona Beach; FL; USA, 2013.

[53] L. M'adler, H. Kammler, R. Mueller and S. Pratsinis, "Controlled synthesis of nanostructured particles by flame spray Pyrolysis," *Aerosol Science,* vol. 33, p. 369–389, 2002.

[54] T. J. Brunner, R. N. Grass and W. J. Stark, "Glass and bioglass nanopowders by flame synthesis," *Chem. Commun.,* p. 1384–1386, 2006.

[55] J. S. Cho and Y. C. Kang, "Synthesis of spherical shape borate-based bioactive glass powders prepared by ultrasonic spray pyrolysis," *Ceramics International,* vol. 35, p. 2103–2109, 2009.

[56] K. Matsuzaki, D. Aray, N. Taneda, T. Mukaiyama and M. Ikemura, "Continuous silica glass fiber produced by sol-gel process," *Journal of Non-Crystalline Solids,* vol. 112, pp. 437-441, 1989.

[57] M. Allahverdi, R. A. L. Drew and J. O. Strom-Olsen, "Melt-extracted oxide ceramic fibres - the fundamentals," *Journal of Materials Science,* vol. 31, pp. 1035-1042, 1996.

[58] F. Quintero, J. Pou, R. Comesana, F. Lusquinos, A. Riveiro, A. B. Mann, R. G. Hill, Z. Y. Wu and J. R. Jones, "Laser spinning of bioactive glass nanofibers," *Adv. Funct. Mater.,* vol. 19, p. 3084–3090, 2009.

[59] C. Gao, Q. Gao, Y. Li, M. N. Rahaman, A. Teramoto and K. Abe, "Preparation and in vitro characterization of electrospun PVA scaffolds coated with bioactive glass for bone regeneration," *Biomed. Mater. Res. Part A,* vol. 100A, p. 1324–1334, 2012.

[60] M. N. Rahaman, Ceramic processing and sintering, 2nd edition, New York: Marcel Dekker, Inc., 2005.

[61] P. Sepulveda, J. R. Jones and L. L. Hench, "Characterization of melt-derived 45S5 and sol-gel–derived 58S bioactive glasses," *J. Biomed. Mater. Res. (Appl Biomater),* vol. 58, p. 734–740, 2001.

[62] I. A. Silver, J. Deas and M. E. ska, "Interactions of bioactive glasses with osteoblasts in vitro: effects of 45S5 Bioglass®, and 58S and 77S bioactive glasses on metabolism,

intracellular ion concentrations and cell viability," *Biomaterials,* vol. 22, pp. 175-185, 2001.

[63] P. Sepulveda, J. R. Jones and L. L. Hench, "Bioactive sol-gel foams for tissue repair," *J. Biomed. Mater. Res.,* vol. 59, p. 340–348, 2002.

[64] W. Xia and J. Chang, "Preparation and characterization of nano-bioactive-glasses (NBG) by a quick alkali-mediated sol–gel method," *Materials Letters ,* vol. 61, p. 3251–3253, 2007.

[65] D. C. BRADLEY, "Metal Alkoxides as Precursors for Electronic and Ceramic Materials," *Chem. Rev. ,* vol. 89, pp. 1317-1322, 1989.

[66] M. Catauro, M. Raucci, F. D. Gaetano and A. Marotta, "Antibacterial and bioactive silver-containing Na_2O x CaO x $2SiO_2$ glass prepared by sol-gel method," *J. Mater. Sci. Mater. Med.,* vol. 15, pp. 831-837, 2004.

[67] Y. Zhao, M. T. Carvajal, Y.-Y. Won and M. T. Harris, "Preparation of Calcium Alginate Microgel Beads in an Electrodispersion Reactor Using an Internal Source of Calcium Carbonate Nanoparticles," *Langmuir,* vol. 23, pp. 12489-12496, 2007.

[68] D. Stephan and S. Wistuba, "Crystal structure refinement and hydration behaviour of doped tricalcium aluminate," *Cement and Concrete Research,* vol. 36, p. 2011–2020, 2006.

[69] S. Chang and T. Ring, "Map of gel times for three phase region tetraethoxysilane, ethanol and water," *Journal of Non-Crystalline Solids,* vol. 147&148, pp. 56-61, 1992.

[70] C. Wu, Y. Luo, G. Cuniberti, Y. Xiao and M. Gelinsky, "Three-dimensional printing of hierarchical and tough mesoporous bioactive glass scaffolds with a controllable pore architecture, excellent mechanical strength and mineralization ability," *Acta Biomaterialia,* vol. 7, pp. 2644-2650, 2011.

[71] H. Demirkiran, A. Mohandas, M. Dohi, A. Fuentes, K. Nguyen and P. Aswath, "Bioactivity and mineralization of hydroxyapatite with bioglass as sintering aid and bioceramics with $Na_3Ca_6(PO_4)_5$ and $Ca_5(PO_4)_2SiO_4$ in a silicate matrix," *Materials Science and Engineering C,* vol. 30, p. 263–272, 2010.

[72] T. Kida, Y. Miyachi, K. Shimanoe and N. Yamazoe, "NASICON thick film-based CO_2 sensor prepared by a sol–gel method," *Sensors and Actuators B,* vol. 80, pp. 28-32, 2001.

[73] A. Martuccia, S. Sartori, M. Guglielmi, M. D. Vona, S. Licoccia and E. Traversa, "NMR and XRD study of the influence of the P precursor in sol-gel synthesis of NASICON powders and films," *Journal of the European Ceramic Society,* vol. 22, p. 1995–2000,

2002.

[74] D. Puppi, F. Chiellini, A. Piras and E. Chiellini, "Polymeric materials for bone and cartilage repair," *Progress in Polymer Science (Oxford),* vol. 35, pp. 403-440, 2010.

[75] K. M. Nampoothiri, N. R. Nair and R. P. John, "An overview of the recent developments in polylactide (PLA) research," *Bioresource Technology,* vol. 101, pp. 8493-8501, 2010.

[76] Y. Tokiwa and B. P. Calabia, "Biodegradability and biodegradation of poly(lactide)," *Appl Microbiol Biotechnol,* vol. 72, p. 244–251, 2006.

[77] "NatureWorks LLC," 10 5 2013. [Online]. Available: http://www.natureworksllc.com.

[78] R. Murugan and S. Ramakrishna, "Development of nanocomposites for bone grafting," *Composites Science and Technology,* vol. 65, p. 2385–2406, 2005.

[79] S. K. Misra, D. Mohn, T. J. Brunner, W. J. Stark, S. E. Philip, I. Roy, V. Salih, J. C. Knowles and A. R. Boccaccini, "Comparison of nanoscale and microscale bioactive glass on the properties of P(3HB)/Bioglass® composites," *Biomaterials,* vol. 29, pp. 1750-1761, 2008.

[80] C. Migliaresi, A. D. L. L. Fambri and D. Cohn, "The Effect of Thermal History on Crystallinity of Different Molecular Weight PLLA Biodegradable Polymers," *Clinical Materials,* vol. 8, pp. 111-118, 1991.

[81] K. Fukushima, C. Abbate, D. Tabuani, M. Gennari and G. Camino, "Biodegradation of poly(lactic acid) and its nanocomposites," *Polymer Degradation and Stability,* vol. 94, p. 1646–1655, 2009.

[82] K. A. Athanasiou, C. M. Agrawal, F. A. Barber and S. S. Burkhart, "Orthopaedic Applications for PLA-PGA Biodegradable Polymers," *The Journal of Arthroscopic and Related Surgery,* vol. 14, p. 726–737, 1998.

[83] G. Ozkoc and S. Kemaloglu, "Morphology, Biodegradability, Mechanical, and Thermal Properties of Nanocomposite Films Based on PLA and Plasticized PLA," *Journal of Applied Polymer Science,* vol. 114, p. 2481–2487, 2009.

[84] J. H. Lee, T. G. Park, H. S. Park, D. S. Lee, Y. K. Lee, S. C. Yoon and J.-D. Nam, "Thermal and mechanical characteristics of poly(l-lactic acid) nanocomposite scaffold," *Biomaterials,* vol. 24, p. 2773–2778, 2003.

[85] C. Migliaresi, L. Fambri and D. Cohn, "A study on the in vitro degradation of poly(lactic acid)," *Journal of Biomaterials Science, Polymer Edition,* vol. 5, pp. 591-606, 1994.

[86] J. M. Anderson and M. S. Shive, "Biodegradation and biocompatibility of PLA and PLGA microspheres," *Advanced Drug Delivery Reviews,* vol. 28, p. 5–24, 1997.

[87] A. R. Boccaccini, J. J. Blaker, V. Maquet, W. Chung, R. Jerome and S. N. Nazhat, "Poly(D,L-lactide) (PDLLA) foams with TiO_2 nanoparticles and PDLLA/TiO_2-Bioglass® foam composites for tissue engineering scaffolds," *J. MATER. SCI.,* vol. 41, p. 3999–4008, 2006.

[88] L.-T. Lim, R. Auras and M. Rubino, "Processing technologies for poly(lactic acid)," *Progress in Polymer Science,,* vol. 33, p. 820–852, 2008.

[89] S. Saeidlou, M. A. Huneault, H. Li and C. B. Park, "Poly(lactic acid) crystallization," *Progress in Polymer Science,* vol. 37, pp. 1657-1677, 2012.

[90] T. Chen, Y. Zhou and W.-S. Tan, "Influence of lactic acid on the proliferation, metabolism, and differentiation of rabbit mesenchymal stem cells," *Cell Biol Toxicol,* vol. 25, p. 573–586, 2009.

[91] L. Wei, N. Hu and Y. Zhang, "Synthesis of Polymer—Mesoporous Silica Nanocomposites," *Materials,* vol. 3, pp. 4066-4079, 2010.

[92] Y. Xie, C. A. Hill, Z. Xiao, H. Militz and C. Mai, "Silane coupling agents used for natural fiber/polymer composites: A review," *Composites: Part A,* vol. 41, p. 806–819, 2010.

[93] J. Santos, L. J. Jhat and F. J. Monteiro, "Surface modifications of glass reinforced hydroxyapatite composites," *Biomaterials,* vol. 16, pp. 521-526, 1995.

[94] X. Li, S. Cai, W. Zhang, G. Xu and W. Zhou, "Effect of pH values on surface modification and solubility of phosphate bioglass-ceramics in the CaO–P_2O_5–Na_2O–SrO–ZnO system," *Applied Surface Science,* vol. 255, p. 9241–9243, 2009.

[95] Z. Mladenovi, A. Sahlin-Platt, Å. Bengtsson, M. Ransj and A. Shchukarevb, "Surface characterization of bone graft substitute materials conditioned in cell culture medium," *surface and interface analysis,* vol. 42, pp. 452-456, 2010.

[96] C. Wu, Y. Zhang, X. Ke, H. Zhu, C. Yong, W. Ross and X. Yin, "Bioactive mesopore-bioglass microspheres with controllable protein-delivery properties by biomimetic surface modification," *Journal of Biomedical Materials Research Part A,* vol. 95, pp. 476-485, 2010.

[97] A. Perro and V. N. Manoharan, "Bulk Synthesis of Polymer-Inorganic Colloidal Clusters," *Langmuir,* vol. 26, p. 18669–18675, 2010.

[98] B. Arkles, "Silane Coupling Agents: Connecting Across Boundaries (second version),"

Gelest Inc., 2006.

[99] R. S. Pryce and L. L. Hench, "Tailoring of bioactive glasses for the release of nitric oxide as an osteogenic stimulus," *J. Mater. Chem.,* vol. 14, p. 2303 – 2310, 2004.

[100] M. Abboud, M. Turner, E. Duguet and M. Fontanille, "PMMA-based composite materials with reactive ceramic fillers Part 1.—Chemical modification and characterisation of ceramic particles," *J. Mater. Chem.,* vol. 8, p. 1527–1532, 1997.

[101] A. Perro, S. Reculus, S. Ravaine, E. Bourgeat-Lami and E. Duguet, "Design and synthesis of Janus micro- and nanoparticles," *J. Mater. Chem.,* vol. 15, p. 3745–3760, 2005.

[102] K. Kailasam, S. Mascotto, S. Gross, C. Maccato and K. Muller, "Alkyl chain grafting on silica–zirconia mixed oxides: preparation and characterization," *J. Mater. Chem.,* vol. 20, p. 2345–2355, 2010.

[103] M. S. Silverstein, "PolyHIPEs: Recent advances in emulsion-templatedporous polymers," *Prog. Polym. Sci.,* vol. 39, p. 199– 234, 2014.

[104] S.-T. Lee, C. B. Park and N. S. Ramesh, Polymeric Foams: Science and Technology, Boca Raton, FL: Taylor and Francis Group, 2007.

[105] X. Liu and P. X. Ma, "Polymeric Scaffolds for Bone Tissue Engineering," *Ann. Biomed. Eng.,* vol. 32, no. 3, p. 477–486, 2004.

[106] F. Dehghani and N. Annabi, "Engineering porous scaffolds using gas-based techniques," *Curr. Opin. Biotechnol.,* vol. 22, p. 661–666, 2011.

[107] E. Reverchon and S. Cardea, "Supercritical fluids in 3-D tissue engineering," *J. Supercrit. Fluids,* vol. 69, p. 97–107, 2012.

[108] T. Serra, J. Planell and M. Navarro, "High-resolution PLA-based composite scaffolds via 3-D printing technology," *Acta Biomaterialia,* vol. 9, no. 3, p. 5521–5530, 2013.

[109] S. Yang, K.-F. Leong, Z. Du and C.-K. Chua, "The Design of Scaffolds for Use in Tissue Engineering. Part I. Traditional Factors," *Tissue Eng,* vol. 7, no. 6, p. 679–689, 2001.

[110] D.-M. Wang and J.-Y. Lai, "Recent advances in preparation and morphology control of polymeric membranes formed by nonsolvent induced phase separation," *Current Opinion in Chemical Engineering,* vol. 2, p. 229–237, 2013.

[111] M. D. Luccio, R. Nobrega and C. P. Borges, "Microporous anisotropic phase inversion membranes from bisphenol-A polycarbonate: study of a ternary system," *Polymer,* vol. 41, p. 4309–4315, 2000.

[112] F. W. Altena and C. A. Smolders, "Calculation of Liquid-Liquid Phase Separation in a Ternary System of a Polymer in a Mixture of a Solvent and a Nonsolvent," *Macromolecules,* vol. 15, pp. 1491-1497, 1982.

[113] T.-H. Young, L.-P. Cheng, D.-J. Lin, L. Fane and W.-Y. Chuang, "Mechanisms of PVDF membrane formation by immersion-precipitation in soft (1-octanol) and harsh (water) nonsolvents," *Polymer,* vol. 40, p. 5315–5323, 1999.

[114] J.-Y. Lai, S.-F. Lin, F.-C. Lin and D.-M. Wang, "Construction of Ternary Phase Diagrams in Nonsolvent/Solvent/PMMA Systems," *J. Polym. Sci.: Part B: Polym. Phys.,* vol. 36, p. 607–615, 1998.

[115] Y.-M. Wei, Z.-L. Xu, X.-T. Yang and H.-L. Liu, "Mathematical calculation of binodal curves of a polymer/solvent/nonsolvent system in the phase inversion process," *Desalination,* vol. 192, p. 91–104, 2006.

[116] Y. S. Soh, J. H. Kim and C. C. Gryte, "Phase behaviour of polymer/solvent/non-solvent systems," *Polymer,* vol. 36, pp. 3711-3717, 1995.

[117] H.-. P. Hentze and M. Antonietti, "Porous polymers and resins for biotechnological and biomedical applications," *Rev. Mol. Biotechnol.,* vol. 90, p. 27–53, 2002.

[118] J. G. Wijmans, J. Kant, M. H. V. Mulder and C. A. Smolders, "Phase separation phenomena in solutions of polysulfone in mixtures of a solvent and a nonsolvent: relationship with membrane formation," *Polymer,* vol. 26, p. 1539–1545, 1985.

[119] P. S. T. Machado, A. C. Habert and C. P. Borges, "Membrane formation mechanism based on precipitation kinetics and membrane morphology: flat and hollow fiber polysulfone membranes," *J. Membr. Sci.,* vol. 155, pp. 171-183, 1999.

[120] Y. Yang, J. Zhao, Y. Zhao, L. Wen, X. Yuan and Y. Fan, "Formation of porous PLGA scaffolds by a combining method of thermally induced phase separation and porogen leaching," *Journal of Applied Polymer Science,* vol. 109, no. 2, pp. 1232 - 1241, 2008.

[121] Z. Hong, R. L. Reis and J. F. Mano, "Preparation and in vitro characterization of scaffolds of poly(L-lactic acid) containing bioactive glass ceramic nanoparticles," *Acta Biomater.,* vol. 4, p. 1297–1306, 2008.

[122] J.-S. Chen, S.-L. Tu and R.-Y. Tsay, "A morphological study of porous polylactide scaffolds prepared by thermally induced phase separation," *J. Taiwan Inst. Chem. Eng.,* vol. 41, p. 229–238, 2010.

[123] F. J. Hua, G. E. Kim, J. D. Lee, Y. K. Son and D. S. Lee, "Macroporous Poly(L-lactide)

Scaffold 1. Preparation of a Macroporous Scaffold by Liquid–Liquid Phase Separation of a PLLA–Dioxane–Water System," *J. Biomed. Mater. Res. (Appl. Biomater.),* vol. 63, p. 161–167, 2002.

[124] F. J. Hua, T. G. Park and D. S. Lee, "A facile preparation of highly interconnected macroporous poly(D,L-lactic acid-co-glycolic acid) (PLGA) scaffolds by liquid–liquid phase separation of a PLGA–dioxane–water ternary system," *Polymer,* vol. 44, p. 1911–1920, 2003.

[125] Y. Xin, T. Fujimoto and H. Uyama, "Facile fabrication of polycarbonate monolith by non-solvent induced phase separation method," *Polymer,* vol. 53, p. 2847–2853, 2012.

[126] Y. S. Nam and T. G. Park, "Biodegradable polymeric microcellular foams by modified thermally induced phase separation method," *Biomaterials,* vol. 20, pp. 1783-1790, 1999.

[127] R. A. Zoppi, S. Contant, E. A. R. Duek, F. R. Marques, M. L. F. Wada and S. P. Nunes, "Porous poly(l-lactide) films obtained by immersion precipitation process: morphology, phase separation and culture of VERO cells," *Polymer,* vol. 40, p. 3275–3289, 1999.

[128] Q. Xing, X. Dong, R. Li, H. Yang, C. C. Han and D. Wang, "Morphology and performance control of PLLA-based porous membranes by phase separation," *Polymer,* vol. 54, p. 5965–5973, 2013.

[129] T. Tanaka, T. Nishimoto, K. Tsukamoto, M. Yoshida, T. Kouya, M. Taniguchi and D. R. Lloyd, "Formation of depth filter microfiltration membranes of poly(l-lactic acid) via phase separation," *journal of membrane science,* vol. 396, pp. 101-109, 2012.

[130] D. M. Koenhen, M. H. V. Mulder and C. A. Smolders, "Phase Separation Phenomena During the Formation of Asymmetric Membranes," *J. Appl. Polym. Sci.,* vol. 21, pp. 199-215, 1977.

[131] L. H. Sperling, Introduction to physical polymer science, 4th edition, New Jersey: John Wiley & Sons Inc., 2006.

[132] A. Razmjou, J. Mansouri and V. Chen, "The effects of mechanical and chemical modification of TiO_2 nanoparticles on the surface chemistry, structure and fouling performance of PES ultrafiltration membranes," *journal of membrane science,* vol. 378, p. 73 – 84, 2011.

[133] S. Balta, A. Sotto, P. Luis, L. Benea, B. V. d. Bruggen and J. Kim, "A new outlook on membrane enhancement with nanoparticles: The alternative of ZnO," *Journal of Membrane Science,* vol. 389, p. 155– 161, 2012.

[134] E. Reverchon, P. Pisanti and S. Cardea, "Nanostructured PLLA-Hydroxyapatite Scaffolds Produced by a Supercritical Assisted Technique," *Ind. Eng. Chem. Res.,* vol. 48, p. 5310–5316, 2009.

[135] M. Catauro, F. Papale, G. Roviello, C. Ferone, F. Bollino, M. Trifuoggi and C. Aurilio, "Synthesis of SiO_2 and CaO rich calcium silicate systems via sol–gel process: bioactivity, biocompatibility, and drug delivery tests," *J. Biomed. Mater. Res. A,* vol. 102, no. 9, p. 3087–3092, 2014.

[136] D. Carta, D. Pickup, J. Knowles, M. Smith and R. Newport, "Sol-gel synthesis of the P_2O_5–CaO–Na_2O–SiO_2 system as a novel bioresorbable glass," *J. Mater. Chem.,* vol. 15, p. 2134–2140, 2005.

[137] A. Lucas-Girot, F. Mezahi, M. Mami, H. Oudadesse, A. Harabi and M. L. Floch, "Sol–gel synthesis of a new composition of bioactive glass in the quaternary system SiO_2–CaO–Na_2O–P_2O_5 Comparison with melting method," *J. Non-Cryst. Solids,* vol. 357, p. 3322–3327, 2011.

[138] V. Cannillo and A. Sola, "Potassium-based composition for a bioactive glass," *Ceram. Int.,* vol. 35, p. 3389–3393, 2009.

[139] A. Balamurugan, G. Balossier, S. Kannan, J. Michel, A. Rebelo and J. Ferreira, "Development and in vitro characterization of sol–gel derived CaO–P_2O_5–SiO_2–ZnO bioglass," *Acta Biomater.,* vol. 3, p. 255–262, 2007.

[140] G. Gheysen, P. Ducheyne, L. Hench and P. deMeester, "Bioglass composites: a potential material for dental application," *Biomaterials,* vol. 4, p. 81–84, 1983.

[141] M. Woodhouse, G.S.Herman and B. Parkinson, "Combinatorial approach to identification of catalysts for the photoelectrolysis of water," *Chem. Mater. ,* vol. 17, p. 4318–4324, 2005.

[142] Y.J.Wee, J. Kim and H. Ryu, "Biotechnological production of lactic acid and its recent applications," *Food Technol. Biotechnol.,* vol. 44, p. 163–172, 2006.

[143] E. Rezabeigi, P. Proa-Flores, R. Drew and P.Wood-Adams, "A novel nitrate-free sol–gel process for production of 45S5 Bioglass®," in *Proc.Am. Soc. Compos.*, Montreal, 2011.

[144] M. Vallet-Regí, C. Ragel and A. Salinas, "Glasses with medical applications," *Eur. J. Inorg. Chem.,* vol. 6, p. 1029–1042, 2003.

[145] M. Eggersdorfer, D. Kadau, H. Herrmann and S. Pratsinis, "Fragmentation and restructuring of soft-agglomerates under shear," *J. Colloid Interface Sci.,* vol. 342, p. 261–268, 2010.

[146] S. Yoo and C.K.Kim, "Effects of the diluent mixing ratio and conditions of the thermally induced phase-separation process on the pore size of microporous polyethylene membranes," *J. Appl. Polym. Sci.,* vol. 3, pp. 154-162, 2008.

[147] S. Chaeichian, P. Wood-Adams and S. Hoa, "In situ polymerization of polyesterbased hybrid systems for the preparation of clay nanocomposites," *Polymer 2013;54:1512e23,* vol. 54, pp. 1512-1523, 2013.

[148] F. Campbell, Phase diagrams: understanding the basics [chapter 10], Ohio: ASM International, 2012.

[149] Y. Su and X. Jian, "Phase separation and theta-compositions of PPES/NMP/nonsolvent systems," *J. Mater. Sci. Technol.,* vol. 21, pp. 430-432, 2005.

[150] I. Smallwood, Handbook of organic solvent properties, London: Hodder Headline Group, 1996.

[151] T. Tanaka and D. R. Lloyd, "Formation of poly(l-lactic acid) microfiltration membranes via thermally induced phase separation," *J. Membr. Sci.,* vol. 238, p. 65–73, 2004.

[152] S. Yoneda, W. Han, U. Hasegawa and H. Uyama, "Facile fabrication of poly(methyl methacrylate) monolith via thermally induced phase separation by utilizing unique cosolvency," *Polymer 2014;55:,* vol. 55, pp. 3212-3216, 2014.

[153] C. Sundback, T. Hadlock, M. Cheney and J. Vacanti, "Manufacture of porous polymer nerve conduits by a novel low-pressure injection molding process," *Biomaterials,* vol. 24, pp. 819e-30, 2003.

[154] K.-H. Shin, I.-H. Jo, S.-E. Kim, Y.-H. Koh and H.-E. Kim, "Nonsolvent induced phase separation (NIPS)-based 3D plotting for threedimensionally macrochanneled poly(ε-caprolactone) scaffolds with highly porous frameworks," *Mater. Lett.,* vol. 122, pp. 348-851, 2014.

[155] E. Rezabeigi, P. Wood-Adams and R. Drew, "Isothermal ternary phase diagram of the polylactic acid-dichloromethane-hexane system," *Polymer,* vol. 55, pp. 3100-3106, 2014.

[156] C. García-Gonzalez, M. Alnaief and I. Smirnova, "Polysaccharide-based aerogelsdpromising biodegradable carriers for drug delivery systems," *Carbohydr. Polym.,* vol. 86, pp. 1425-1438, 2011.

[157] M. Mosquera, M. Bejarano, N. Rosa-Fox and L. Esquivias, "Producing crack-free colloid-polymer hybrid gels by tailoring porosity," *Langmuir,* vol. 19, pp. 951-957, 2003.

[158] M. Tang, Y. Dong, M. Stevens and C. Williams, "Tailoring polylactide degradation:

copolymerization of a carbohydrate lactone and S,S-lactide," *Macromolecules,* vol. 43, pp. 7556-7564, 2010.

[159] J.-R. Sarasua, R. Prud'homme, M. Wisniewski, A. Borgne and N. Spassky, " Crystallization and melting behavior of polylactides," *Macromolecules,* vol. 31, pp. 3895-3905., 1998.

[160] J. Blaker, V. Maquet, R. Jerome and S. N. A. Boccaccini, "Mechanical properties of highly porous PDLLA/bioglass® composite foams as scaffolds for bone tissue engineering," *Acta Biomater.,* vol. 1, pp. 643-652, 2005.

[161] S. Fakirov, E. Fischer, R. Hoffmann and G. Schmidt, "Structure and properties of poly(ethylene terephthalate) crystallized by annealing in the highly oriented state: 2. Melting behaviour and the mosaic block structure of the crystalline layers," *Polymer,* vol. 18, pp. 1121-1129, 1977.

[162] K. Asadi, H. Wondergem, R. Moghaddam, C. McNeill, N. Stingelin, B. Noheda and e. al, "Spinodal decomposition of blends of semiconducting and ferroelectric polymers," *Adv. Funct. Mater. ,* vol. 21, pp. 1887-1894, 2011.

[163] L. McCusker, F. Liebau and G. Engelhardt, "Nomenclature of structural and compositional charactrictics of ordered microporous and mesoporous materials with inorganic hosts," *Pure. Appl. Chem.,* vol. 73, no. 2, pp. 381-394, 2001.

[164] A. Deng, A. Chen, S. Wang, Y. Li, Y. Liu, X. Cheng and e. al, "Porous nanostructured poly-l-lactide scaffolds prepared by phase inversion using supercritical CO_2 as a nonsolvent in the presence of ammonium bicarbonate particles," *J. Supercrit. Fluids,* vol. 77, pp. 110-116, 2013.

[165] M. Muthukumar, "Nucleation in polymer crystallization," *Adv. Chem. Phys.,* vol. 128, pp. 1-63, 2004.

[166] E. Rezabeigi, P. M. Wood-Adams and R. A. Drew, "Synthesis of 45S5 Bioglass® via a straightforward organic, nitrate-free sol-gel process," *Materials Science and Engineering: C,* vol. 40, p. 248–252, 2014.

[167] K. C. Shin, B. S. Kim, J. H. Kim, T. G. Park, J. D. Nama and D. S. Lee, "A facile preparation of highly interconnected macroporous PLGA scaffolds by liquid–liquid phase separation II," *Polymer,* vol. 46, p. 3801–3808, 2005.

[168] F. J. Hua, J. D. Nam and D. S. Lee, "Preparation of a Macroporous Poly(l-lactide) Scaffold by Liquid-Liquid Phase Separation of a PLLA/1,4-Dioxane/Water Ternary System in the

Presence of NaCl," *Macromol. Rapid Commun.,* vol. 22, pp. 1053-1057, 2001.

[169] E. Rezabeigi, P. M. Wood-Adams and R. A. Drew, "Production of porous polylactic acid monoliths via nonsolvent induced phase separation," *Polymer,* vol. 55, pp. 6743-6753, 2014.

[170] P. J. Launer, "Infrared analysis of organosilicon compounds: Spectra-structure correlations,," Laboratory For Materials, Inc., New York, 1987.

[171] E. Rezabeigi, P. M. Wood-Adams and R. A. Drew, "Surface Modification of Sol-Gel-Derived 45S5 Bioglass® for Incorporation in Polylactic Acid (PLA)," in *Advances in Bioceramics and Porous Ceramics VI (eds R. Narayan, P. Colombo, S. Kirihara and S. Widjaja), John Wiley & Sons, Inc.,*, Hoboken, NJ, USA, 2013.

[172] G. Theodorou, O. M. Goudouri, E. Kontonasaki, X. Chatzistavrou, L. Papadopoulou, N. Kantiranis and K. M. Paraskevopoulos, "Comparative Bioactivity Study of 45S5 and 58S Bioglasses in Organic and Inorganic Environment," *Bioceramics Development and Applications,* vol. 1, pp. 1-4, 2011.

[173] N. Barroca, A. Daniel-da-Silva, P. Vilarinho and M. Fernandes, "Tailoring the morphology of high molecular weight PLLA scaffolds through bioglass addition," *Acta Biomaterialia,* vol. 6, p. 3611–3620, 2010.

[174] H.-C. Liu, I.-C. Lee, J.-H. Wang, S.-H. Yang and T.-H. Young, "Preparation of PLLA membranes with different morphologies for culture of MG-63 Cells," *Biomaterials,* vol. 25, p. 4047–4056, 2004.

[175] X. Shan, W. Qin and Y. Dai, "Dependence of extraction equilibrium of monocarboxylic acid from aqueous solutions on the relative basicity of extractant," *Chemical engineering science,* vol. 61, pp. 2574-81, 2006.

Appendix

Appendix A

Appendix A contains additional information about Chapter 5.

A1. Handling and solvent exchange of the fragile, wet gels

The gels from low PLA concentration mixtures are more fragile and cannot be removed from the glass vessel prior to the solvent exchange. In this case, methanol is poured on top of the gel and allowed to diffuse through the monolith (the methanol is completely replaced 4 times). These gels, which are then much more rigid, are subjected to the immersion solvent exchange process as described in section 5.2.2. Thorough solvent exchange plays an important role in the subsequent drying step by strengthening the monolith and lowering the capillary forces.

A2. Effect of nonsolvent/solvent ratio on crystallinity

From Fig. 5.8 and Fig. A.1, we can conclude that PLA in DCM concentration has a more significant effect on the overall crystallinity of the foams compared to that of the nonsolvent/solvent ratio.
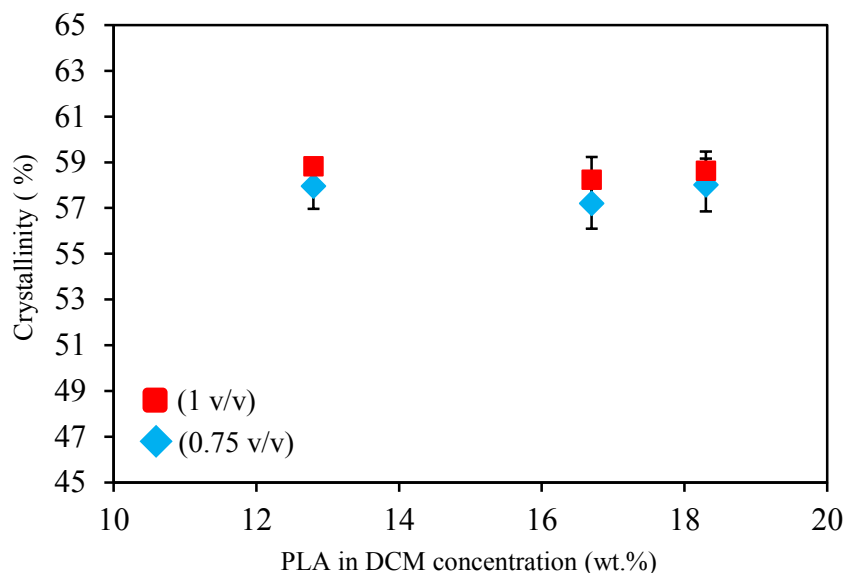
Fig. A. 1. The effect of nonsolvent/solvent ratio (v/v) on crystallinity of the monoliths with the same initial PLA in DCM concentration (n= 3).

A3. Permeability of the PLA foams

We performed a simple permeability test using an isopropyl alcohol-based suspension of graphite flakes (D = ~ 2 μm in average). As shown in Fig. A. 2, a foam specimen (13 wt.%, 1 v/v, -23 °C) whose microstructure is shown as Fig. 5.6 a, c and e, is immersed in the suspension. The sample initially floats on top of the suspension since its density is very low (0.12 ± 0.02 g/cm^3), but after a few seconds it becomes saturated and sinks below the surface. After 5 minutes, the sample is taken out and allowed to dry in air followed by vacuum. After gently cleaning the surface, the sample is cut and visually investigated. The graphite flakes penetrated the foam even in this short soaking time indicating relatively good interconnectivity.

In addition to the mesopores structure, there are many micron-sized defects/channels in the microstructure of PLA foams connecting the large spherical pores together (Fig. A. 3).
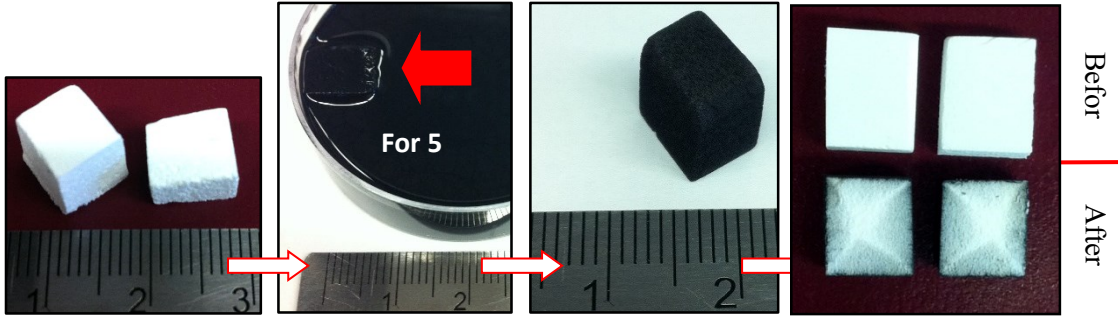
Fig. A. 2. The steps of the permeability test on foam (13 wt.%, 1 v/v, -23 °C) using an isopropyl alcohol-based suspension containing of graphite flakes.
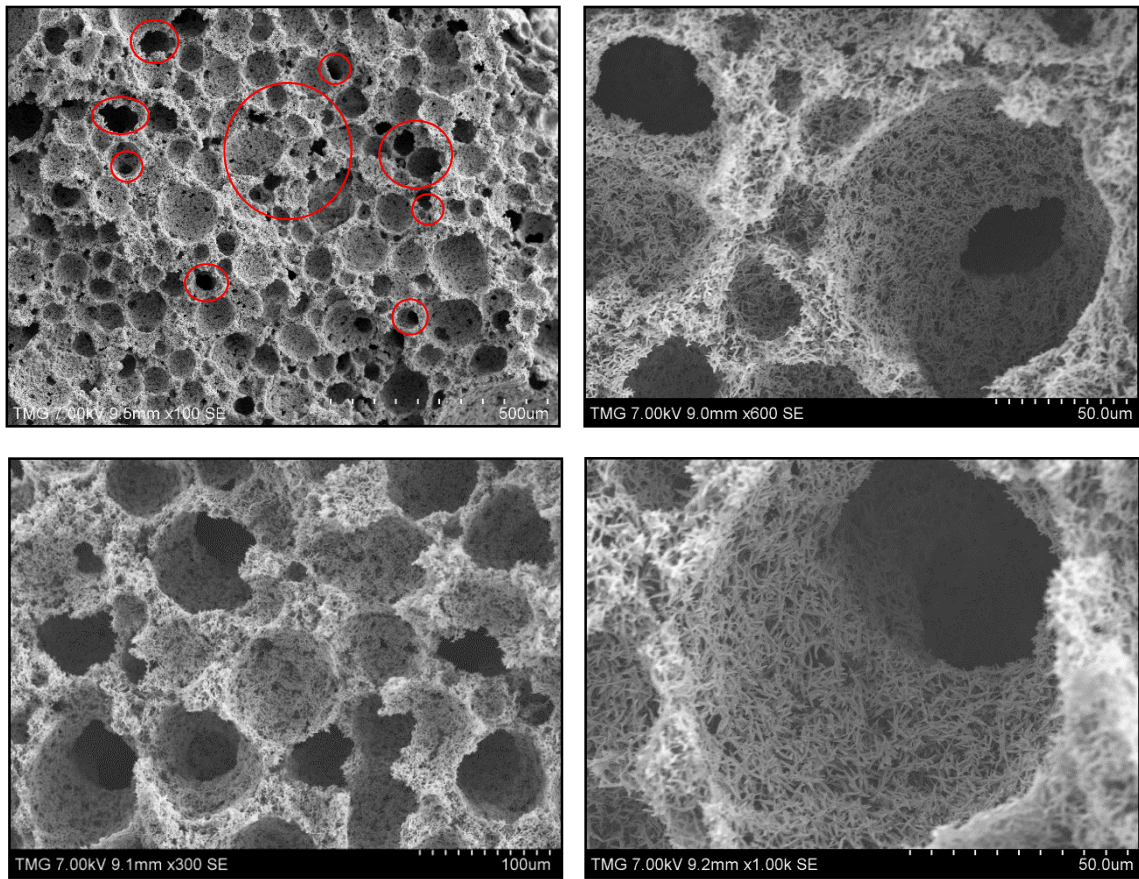

Fig. A. 3. Some examples of SEM images of foam (13 wt.%, 1 v/v, -23 °C) showing interconnectivity.

Appendix B

Appendix B contains additional information about Chapter 6.

B1. Mesoporous morphology of foams

According to the SEM images (Fig. B. 1), the needle-like mesoporous morphology of pure PLA foams is almost the same as that of the foams containing surface modified glass particles incorporated via solvent DCM (route i).
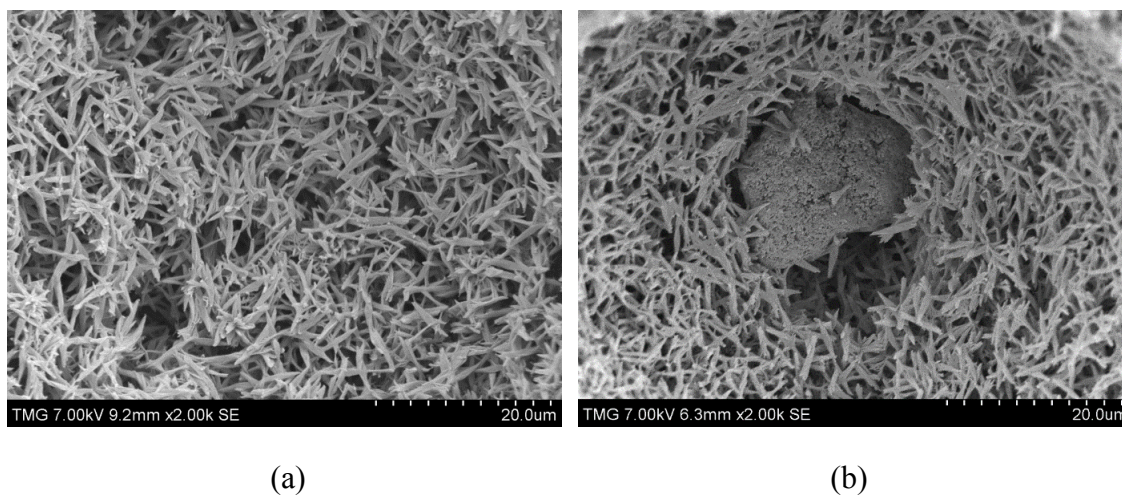

(a)   (b)

Fig. B. 1. SEM images (× 2000) of mesoporous structure of the pure PLA (a) and composite (b) foams prepared from system (13 wt.%). Note that this composite system is produced via route i (DCM).

Appendix C

Two conference papers are also published based on the primary results presented in Chapters 3 and 6, which are not included in this thesis.

1. E. Rezabeigi, , P. M. Wood-Adams, and R. A.L. Drew, "Surface Modification of Sol-Gel-Derived 45S5 Bioglass® for Incorporation in Polylactic Acid (PLA)", Advances in Bioceramics and Porous Ceramics VI (eds R. Narayan, P. Colombo, S. Kirihara and S. Widjaja), John Wiley & Sons, Inc., Hoboken, NJ, USA, vol. 34, no. 6, pp. 107 – 112, 2013[1].

2. E. Rezabeigi, P.M. Proa-Flores, R.A.L. Drew, P. Wood-Adams, "A novel nitrate-free sol–gel process for production of 45S5 Bioglass®", Proc.Am. Soc. Compos. 1 pp. 34 – 42, 2011[2].

---

1. 37th International Conference & Exposition on Advanced Ceramics and Composites, Daytona Beach, Florida, January 27 - February 1, 2013.

2. 26th ASC technical conference/Second joint US-Canada conference on composites, Montreal, Quebec, September 26 - 28, 2011.